Shallow Overturning Circulations of the Tropical-Subtropical Oceans

Friedrich A. Schott

IFM-GEOMAR Leibniz Institut für Meereswissenschaften an der Universität Kiel, Kiel, Germany

Julian P. McCreary, Jr.

International Pacific Research Center, University of Hawaii, Honolulu, Hawaii

Gregory C. Johnson

NOAA/Pacific Marine Environmental Laboratory, Seattle, Washington

The Subtropical Cells (STCs) of the Pacific and Atlantic Oceans connect the subtropical subduction regions of both hemispheres to the eastern, equatorial upwelling regimes by equatorward thermocline and poleward surface flows. In the Indian Ocean, where equatorial upwelling is absent, a cross-equatorial cell (CEC) connects the southern-hemisphere subduction regime with upwelling regions north of the equator, and it is closed by southward, cross-equatorial Ekman/Sverdrup transport at the ocean surface. We review here the theory explaining the mean features of the STCs and CEC, the observational evidence for their various branches, and results of realistic model simulations. A topic of particular interest is the partition of the equatorward STC branch between interior and western-boundary pathways. Observational results are only now beginning to reveal the structure of the interior pathways, and model results of these flows vary with model type and the wind forcing applied. We also review studies of STC variability, which has been hypothesized to play a role in climate variability. Existing work indicates that wind-driven STC transport variations ($\mathbf{v}'\overline{T}$ processes) are more important than advection of subducted temperature anomalies by the mean STC currents (the $\overline{\mathbf{v}}T'$ processes) in generating equatorial sea-surface temperature anomalies and, hence, climate variability.

1. INTRODUCTION

The Subtropical Cells (STCs) are shallow overturning circulations confined to the upper 500 m. In the Atlantic and Pacific Oceans, they connect subduction zones of the eastern, subtropical ocean with upwelling zones in the tropics. In addition to the dominant equatorial upwelling regimes, upwelling in off-equatorial regions (e.g., the Costa Rica Dome and the Peruvian coast in the Pacific, and the Guinea and Angola domes in the Atlantic) also has to be considered as a potential STC driver; so far, very little is known about these upwelling regimes, but offshore Ekman transports suggest that their contribution may not be negligible. The subsurface STC branches carry thermocline water to the equator either in western boundary currents after circulating across the basin in the Subtropical Gyres or directly in the ocean interior. They are closed by poleward surface currents, largely Ekman transports, that return the upwelled waters to the subtropics (e.g.,

Earth Climate: The Ocean-Atmosphere Interaction
Geophysical Monograph Series 147

10.1029/147GM15

McCreary and Lu [1994]; *Liu et al.* [1994]; *Lu et al.* [1998]; *Johnson and McPhaden* [1999]; *Malanotte-Rizzoli et al.* [2000]).

In contrast to the other two oceans, the Indian Ocean does not possess an equatorial upwelling zone because its annual-mean equatorial winds are westerly. As a result, its shallow cells differ markedly from those in the other two oceans. One cell, the Cross-Equatorial Cell (CEC), has its descending branches in the eastern subtropics of the southern hemisphere but its upwelling branches in the northern hemisphere, thereby requiring cross-equatorial flow [*Schott et al.*, 2002a; *Miyama et al.*, 2003]. Another, the Indian Ocean STC, is associated with upwelling driven by the Ekman divergence from 2–12ºS at the northern edge of the Southeast Trades [*McCreary et al.*, 1993; *Murtugudde et al.*, 1999; *Webster et al.*, 1999], and hence is confined to the southern hemisphere.

The STCs provide the cool subsurface water that is required to maintain the tropical thermocline. For this reason, STC variability has been hypothesized to be important for the decadal modulation of ENSO and for Pacific decadal variability, and it may affect Atlantic equatorial SST as well. In the Indian Ocean, a recently identified climate anomaly, the Indian Ocean Dipole (IOD) or Zonal Mode (IOZM), has been associated with changes in the 2–12ºS upwelling regime and, hence, variations in the Indian Ocean STC [*Xie et al.*, 2002; *Feng and Meyers*, 2003].

STC pathways are complicated by their interaction with the other ocean currents, particularly with the interocean circulations in each basin, namely, the northward flow of warm water in the Atlantic by the Meridional Overturning Circulation (MOC) with a transport of about 15 Sv [*Ganachaud and Wunsch*, 2001; *Lumpkin and Speer*, 2003], and the circulation driven by the Indonesian Throughflow (ITF) in the Pacific with a transport of 10–15 Sv [*Ganachaud et al.*, 2000; *Sloyan et al.*, 2003]. One result of these interactions is that the southern STC is stronger than the northern one in both oceans [*Johnson and McPhaden*, 1999; *Sloyan et al.*, 2003; *Zhang et al.*, 2003; *Fratantoni et al.*, 2000; *Lazar et al.*, 2002].

The STCs also interact with even shallower overturning cells confined to the tropics. In the Atlantic and Pacific, the shallow Tropical Cells (TCs) are associated with downwelling driven by the decrease of the poleward Ekman transport 4–6º off the equator [*Liu et al.*, 1994; *McCreary and Lu*, 1994; *Molinari et al.*, 2003]. Interestingly, although the TCs are strong in zonal integrations along constant depths, they are much diminished in integrations carried out along isopycnal layers, indicating that they have little influence on heat transport [*Hazeleger et al.*, 2000]. Their existence implies that any measure of STC strength must be defined poleward of the TC convergences, that is, closer to the dynamical intersection between the tropics and subtropics (near 8–10º say). In the Indian Ocean, the CEC interacts with a shallow equatorial roll, analogous to the TCs (or to the Equatorial Cell defined by *McCreary and Lu* [1994]) but driven by meridional winds; it distorts the southward, cross-equatorial pathway of the CEC, requiring that it takes place about 50 m below the surface [*Schott et al.*, 2003; *Miyama et al.*, 2003].

Finally, the off-equatorial undercurrents in the Atlantic and Pacific have to be considered when discussing STCs. In the Pacific, they are referred to as North and South Subsurface Countercurrents (NSCC and SSCC) or simply Tsuchiya Jets [*Tsuchiya*, 1972], whereas in the Atlantic they are called North and South Equatorial Undercurrents (NEUC and SEUC). They are attached to the EUC in the western Pacific [*Rowe et al.*, 2000], but are clearly separated from the EUC in the western Atlantic [*Schott et al.*, 1998; *Bourles et al.*, 1999b]. The fate of these currents is not clear. They diverge poleward toward the east [*Johnson and Moore*, 1997], and hence may upwell in the aforementioned off-equatorial regions or partially recirculate in the other mid-depth equatorial currents [*Rowe et al.*, 2000]. Although most of their transport is located deeper than the EUC, their shallow portions overlap with the deeper part of the EUC. Thus, they can potentially impact the STCs by partially blocking the equatorward transport of thermocline water to the equator, instead carrying water eastward where it may upwell along the eastern boundary or in domes. Even more fundamentally, they can perhaps be considered part of the STCs themselves, a deep off-equatorial branch.

Our review is organized as follows. In Section 2, we discuss the theoretical concepts that explain the basic properties of mean STC pathways. Next, we review observations and model simulations for the individual oceans in Sections 3–5. In Section 6, we present observational and modeling evidence on STC variability, and discuss its potential role in climate variability. We close (Section 7) with a summary of our conclusions and a brief outlook on needed research.

2. STEADY-STATE THEORY

In this section, we discuss basic properties of steady-state STCs (their existence, strength, equatorward extension, and subsurface pathways) using a $2^1/_2$-layer model, the simplest system that can represent all the STC branches. Its advantage is that analytic solutions can be obtained in which basic STC properties are clearly expressed [*Luyten et al.*, 1983; *Pedlosky*, 1987, 1988, 1991; *Pedlosky and Samelson*, 1989; *McCreary and Lu*, 1994; *Liu*, 1994], allowing their underlying dynamics to be readily identified and their sensitivity to model parameters assessed. Among these studies, only *McCreary and Lu* [1994] obtained solutions in a closed basin, allowing the existence of a complete STC. Here, then, we focus on results from that paper.

As noted here and discussed in greater detail in Sections 3–5, similar dynamics appear to be at work both in the real ocean and in solutions to oceanic GCMs. Also see *Liu et al.* [1994] for a discussion of basic STC properties from a GCM perspective.

2.1. Model Overview

The model equations are

$$f\mathbf{k}\times\mathbf{v}_i + \nabla p_i = \delta_{1i}\tau^x(y)\mathbf{i}/h_i,$$
$$\nabla\cdot(h_i\mathbf{v}_i) = -(-1)^i w_1, \qquad (1)$$

where i=1,2 is a layer index, h_i and $\mathbf{v}_i = (u_i, v_i)$ are the thickness and velocity fields of layer i, the pressures are $p_1 = g'_{12}h_1 + g'_{23}h$ and $p_2 = g'_{23}h$, $h = h_1 + h_2$, $g'_{ij} = g(\rho_j - \rho_i)/\rho_o$, $\mathbf{i}$ and $\mathbf{k}$ are unit vectors in the zonal and vertical directions, and δ_{1i} is the Kronecker symbol–δ (that is, $\delta_{11} = 1$ and $\delta_{12} = 0$). Water can transfer between layers at the rate w_1, allowing for the existence of upwelling and downwelling STC branches. To allow for analytic solutions, w_1 is restricted to the values $\pm\infty$ or 0. Horizontal mixing is not explicitly included in (1), but is assumed to be present in boundary layers.

McCreary and Lu [1994] obtained analytic solutions to (1) in the rectangular basin shown in Figure 1 with $y_n = L = 50°$, subject to the constraints that h_1 and h_2 are fixed to constant values H_1 and H_2, respectively, along the eastern boundary of the basin. The solutions were forced by zonally independent wind fields, $\tau^x(y)$, with peak westerlies at 37.5°N, peak easterlies at 12.5°N, and hence a region of negative curl for 12.5°N < y < 37.5°N (as in the thick $\tau^x(y)$ curve in Figure 1).

Figure 1 also indicates the different dynamical regimes of the solution. In Region 1 ($y > y_d = 18°$), h_1 is kept fixed to H_1. In this region, then, layer 1 behaves like a constant-thickness mixed layer, in which water instantly transfers between the layers (i.e., $w_1 = \pm\infty$) in response to Ekman pumping; in particular, when $w_{ek} < 0$ water instantly subducts from layer 1 to layer 2. In Region 2 ($\delta_e < y < y_d$), no entrainment or detrainment is allowed ($w_1 = 0$), so that h_1 is allowed to adjust freely; thus, there is no subduction in the model equatorward of y_d, consistent with its observed weakening at low latitudes. In Region 3 ($y < \delta_e$), the equatorial boundary region, there is upwelling but no detrainment ($w_1 > 0$). The lines $y = y_n - \delta_n$ and $x = \delta_w$ designate edges of frictional boundary currents attached to the northern and western boundaries, respectively.

With the above specifications, the physical situation in Region 2 is essentially the same as in the *Luyten et al.* [1983] study with y_d corresponding to their "ventilation latitude," the two systems differing only in that *Luyten et al.* [1983] assumed $H_1 = 0$ (i.e., an infinitesimally thin mixed layer in Region 1). Regions 1 and 2 are the regions considered by *Liu*

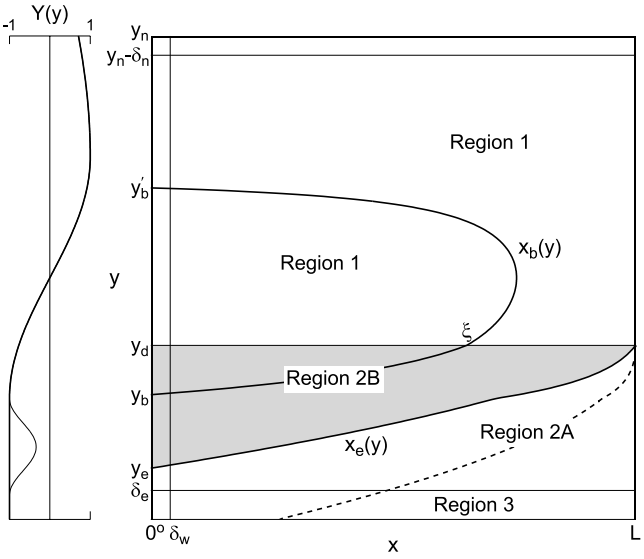

Figure 1. A schematic diagram illustrating the structure of the analytic solution of *McCreary and Lu* [1994]. Two wind profiles, $Y(y)$, are plotted at the left margin, where $\tau^x(y) = \tau_o Y(y)$ and $\tau_o = 0.6$. Parameter values for the solid x_e and x_b curves are $g'_{12} = 1.96$ cm s^{-2} and $g'_{23} = 3.675$ cm s^{-2}, $H_1 = 50$ m, and $H_2 = 200$ m, whereas for the dashed x_e curve $g'_{12} = 1.23$ cm s^{-2} and $H_2 = 150$ m.

[1994]. Regions 2 and 3 correspond to the domain considered by *Pedlosky* [1987, 1988, 1991] and *Pedlosky and Samelson* [1989], who investigated pathways by which subducted water flows to the equator to join the EUC.

2.2. STC Existence and Strength

The net upper-layer transport that flows across y_d is given by

$$M_1(y_d) = -L\frac{\tau_d^x}{f_d}\left(1 - \frac{2H_1}{D + \sqrt{D^2 - 2L\tau_d^x/g'_{23}}}\right) \qquad (2)$$

where $D = H_1 + H_2$, $\tau_d^x = \tau^x(y_d)$, and $f_d = f(y_d)$. It is determined by the Ekman drift across y_d, $-L\tau_d^x/f_d$, and by the upper-layer geostrophic flow. The geostrophic transport always tends to counteract the Ekman transport, but is never strong enough to reverse it since $\tau_d^x > 0$ and hence

$$\sqrt{D^2 - 2L\tau_d^x/g'_{23}} > D \geq H_1.$$

Indeed, for realistic parameter choices and forcing, the geostrophic contribution is relatively small so that $M_1(y_d)$ is largely determined by the Ekman transport [*McCreary and Lu*, 1994].

Because $w_1 = 0$ in Region 2, it follows from the upper-layer continuity equation that $M_1(y) = M_1(y_d)$ *everywhere* in Region

2, so that $M_1(y_d)$ measures the strength of the upper branch of the model's STC. Mass conservation also requires that the corresponding lower-layer transport is $M_2(y) = -M_1(y_d)$, so that (2) also measures the strength of the STC's lower branch. Thus, $M_1(y_d)$ is really the driving force for subsurface equatorward flow: By draining upper-layer water from the tropics, it requires a compensating subsurface flow.

It is rather surprising that $M_1(y_d)$ is determined *entirely* by properties along $y = y_d$, and does not depend on details of the forcing inside either Region 1 or Region 2. In particular, it does not depend on the strength of the wind curl in Region 1, as might be expected: If there is no change in τ_d^x, an increase (decrease) in wind curl in Region 1 only leads to a strengthening (weakening) of the Subtropical Gyre. This result clearly depends on the model property that subduction cuts off along a *single* latitude, y_d. Nevertheless, it is supported in several studies that do not adopt this restriction. For example, in *Liu and Philander's* [1995] idealized GCM solutions, STC strength is almost unchanged in solutions forced by wind fields in which the midlatitude wind curl differs by a factor of two. *Nonaka et al.* [2002] concluded that the STC strength in their GCM solutions was set by zonal winds in the bands 17.5°S < y < 7.5°S and 7.5°N < y < 22.5°N.

2.3. Subsurface Equatorward Flow

In response to negative Ekman pumping ($y \lesssim 37.5$°N), upper-layer water in Region 1 subducts into layer 2, and, according to (2), some of it is driven across y_d into Region 2. In Region 2, equation (1) can be solved for a single equation in h,

$$\overline{v}_g h_y + (\overline{u}_g - c_r) h_x = 0, \tag{3}$$

where

$$\overline{u}_g = -\frac{1}{h}\Psi_y, \quad \overline{v}_g = \frac{1}{h}\left(\Psi_x + \frac{\tau^x}{f}\right) = \frac{f}{h\beta} w_{ek}, \tag{4}$$

are the depth-averaged, zonal and meridional geostrophic currents in both layers,

$$\Psi = (1/\beta)\int_L^x \text{curl } \tau \, dx$$

is the Sverdrup transport streamfunction, $c_r = (\beta/f^2)\ g'_{12}(h_1 h_2/h)$, and $\beta = f_y$ [*Luyten et al.*, 1983; *Luyten and Stommel*, 1986]. According to (3), isolines of h are parallel to the characteristic curves, $x_c(s)$ and $y_c(s)$, obtained by integrating the equations

$$\frac{dx_c}{ds} = \overline{u}_g - c_r, \quad \frac{dy_c}{ds} = \overline{v}_g, \tag{5}$$

where s is a time-like variable, the integration requiring that h is specified on some boundaries of the domain. Since, according to (1), isolines of h are also identifiable with geostrophic streamlines of layer-2 flow, so are the characteristics.

Region 2 is divided into two subregions, Regions 2A and 2B (Figure 1), by the lower-layer characteristic, $x_e(y)$, that emanates from the point (L, y_d),

$$x_e(y) = L - \frac{g'_{12}\beta}{f\tau_y^x - \beta\tau^x}\left(1 - \frac{f}{f_d}\right)\left[\frac{1}{2}\left(1 - \frac{f}{f_d}\right)D^2 + \frac{f}{f_d}DH_1 - \frac{1}{2}\left(1 + \frac{f}{f_d}\right)H_1^2\right]. \tag{6}$$

East of x_e (Region 2A), h is determined by its value along the eastern boundary, D, and this constant value is carried into the interior of Region 2A along characteristics. As a result, $h = D$ throughout Region 2A and there is no layer-2 flow there, the "shadow zone" of the *Luyten et al.* [1983] solution. West of x_e (Region 2B), h is specified by its value along y_d, which increases to the west since $w_e(y_d) < 0$ for the wind profiles considered here. This westward increase of h is carried into the interior of Region 2B, ensuring that there is a region of equatorward flow in layer 2 that extends well into the tropics.

McCreary and Lu [1994] obtained an expression similar to (6) for the lower-layer streamline, $x_b(y)$, that extends to the bifurcation point of the model's low-latitude western boundary current, $(0, y_b)$ (Figure 1). It divides Region 2B into two parts, with water east of x_b flowing to the equator to participate in the STC, and water west of it returning to the subtropics in the western boundary current. It also separates the subduction region in Region 1 into two parts, with only water that subducts east of x_b participating in the STC.

The interesting property of the Region-2 response is that there is *any* penetration of layer-2 water into the tropics at all. This property is entirely due to the nonlinear terms in (1), that is, the terms that involve h_i. (In a linear model, the variable thicknesses h_i in the nonlinear terms are replaced by externally specified constants H_i, typically assumed to be uniform throughout the basin.) The nonlinearities are the source of the term proportional to $\overline{v}_g$ in (3), which, according to (5), accounts for the meridional displacement of characteristics. Consistent with this result, $x_e(y)$ becomes a straight line along $y = y_d$ in the limit that the forcing, and hence the expression $\left(f\tau_y^x - \beta\tau^x\right)$ tends to zero.

2.4. Interior and Western-Boundary Pathways

In Figure 1, all of layer-2 first flows across the basin before moving to the equator in a western boundary current, but it can

also flow to the equator in the interior ocean. The equatorial limit of (6) is,

$$x_e(0) = L + \frac{g'_{12}}{2\tau^x(0)} H_2(H_2 + 2H_1), \quad (7)$$

which is well defined even though the equator lies outside the range of validity of (1). Since there are no lower-layer currents in Region 2A, a necessary condition for lower-layer water to flow to the equator in the interior ocean is that $x_e(0) > 0$, that is, the shadow-zone boundary intersects the equator.

The value of $x_e(0)$ can be positive or negative for realistic parameter choices, with $x_e(0)$ being positive for larger L and $|\tau^x(0)|$ and smaller g'_{12} and H_2 (as in the dashed curve in Figure 1). The dependency on L suggests that the existence of an interior pathway is more likely in the Pacific Ocean than the Atlantic. The dependency on the latter two parameters suggests that, in the real ocean, water from shallower thermocline levels is more likely to move to the equator in the interior ocean. As we shall see, these dependencies are consistent with both observed and modelled properties (Sections 3–5).

Provided there is an Intertropical Convergence Zone (ITCZ, as in the thin τ^x curve in Figure 1), however, the inequality $x_e(0) > 0$ is not a sufficient condition for the existence of an interior pathway. If the ITCZ is sufficiently weak, $x_e(y)$ first bends more sharply to the west on the northern flank of the ITCZ where $|w_{ek}|$ is small, and then bends back to the east on the southern flank where it is large. If the ITCZ is sufficiently strong, $x_e(y)$ intersects the western boundary *before* it can loop back, and so layer-2 flow follows the western-boundary pathway to the equator even though $x_e(y) > 0$. If the ITCZ is strong enough for $w_{ek} > 0$, then no interior pathway is possible.

The idea of the ITCZ being a barrier for equatorward flow in the Pacific Ocean was discussed by *Lu and McCreary* [1995], since in their solution to a $2^1/_2$-layer model the interior pathway was completely eliminated by the ITCZ. As discussed in Section 3, however, interior pathways exist at shallow levels in GCM solutions [*Liu et al.*, 1994; *Blanke and Raynaud*, 1997; *Rothstein et al.*, 1998]. *Liu and Huang* [1998] suggested that the lack of an interior pathway in the *Lu and McCreary* [1995] solution was their value of H_2 being somewhat too thick, an idea supported by *Lu et al.* [1998; see Figure 7].

3. PACIFIC OCEAN

The STCs have been better documented and quantified in the Pacific Ocean than in the other two oceans, mainly because their equatorward branches are located within the region occupied by the ENSO signal, which is relatively well sampled by moored arrays and repeat shipboard sections. In this section (and in Sections 4 and 5 as well), we first describe key properties of the wind field that drives the STCs, then review observations of their individual (subduction, equatorward, upwelling, and poleward) branches, and conclude with a discussion of several modeling studies designed to simulate them.

3.1. Wind-stress Fields and Ekman Transport Divergences

The annual-mean wind-stress field from the NCEP reanalysis (Figure 2a) shows the tradewind circulations in each hemisphere with the ITCZ just north of the equator. A band of positive (or weakened negative) Ekman pumping, w_{ek} = curl (τ/f) (Figure 2b) associated with these winds extends across the interior ocean under the ITCZ. As discussed in Section 2.4 and below, it acts to inhibit the possible interior STC pathways in the northern hemisphere. Note, however, that values of w_{ek} remain negative within the band from about the dateline to 140°W, providing a "window" for the existence of interior pathways; details of the window depend on the wind-stress climatology used, but it is always there. In the southern hemisphere, there is no region of positive w_{ek} in the eastern and central ocean, allowing the possibility for interior pathways over a broader longitudinal range. On the other hand, details of the curl structure and its role for STC pathways are still evolving. For example, *Kessler et al.* [2003] recently derived w_{ek} near the equator on a finer scale from scatterometer winds, finding a conspicuous band of positive w_{ek} along about 1°N between 150–100°W; the presence of this band results in a more realistic Sverdrup circulation than for existing wind-stress and reanalysis products, yielding a stronger EUC and northern branch of the South Equatorial Current (SEC).

As discussed in Section 2.2, the STCs are forced by the poleward transport of near-surface, equatorial waters across the latitudes where subduction cuts off in each hemisphere, roughly the equatorward boundaries of the Subtropical Gyres; moreover, that divergence is composed primarily of Ekman transport. The location of the subduction cut-off latitudes is not precisely known in the real ocean. They must be chosen poleward of the Tropical Cell convergence, about 4–6° north and south of the equator, and we define them here to be 10°N/10°S.

The annual-mean value of the poleward NCEP Ekman transports divergence across these latitudes is 54 Sv (and similarly, 58 Sv for the ERS-1,2 scatterometer stresses), providing an estimate of the upper limit for equatorial upwelling discussed next. The longitudinal distribution of the meridional Ekman transports along 10°N has its maximum contribution to the total divergence in the center of the basin, while at 10°S the maximum southward contributions are further to the east, as shown in Figure 2b.

The area integral of positive w_{ek} in Figure 2b in the region $x > 100$°W, 5°N > $y > 20$°N plus the line integral of offshore

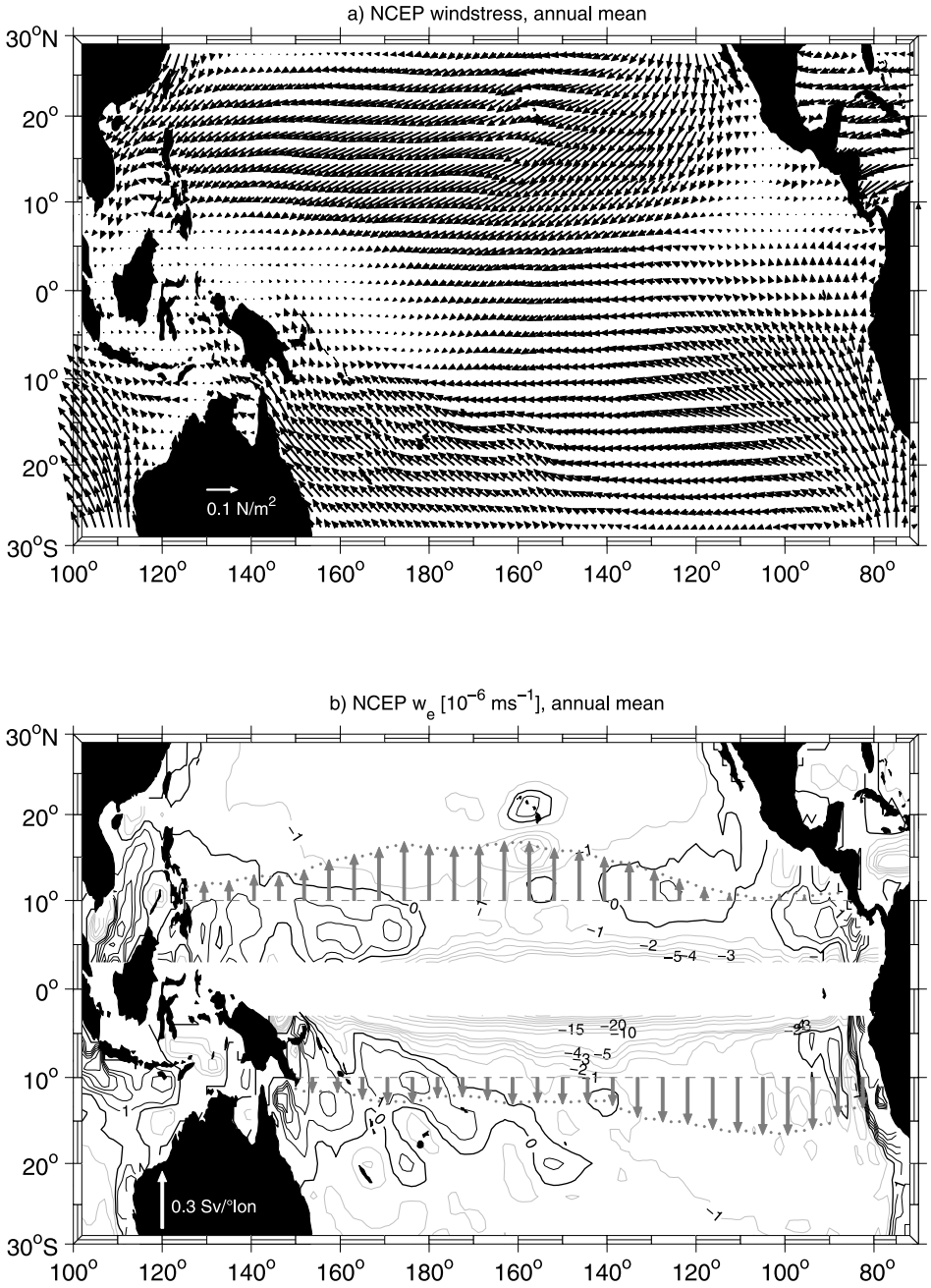

Figure 2. a) Mean wind stress and b) Ekman pumping (outside ± 3° latitude belt) for Pacific from NCEP reanalysis 1990-1999; also shown are meridional Ekman transports (vector at lower left = 0.3 Sv/degree longitude) across 10°N and 10°S.

Ekman transport along the coast, is 2.2 Sv, providing an upper limit for off-equatorial upwelling in the Costa Rica Dome. Similarly, the area integral of positive w_{ek} for $x > 85°W$, $20°S > y > 5°S$ plus the coastal Ekman divergence driven by the alongshore winds is 7.7 Sv, yielding a total eastern boundary Ekman divergence of about 10 Sv. Some amount of this eastern upwelling occurs within the 10ºS to 10ºN latitude range and thus contributes to the Ekman divergence across 10°N/10°S; thus, this amount must be subtracted from the 10°N/10°S divergence to estimate open-ocean equatorial upwelling.

The variations of the Ekman divergence across 10°N and 10°S for the Pacific (Plate 1) shows variations of about 5 Sv amplitude at interannual and longer timescales, which do not

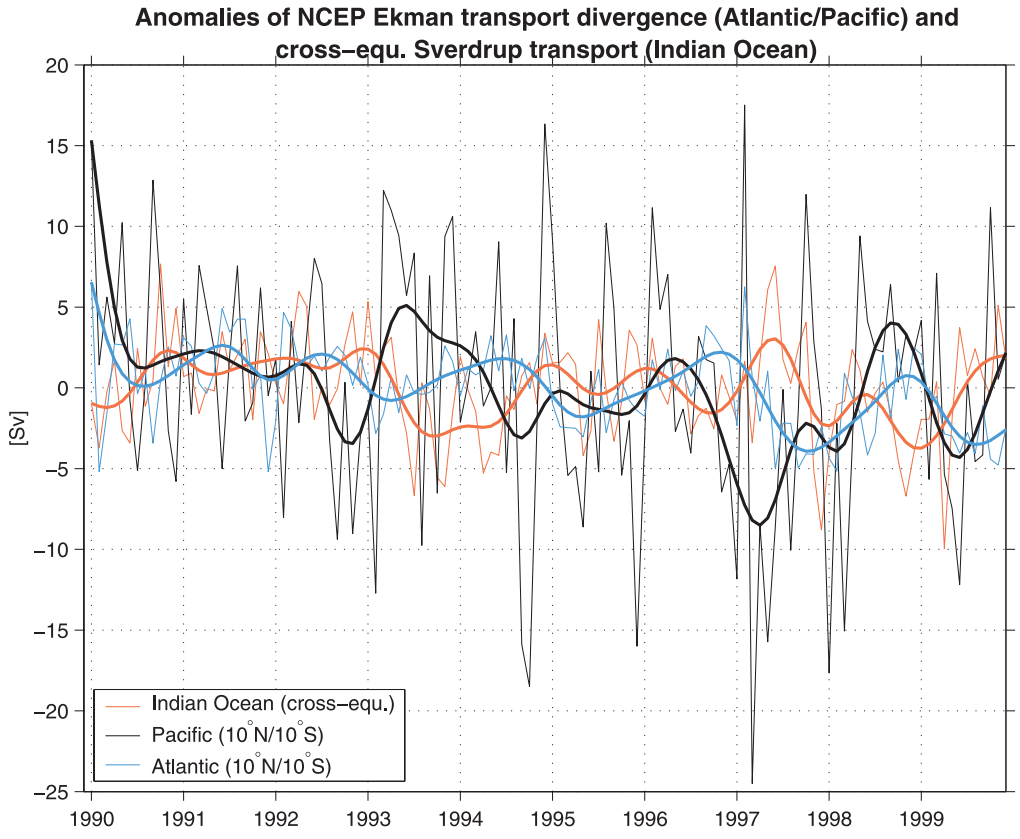

Plate 1. Time series 1990–1999 of equatorial Ekman transport divergence (in Sv) for the Pacific (black) and Atlantic (blue), calculated for the band 10°S–10°N and coast to coast, and of cross-equatorial Sverdrup transport for the Indian Ocean (red) from NCEP reanalysis wind stresses. Thin curves are for monthly means, heavy curves for low-passed interannual variability.

occur in any obvious association with El Niño/La Niña events; however, if the divergence is calculated closer to the equator, at 3°N/3°S say, a relationship to ENSO appears (see Section 6).

3.2. Observations

For convenience, we organize the discussion in this section to follow the subsurface branch of the North and South STCs from their sources (subduction) to their sinks (upwelling). We conclude by noting key properties of their surface return flows.

3.2.1. Subduction. Estimating subduction rates is an involved process that requires knowledge of oceanic density structure and air-sea fluxes, and these estimates have been limited to the annual mean [*Marshall et al.*, 1993]. Analyses suggest that subduction rates are fairly high in a band across the subtropical North Pacific, but highest in the west [*Qiu and Huang*, 1995]. These high subduction rates lead to an enhanced presence of certain density classes within the pycnocline, namely, regions of reduced stratification known as "mode waters".The most eastward and equatorward of these mode waters [*Hautala and Roemmich*, 1998] are the ones that flow westward and equatorward to participate in the STCs. Using *Hellermann and Rosenstein* [1983] wind stresses and hydrographic climatology from *Levitus* [1982], *Qiu and Huang* [1995] estimated a total subduction of 35 Sv for the North Pacific. By calculating geostrophic pathways of the subducted waters, they showed that most of the subducted water returns northward through the NEC (north of the bifurcation in the Mindanao Current) and then via the Kuroshio, but the authors did not estimate the southward transfer into the STC.

In the South Pacific, the highest subduction rates are at the equatorward and eastward edges of the subtropics, extending even into the tropics [*Huang and Qiu*, 1998; *Karstensen and Quadfasel*, 2002], and they are associated with a prominent low-latitude mode water [*Wong and Johnson*, 2003]. Using the mean hydrographic data base of *Levitus and Boyer* [1994a,b] and Southampton Oceanographic Center (SOC) air-sea fluxes, *Karstensen and Quadfasel* [2002] determined a total water-mass formation of 44 Sv for the South Pacific. Of this total, 27 Sv are inserted into densities lighter than 26.5 kg m^{-3} that can participate in tropical upwelling (Section 3.2.4). How much of this subduction reaches the East Australian Current and turns southward versus how much enters the STC has not been estimated.

3.2.2. Subsurface equatorward flow.

3.2.2.1. Western-boundary pathways: In the South Pacific, subsurface waters flow to the equator in the New Guinea Coastal Undercurrent (NGCU). Water flows to the NGCU primarily through two channels: the Vitiaz Strait between Papua New Guinea and New Britain, and the St. Georges Channel between New Britain and New Ireland [*Butt and Lindstrom*, 1994]. The inverse model result of *Sloyan et al.* [2003] yielded a transport of 14.7±1.5 Sv westward for the NGUC. They further concluded that the NGUC overshoots the equator and retroflects back southeastward to supply the EUC (Plate 2), as suggested earlier by *Tsuchiya et al.* [1989]. At 143°E, the EUC transport in the density range 25.5 kg $m^{-3} < \sigma_\theta < 26.3$ kg m^{-3} essentially balances with the NGUC supply.

In the northern hemisphere, the Mindanao Current (MC) flows southward along the Philippine Islands. Analysis of eight CTD/ADCP surveys off Mindanao along 8°N [*Wijffels et al.*, 1995] showed a southward MC transport of 23±4 Sv above $\sigma_\theta = 26.7$ kg m^{-3} (around 350 m); 15 Sv of this transport falls into the density range $\sigma_\theta = 23$–26.2 kg m^{-3} [*Liu and Philander*, 2001] and is used here in our schematic diagram (Plate 2). Just south of Mindanao (about 5°N), 9±3 Sv of the MC flows into the Celebes Basin to provide much of the water for the ITF [*Gordon et al.*, 1999], the rest (14±5 Sv) turning east to feed the NECC and eventually joining the EUC (*Johnson and McPhaden* [1999]; Plate 2). It is not likely that all of this water reaches the EUC, however, as some of the denser MC waters contribute a relatively fresh signature that is advected eastward in the northern part of the NSCC [*Johnson and McPhaden*, 1999], which itself carries about 7 Sv across 165°E [*Sloyan et al.*, 2003], and some of the lighter MC waters are too light to supply the EUC.

3.2.2.2. Interior pathways: While there are substantial difference between different wind stress products [*Kessler et al.*, 2003], the possibility of an interior pathway is allowed by the property that w_{ek} remains generally negative in the central Pacific (Figure 2b). Such pathways with interior flow to the equator in the northern hemisphere were first suggested by tracer studies [*Fine et al.*, 1987]. Moreover, distributions of salinity, acceleration potential, and potential vorticity (Figure 3) all point toward the presence of a circuitous, southward, interior flow, with a strong westward component north of the ITCZ in the North Equatorial Current (NEC), an eastward component in latitude band of the NECC, and westward flow in the northern branch of the SEC. By contrast, southern-hemisphere distributions all show a direct northwestward route toward the equator within the southern branch of the SEC.

From historical CTD data, *Johnson and McPhaden* [1999] estimated the relative contributions of the equatorward geostrophic flows in the interior ocean above a neutral density of about γ_n = 26 kg m^{-3} to be 5±1 Sv and 15±3 Sv in the North and South Pacific, respectively (Figure 4). In that study, the bulk of the equatorward thermocline transport

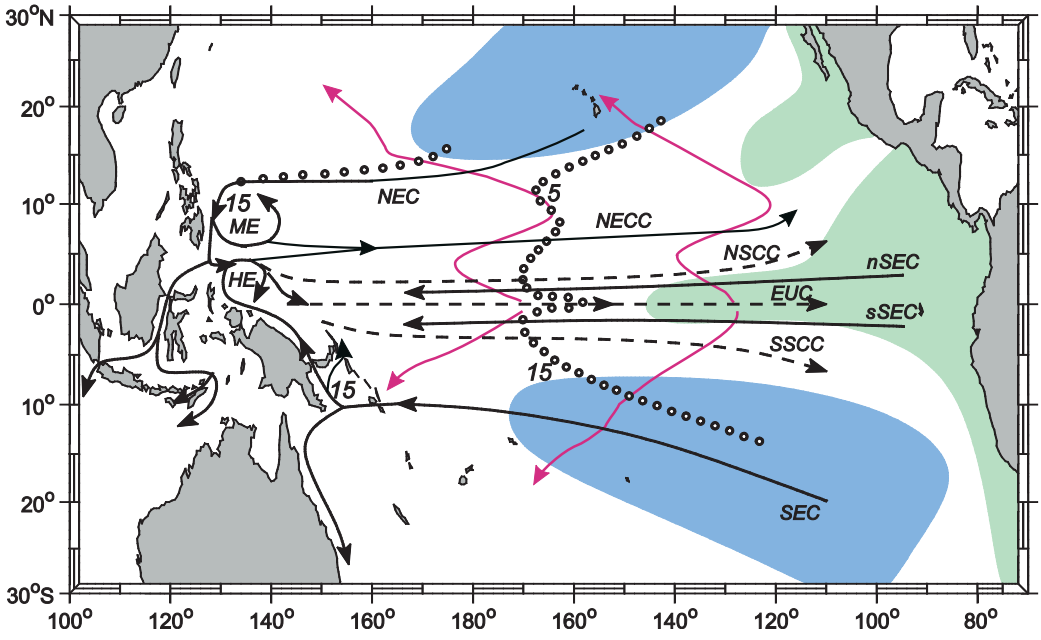

Plate 2. Schematic representation of the Pacific circulation branches, subduction (blue) and upwelling (green) zones that participate in the STC. Current branches participating in STC flows are NEC = North Equatorial Current; nSEC, sSEC = South Equatorial Current north and south of the equator; NECC = North Equatorial Countercurrent; EUC = Equatorial Undercurrent; NSCC, SSCC = North and South Subsurface Countercurrent; ME = Mindanao Eddy; HE = Halmahera Eddy. Interior equatorward thermocline pathways dotted, with interior equatorward transport estimates (in Sv) marked; selected surface poleward pathways for the central basin (from Figure 6) marked by thin, magenta lines; see text for details.

across 7°S occurs from 160–90°W, whereas the flow between the NEC and the NECC is distributed from 130–180°W (Figure 4). Near-equatorial pathways, however, apparently shift further westward in both hemispheres before merging into the EUC (Plate 2). *Sloyan et al.* [2003] obtained equatorward transports for the density range σ_θ = 23.0–26.3 kg m^{-3}, finding 5.8 Sv across 8°N from 156°E–170°W and 13.6 Sv across 8°S from 170–95°W, confirming the earlier estimates. These results show that about half of the total equatorial Pacific upwelling is supplied by interior meridional flows at the upper thermocline.

3.2.3. Equatorial currents

3.2.3.1. EUC: The EUC shoals from a core depth of 200 m at 143°E to 80 m at 110°W (Figure 5; *Johnson et al.* [2002]). At the western end, across 156°E, its transport is estimated to be 19.8±1.1 Sv. It attains its maximum transport of 30.5±2.0 Sv in the eastern central Pacific at 125°W, and then drops to 16.2±1.9 Sv at 95°E [*Sloyan et al.*, 2003]. Most of its transport is upwelled before it reaches the eastern boundary, but some likely feeds into the Peru-Chile Undercurrent [*Lukas*, 1986].

3.2.3.2. NSCC and SSCC: The North and South Subsurface Countercurrents (NSCC, SSCC) flow eastward in the density range 26.3 kg m^{-3} < σ_θ < 26.9 kg m^{-3} in the western and central equatorial Pacific so that they are located underneath the interior equatorward flow discussed above, but rise across isopycnals on their way east (Figure 5). They are supplied mostly from western boundary currents. In the east, they likely supply water for the off-equatorial upwelling regions along the South American coast and in the Costa Rica Dome. Thus, they should probably be viewed as a deep branch of the STC system. Connections with westward-flowing tropical currents in this density range have also been suggested [*Rowe et al.*, 2000].

The pathways of the subsurface countercurrents shift polewards toward the east (Figure 5; *Rowe et al.* [2000]), as discussed kinematically by *Johnson and Moore* [1997] and dynamically by *McCreary et al.* [2002]. The SSCC transport was estimated to be 6.7±2.2 Sv at 165ºE with its core at 2.5°S, and 6.1±1.9 Sv at 110°W with its core at 5.5°S, with a suggestion of a reduction to 3.8±2.4 Sv at 95°W due to upwelling across the σ_θ = 26.3 kg m^{-3} isopycnal [*Rowe et al.*, 2000; *Sloyan et al.*, 2003]. The NSCC has similar strength, with a transport of 7.6±1.7 Sv at 165°E centered near 2.5°N and 6.4±2.2 Sv at 110°W near 4.5°N. In contrast to the SSCC, the NSCC is only slightly weakened at 95°W, perhaps indicating a larger role of the NSCC for supplying eastern Pacific upwelling.

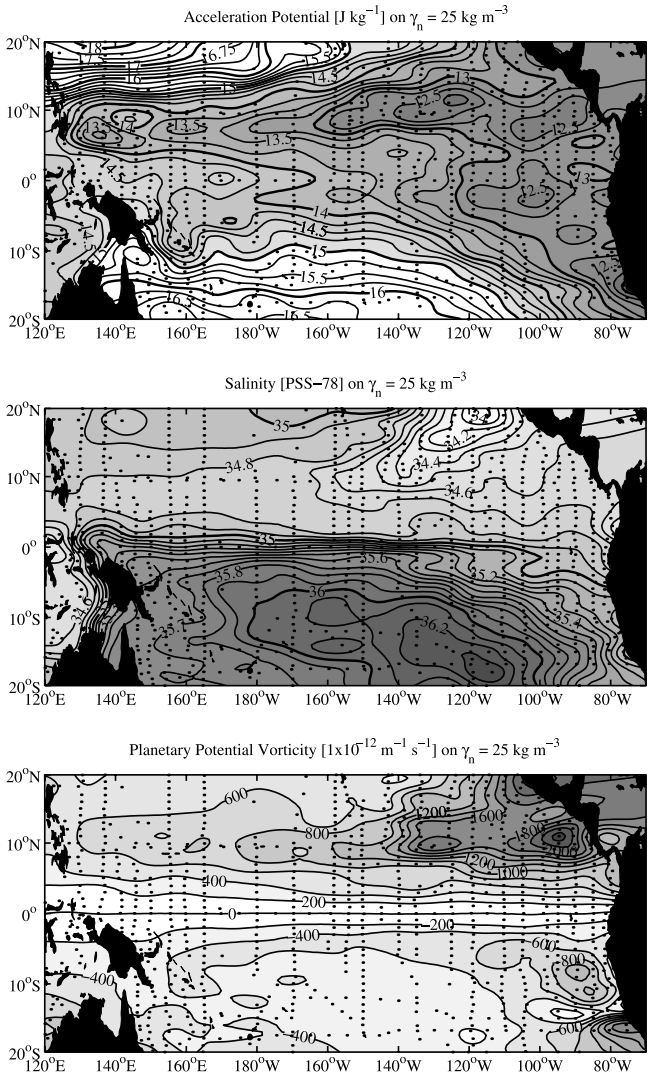

Figure 3. Objective maps of properties on γ_n = 25.0 kg m^{-3}, within the tropical Pacific pycnocline made from binned mean hydrographic profiles (dots), a) acceleration potential relative to 900 db, contour intervals of 0.25 J kg^{-1}; b) salinity, contour intervals of 0.1; c) planetary potential vorticity, contour intervals of 200×10^{-12} m^{-1}s^{-1}. (After *Johnson and McPhaden* [2001].)

3.2.3.3. Tropical cells: Analysis of shipboard sections from 95–170°W taken during the 1990's, mostly during maintenance of the Tropical Atmosphere Ocean (TAO) project [*McPhaden et al.*, 1998] moorings, shows equatorward subsurface flow beneath poleward near-surface Ekman flow, the latter with off-equatorial convergence occurring mostly in the NECC about 7°N [*Johnson et al.*, 2001]. Drifter data suggest a more symmetric off-equatorial convergence with maxima near ±4º having an amplitude about half that of the equatorial divergence [*Johnson*, 2001]. In their inverse model study, *Sloyan et al.* [2003] estimated the overall strength of the TCs

to be 15±13 Sv and 20±11 Sv for the northern and southern TCs, respectively. This diverse evidence of off-equatorial convergence likely indicates the downwelling limbs of the Tropical Cells predicted by models (e.g., *Stommel* [1960]; *Philander and Pacanowski* [1980]; *McCreary* [1985]; *Liu et al.* [1994]; *McCreary and Lu* [1994]). The existence of the TCs implies that the strengths of the STCs' poleward branches need to be evaluated at least poleward of the TC convergences.

3.2.4. Upwelling. The existence of annual-mean equatorial easterlies ensures that most of the upwelling in the tropical ocean occurs along the equator, due to the strong Ekman divergence there. Some water also upwells along the coast of Peru, and there is potential for upwelling in the Costa Rica Dome where thermocline, and even subthermocline, waters are brought very close to the surface.

3.2.4.1. Source depth of upwelled waters: From tracers (^{14}C and CO_2) incorporated into a box model, *Quay et al.* [1983] set an upper limit for the density of water that upwells along the equator to be $\sigma_\theta = 26.5$ kg m^{-3} (a depth of about 225 m). In their recent inverse model study, *Sloyan et al.* [2003] merged CTD data and mean zonal currents from shipboard ADCP data [*Johnson et al.*, 2002] with air-sea flux estimates to obtain a consistent picture of the equatorial Pacific circulation and upwelling. They determined for the central equatorial Pacific that diapycnal upwelling existed only for $\sigma_\theta < 24.0$ kg m^{-3}, with upward velocities in the depth range 100–200 m occurring mostly along isopycnals. For the eastern equatorial Pacific, however, some diapycnal upwelling was found across isopycnals as dense as $\sigma_\theta = 26.3$ kg m^{-3}, corresponding to a depth of about 200 m.

3.2.4.2. Equatorial upwelling: Estimates of upwelling transports for the zonally sloping EUC differ widely depending on whether they are determined across horizontal or isopycnal surfaces. *Wyrtki* [1981] made an early calculation of the upwelling transport across 50 m in an equatorial box extending from 170°E to 100°W and from 5°S to 5°N. Based on estimates of the horizontal-transport convergence across the sides of the box (determined from existing equatorial current measurements, geostrophy, and net Ekman divergence), he reported a range of estimates for the upwelling transport with 51 Sv being his preferred value. *Bryden and Brady* [1985] carried out a similar analysis in a smaller box from 110–140°W for the same latitude range, determining an upwelling transport of 22 Sv across 62.5 m. They also noted that because the thermocline and EUC shoal toward the east, only 7 Sv of that amount actually crossed 23ºC to upwell into the surface layer.

Meinen et al. [2001] determined equatorial upwelling and its variability (see Section 6.1.1) across 50 m in an equatorial

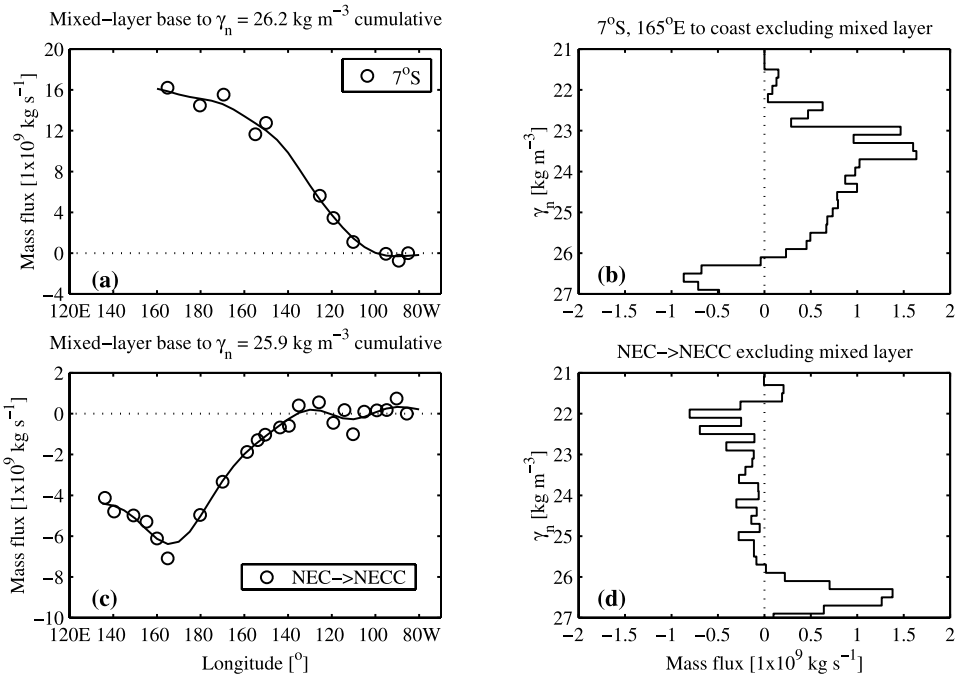

Figure 4. Quasi-meridional interior pycnocline (mixed-layer base to pycnocline base) mass transport (10^9 kg s^{-1}) zonally accumulated from the Americas westward at (a) 7°S and (c) between the North Equatorial Current (NEC) and North Equatorial Countercurrent (NECC) in the Pacific Ocean. The same quantity summed in 0.1 kg m^{-3} γ_n bins at (b) 7°S from 165°E to the Americas and (d) between the NEC and NECC from 135°E to the Americas. (After *Johnson and McPhaden* [1999].)

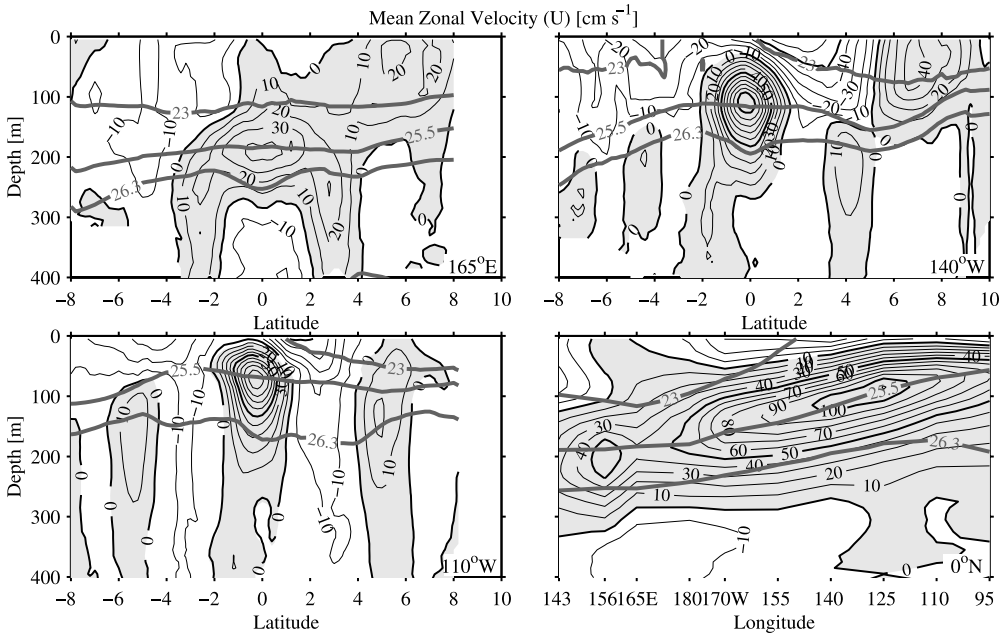

Figure 5. Sections of mean zonal velocity, estimated at 3 different longitudes and along the equator in the Pacific Ocean. Locations marked in the bottom right corner of each section. Contour interval is 10 cm s^{-1}, with enhanced contours at 50 cm s^{-1} intervals; eastward velocities are shaded. Heavy lines correspond to isopycnal surfaces σ_θ = 23.0, 25.5 and 26.3 kg m^{-3} (After Johnson *et al.* [2002].)

box extending from 5°S to 5°N and from 155°E to 95°W. They estimated the upwelling transport by the horizontal transport divergence out of the box, utilizing TAO-mooring and shipboard data, and applying geostrophy and Ekman dynamics. *Meinen et al.* [2001] obtained 24±3 Sv of upwelling across 50 m for that box. Cross-isopycnal transports were significantly smaller, 15 Sv across the 24°C isotherm. The inverse calculation of *Sloyan et al.* [2003] yielded 24±4 Sv of upwelling across the σ_θ = 23.0 kg m^{-3} isopycnal surface in the central Pacific (2°S–2°N, 170–125°W) and 13±4 Sv across σ_θ = 24.0 kg m^{-3} in the eastern equatorial Pacific (125–95°W). A direct velocity-based upwelling estimate [*Johnson et al.*, 2001] is larger than all of these box model estimates, but arguably more uncertain.

3.2.4.3. Peru-Chile coastal upwelling: The EUC surfaces in the east and what remains of it at the Galapagos Islands turns southeastward toward the west coast of South America [*Lukas*, 1986]. It then presumably feeds the poleward-flowing Peru-Chile Undercurrent (PCUC), but conclusive evidence supporting a continuity between these currents has not been provided yet. The PCUC transport at 10°S has been estimated from several hydrographic sections to be 1 Sv, sufficient to supply the coastal upwelling to at least 15°S [*Huyer et al.*, 1991]. This estimate is considerably smaller than the Ekman transport-derived upper bounds mentioned previously for the region. On the other hand, water properties of the PCUC [*Blanco et al.*, 2001] suggest that its source may just as likely be the SSCC, which could reach the eastern boundary south of 10°S.

3.2.4.4. Costa Rica Dome upwelling: Finally, the Costa Rica Dome (near 89°W, 9°N) provides another possible location for upwelling. The top of an extremely sharp thermocline is often located within 10 m of the sea surface within this dome [*Wyrtki*, 1964]. Relative to surrounding waters, surface waters within the dome are slightly cooler, saltier, undersaturated in oxygen, and nutrient-rich, all properties indicative of upwelling. A recent analysis yielded an upwelling transport of about 3.5 Sv [*Kessler*, 2002]. *Johnson and McPhaden* [1999] speculated that Costa Rica Dome upwelling might be associated with northward flow of the NSCC, and *Kessler* [2002] built a stronger case for this connection (see Plate 2). *McCreary et al.* [2002] provided theoretical justification for the idea.

3.2.5. Poleward surface flow. Surface drifter trajectories (Figure 6) clearly show the poleward component of the Ekman flow driven by the easterly trade winds in both hemispheres [*Reverdin et al.*, 1994; *Johnson*, 2001]. The poleward Ekman flows are superimposed on the geostrophic currents, which are predominantly zonal and, except for the NECC and the weaker SECC (not shown in Plate 2), are directed westward.

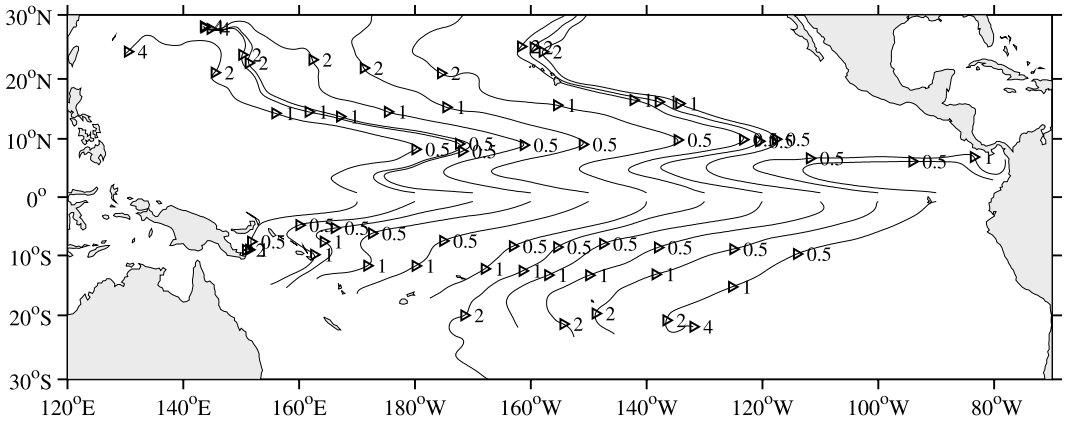

Figure 6. Near-surface trajectories calculated from mean surface drifter velocities; numbers are mean time in years to reach the location from starting points at ±0.75° latitude from equator. (From *Johnson* [2001].)

Shipboard ADCP data give some indication of the vertical distribution of poleward Ekman flow, and it appears that these flows reach below the mixed layer [*Johnson et al.*, 2001].

Interestingly, most of the trajectories for the surface flow reach the subtropics in the western half of the basin (*Johnson* [2001]; Figure 6). Since subduction of the water that participates in the STCs occurs predominantly in the eastern subtropics, there is not an obvious direct and complete closure of the surface and subsurface STC branches within the subtropics (Plate 2), suggesting that the STCs are linked to circulations farther poleward. See *McCreary and Lu* [1994], *Liu et al.* [1994], and *Lu et al.* [1998] for discussions of these linkages in ocean models; in particular, the latter two studies note the interaction of the North Pacific STC with the Subpolar Cell (SPC), a shallow overturning circulation that connects the subtropical and subpolar oceans. In the eastern basin, where the EUC and off-equatorial undercurrents surface, the drifters can also travel eastward (Figure 6).

A cautionary note has to be added here regarding drifter representations of particle pathways for the waters that are upwelled at the equator. Real water parcel followers would have to downwell partially at the TC convergence and thus be removed from the poleward Ekman transports for some time, thereby extending further westward than indicated by the trajectories of Figure 6 or Plate 2.

3.3. Models

A number of modeling studies have investigated the Pacific STCs. Here, we briefly summarize four of them [*Lu et al.*, 1998; *Blanke and Raynaud*, 1997; *Rothstein et al.*, 1998; *Huang and Liu*, 1999] that span a variety of model types. The solutions all capture the overall STC structure, but differ in the strength and location of interior pathways. None of the solutions reproduces the subsurface countercurrents at 3–5° latitude. This shortcoming may not be significant for understanding STCs, however, since the observed equatorward thermocline flow appears to mostly pass over them, but more research on the subject is needed.

Lu et al. [1998] obtained solutions to a $3^1/_2$-layer model, the three active layers representing tropical, thermocline, and upper-intermediate (subthermocline) waters. As for the simpler layer model discussed in Section 2, water is allowed to transfer between layers to parameterize the processes of upwelling, subduction, and diapycnal mixing, and subduction is cut off equatorward of 18°S and 18°N. Solutions are forced by climatological annual-mean winds and by the ITF, which is prescribed as an outflow of 10 Sv from layers 1 and 2 along the western boundary from 1–6°N and a compensating inflow into layer 3 across the open southern boundary.

Figure 7 plots the $\mathbf{v}_2$ field from their main-run solution, together with a number of streamlines that divide the flow field into several subregions and shaded areas indicating where water subducts from layer 1 into layer 2. Streamlines Sz and Bi correspond to the shadow-zone and bifurcation streamlines, x_e and x_b, in Section 2, and the others are defined in the caption to Figure 7. The fate of subducted water varies considerably depending on where it subducts. Only the water that subducts in the two darkest-shaded regions in each hemisphere flows to the equator to join the EUC and, hence, to participate in the STCs.

The layer-3 water imported into the South Pacific first recirculates within the deepest portion of the South Pacific Subtropical Gyre, and then flows north to the equator in a western-boundary current, consistent with the observed flow of subthermocline water. Most of it turns eastward to flow along the equator as the deepest part of the EUC, where it upwells into layers 2 and 1 in the central and eastern oceans. The addition of this water, together with the draining of water

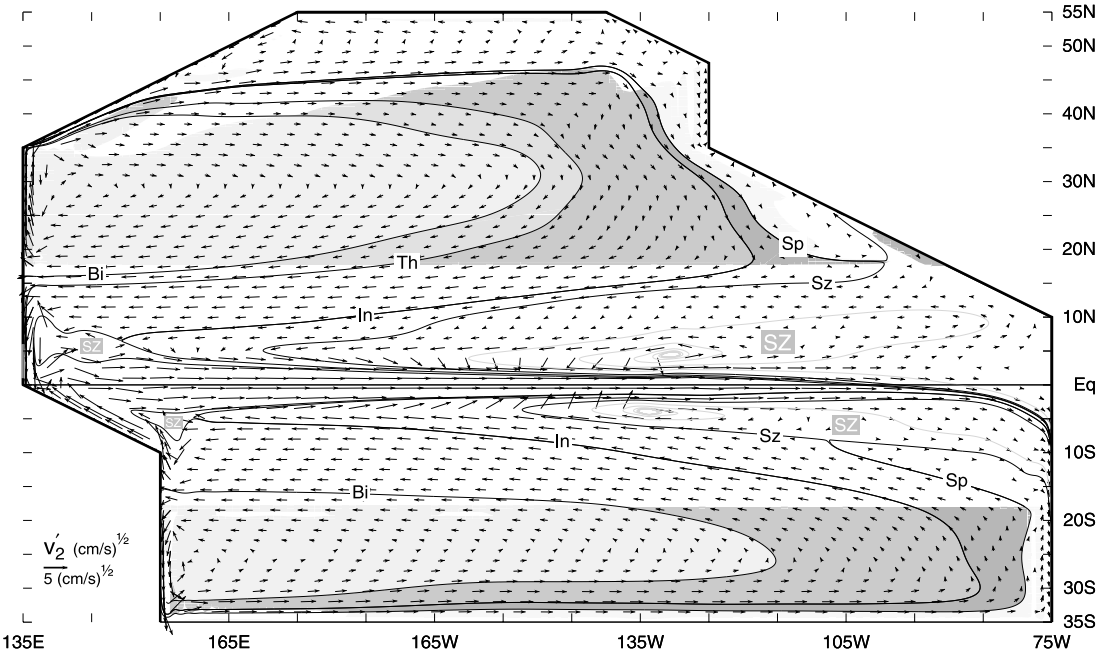

Figure 7. STC-circulation in the $3^1/_2$-layer model of *Lu et al.* [1998]. Horizontal distributions of $\mathbf{v}_2$ with regions where $w_s \neq 0$ shaded. Current arrows are of the vector field $\mathbf{v}'_i = \mathbf{v}_i / |\mathbf{v}_i|^{\frac{1}{2}}$, which has the same direction as $\mathbf{v}_i$ but an amplitude of $|\mathbf{v}_i|^2$; this modification enhances the strength of weak flows relative to stronger ones, allowing them to be more visible in each plot. The shading indicates where layer-1 water subducts into layer 2. The flow field is divided into subregions by streamlines of $\mathbf{v}_2$. Streamline Sp defines the southern boundary of the Subpolar Gyre in layer 2. Streamlines Sz and Bi correspond to the shadow-zone and bifurcation streamlines, x_e and x_b, in Section 2. Streamline In bifurcates in the western basin at 150°E, 6°N, with one branch extending on to the western boundary. Streamline Th intersects the western boundary at the southern edge of the Indonesian passage, so that water between streamlines Th and Bi leaves the basin in the throughflow region. Analogous streamlines are also plotted in the southern hemisphere (the throughflow streamline only existing in the northern hemisphere).

from layers 1 and 2 by the ITF, ensures that the EUC is composed mostly of water of southern-hemisphere origin (63%). In a subsequent study with a different parameterization of layer-2 entrainment, *McCreary et al.* [2002] concluded that the layer-3 equatorial branch upwells rather in the Costa Rica Dome and along the Peruvian coast, thereby generating the NSCC and SSCC, respectively.

Blanke and Raynaud [1997] investigated the sources and sinks of the Pacific EUC, using an OGCM with 30 vertical levels (a 10-m resolution in the top 150 m) and a horizontal resolution of 0.33° near the equator, decreasing to 1.5° poleward of ±47º. The model was forced by *Hellermann and Rosenstein* [1983] wind stresses and *Esbensen and Kushnir* [1981] heat fluxes, and salinity was relaxed to the *Levitus* [1982] surface climatology. There was, however, no explicit representation of the ITF. Pathways of water parcels backtracked from the central equatorial Pacific show source regions for EUC water similar to those discussed in previous sections. Particles reach the EUC via the equatorward western boundary currents but also through windows in the interior ocean via circuitous pathways with large westward excursions before reaching the equatorial interior Pacific.

Rothstein et al. [1998] studied STC pathways, using a σ-coordinate model of the Pacific domain with 11 layers in the upper ocean (roughly the top 700 m) beneath a surface mixed layer and with a horizontal resolution of 0.3° near the equator, increasing to 1° at 50° latitude. The forcing was similar to that for the *Blanke and Raynaud* [1997] study, and the model also did not include the ITF. Pathways of subsurface flow are identified by the Bernoulli function and current vectors (Figure 8). They again show a westward excursion of the equatorward thermocline flow in both hemispheres. In the northern hemisphere, only the waters that subduct in the northeastern subtropics (region III) follow pathways that extend directly to the equator in the interior ocean; the model equatorward transport across 10°N through the 140–160°E window is 3 Sv, of the same order as observational numbers quoted earlier.

Waters that subduct west of about 170°W (region I, Figure 8) do not reach the equator at all but rather bend northward

at the western boundary to remain in the subtropical gyre. Particles subducted in the central subtropical North Pacific at about 170–120°W (region II) travel to the western boundary. Almost all of them bend southward there and then eastward within the NECC to join the EUC in the central ocean. Note the existence of an additional pathway (the 12.5 isoline) that first flows to the equator and then retroflects to join the NECC. In the southern hemisphere, the lack of the ITCZ simplifies the trajectories. Subduction west of 140°W and north of 15°S reaches the EUC via the western boundary, whereas subduction from further east can supply interior pathways.

A further development in Pacific STC studies is the evaluation of the NCEP Pacific Ocean reanalysis product, in which observed temperature data are assimilated into an ocean model (*Huang and Liu* [1999]; see also *Liu and Philander* [2001]). The model has 28 vertical layers, its longitudinal resolution is 1.5°, and its meridional resolution decreases from $^1/_3$° from 10°S–10°N to 1° at midlatitudes. Forcing is by annual-mean NCEP momentum and heat fluxes. The authors presented Lagrangian trajectories obtained by releasing particles at a depth of 50 m along 24°N and 24°S in the North and South Pacific (Figs. 9a,b), confirming the existence of the exchange windows (Figs. 9c,d) discussed above.

Some of the particles released at 24°N take the western-boundary pathway to the equator. Interestingly, they do not join the EUC at the boundary, but rather travel eastward with the NECC until mid-basin and only then extend to the equator (Figure 9a). Water subducted east of about 135°W takes the interior exchange window, first travelling westward with the NEC and then eastward in the NECC before extending to the equator. Similarly, particles released at 24°S have two exchange windows. Water subducted east of about 100°W reaches the equator by the interior exchange window, and the western-boundary exchange window is supplied out of longitude range 170–100°W. Time scales for particles to reach the equatorial zone range from less than 2 years near the western boundary to 15 years in the central subtropics.

Overall, *Huang and Liu* [1999] confirm that the EUC is dominantly supplied out of the South Pacific (where the role of the ITF in comparison to observations needs to be taken into account), and they find that the southern exchange window reaches much further poleward than the northern one (Figs. 9c,d). *Huang and Liu* [1999] also calculated the meridional transports across 10°S and 10°N, obtaining values for the western boundary and northern interior thermocline transports similar to those discussed in the previous sections and marked in Plate 2. Their southern interior thermocline transport is weaker (12 Sv) than estimated from observations (15 Sv), perhaps a consequence of the model not including the ITF.

4. ATLANTIC OCEAN

Only in the western Atlantic (near 35°W) are shipboard ADCP observations sufficiently dense to be comparable to the coverage in the equatorial Pacific and hence to allow quantitative circulation estimates for the STC mean flows [*Schott*

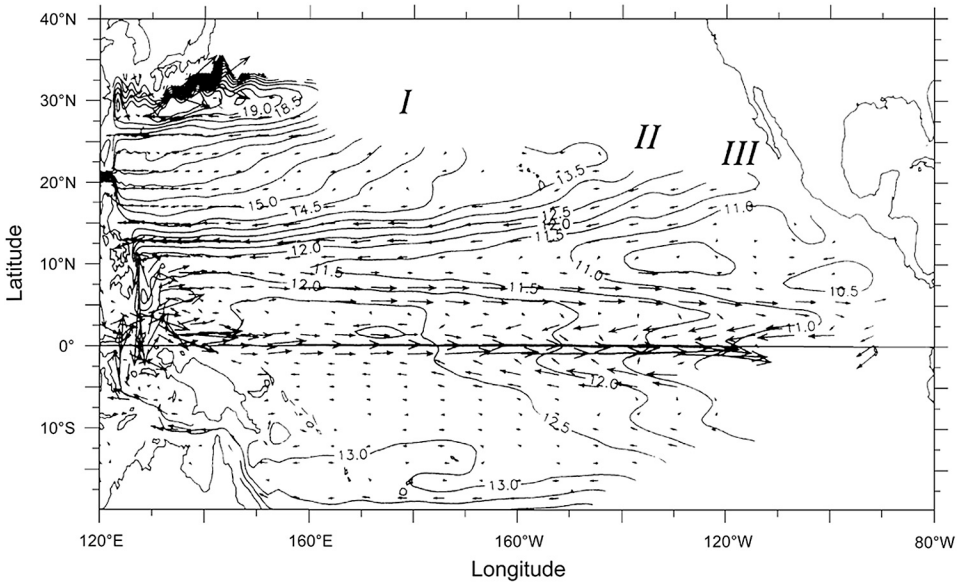

Figure 8. Bernoulli function and current vectors on isopycnal surface σ_θ = 24.0 kg m^{-3} in the *Rothstein et al.* [1998] σ-coordinate model simulation.

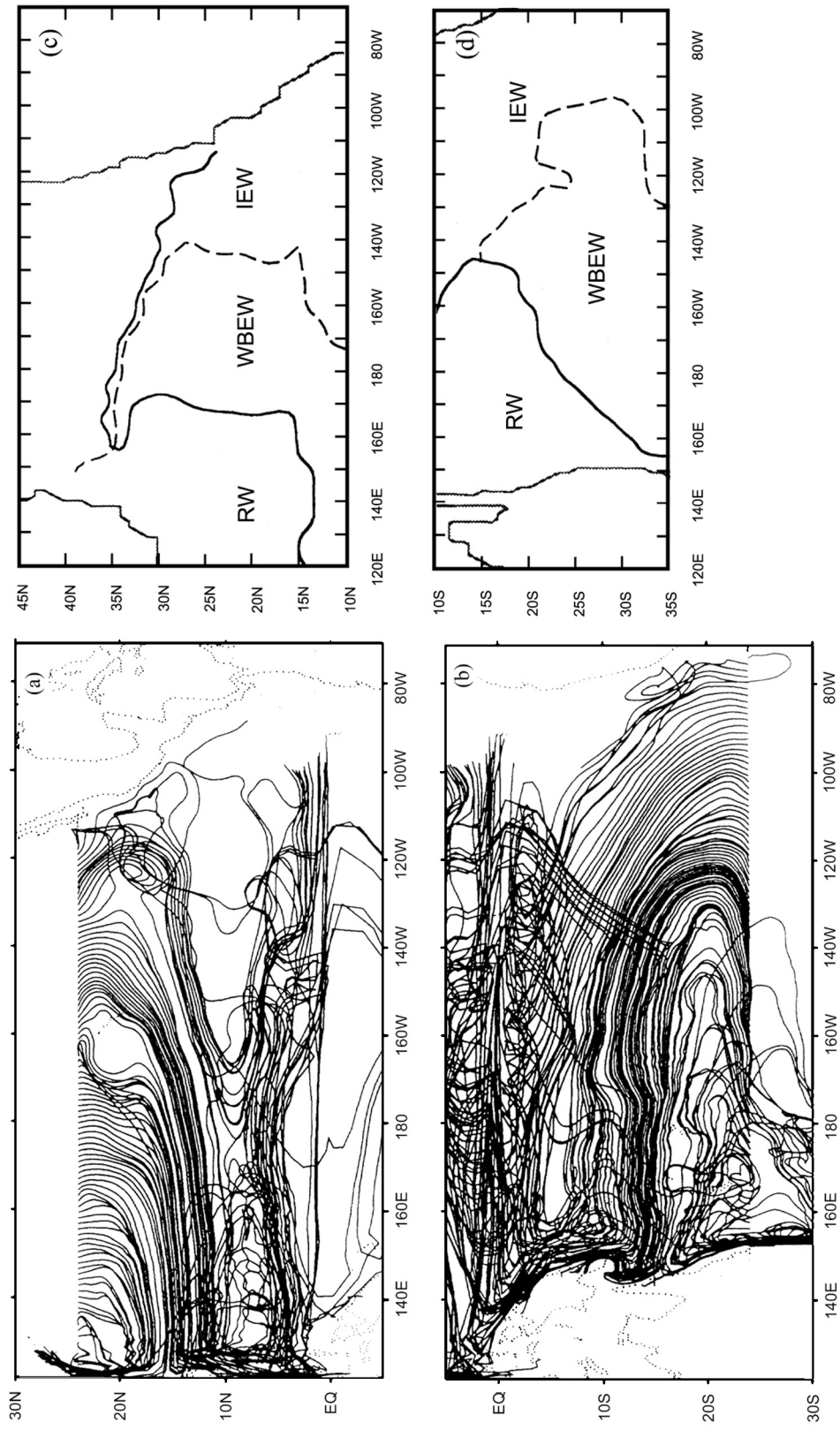

Figure 9. Trajectories of particles released at a) 24°N, b) 24°S in NCEP model study; c) corresponding thermocline water exchange windows in the North Pacific and d) South Pacific (RW = recirculation window, WBEW = western boundary exchange window, IEW = interior exchange window). (From *Huang and Liu* [1999].)

et al., 2003; *Molinari et al.*, 2003]. Farther east, interpretation of observations gets more speculative as the coverage becomes increasingly sparse. Nevertheless, it is clear from the available data that the Atlantic STCs have many features in common with those in the Pacific. One prominent difference, though, is the narrowness of the Atlantic basin, which limits the contribution of interior thermocline pathways to the equatorward transport (Section 2.3).

Another difference is the strong influence of the Atlantic MOC (analogous to the ITF-driven circulation in the Pacific) on the structure of the weaker Atlantic STCs. It carries an estimated 16±3 Sv of warm and intermediate waters from the South to the North Atlantic via the NBC [*Ganachaud and Wunsch*, 2001]. The northward flow reaches northern subtropical latitudes by two routes: 1) by ring shedding from the NBC retroflection; and 2) by eastward detours in the EUC, NEUC, and NECC, with some of the MOC water upwelling to shallower levels along the equator. Recent NBC ring studies [*Garzoli et al.*, 2003; *Johns et al.*, 2003] have shown that the rings contribute 8–9 Sv of South Atlantic NBC water to interhemispheric exchange, about half of the total and a much larger fraction than previously thought. Among other things, the MOC prevents much of the subsurface branch of the North Atlantic STC from reaching the equator.

4.1. Wind-Stress Fields and Ekman-Transport Divergences

The Atlantic ITCZ shows a marked seasonal migration (Figs. 10a,b), moving from its most equatorial position during February to its most northern location near 10ºN during August. The Ekman transports are directed poleward in both hemispheres with a zonally integrated, annual-mean divergence between 10°S and 10°N of 23 Sv for the NCEP reanalysis stresses (and 21 Sv for ERS-1,2 scatterometer stresses). The mean longitudinal distribution of the meridional NCEP Ekman transports across 10°N and 10°S (Figure 10c) shows that they are strongest in the central and western parts of the respective sections. The time series of the Ekman transport divergence across 10°N/10°S (Plate 1) shows variations of about 2 Sv amplitude at interannual but also longer time scales.

The Ekman-pumping velocity field, w_{ek}, for the annual mean winds (Figure 10c) is similar to the North Pacific, with a band of positive (or weakened negative) w_{ek} that extends nearly across the basin in the North Atlantic, limiting the possibility of interior pathways in the northern hemisphere. There is also an area of positive w_{ek} in the eastern tropical-subtropical South Atlantic, allowing a larger longitude range of interior exchange with the tropics. The area integral of positive w_{ek} in Figure 10 in the region $x > 30°W$, $5°N > y > 22°N$ plus the line integral of offshore Ekman transport along the coast, is 4.4 Sv, providing an upper limit for off-equatorial upwelling in the

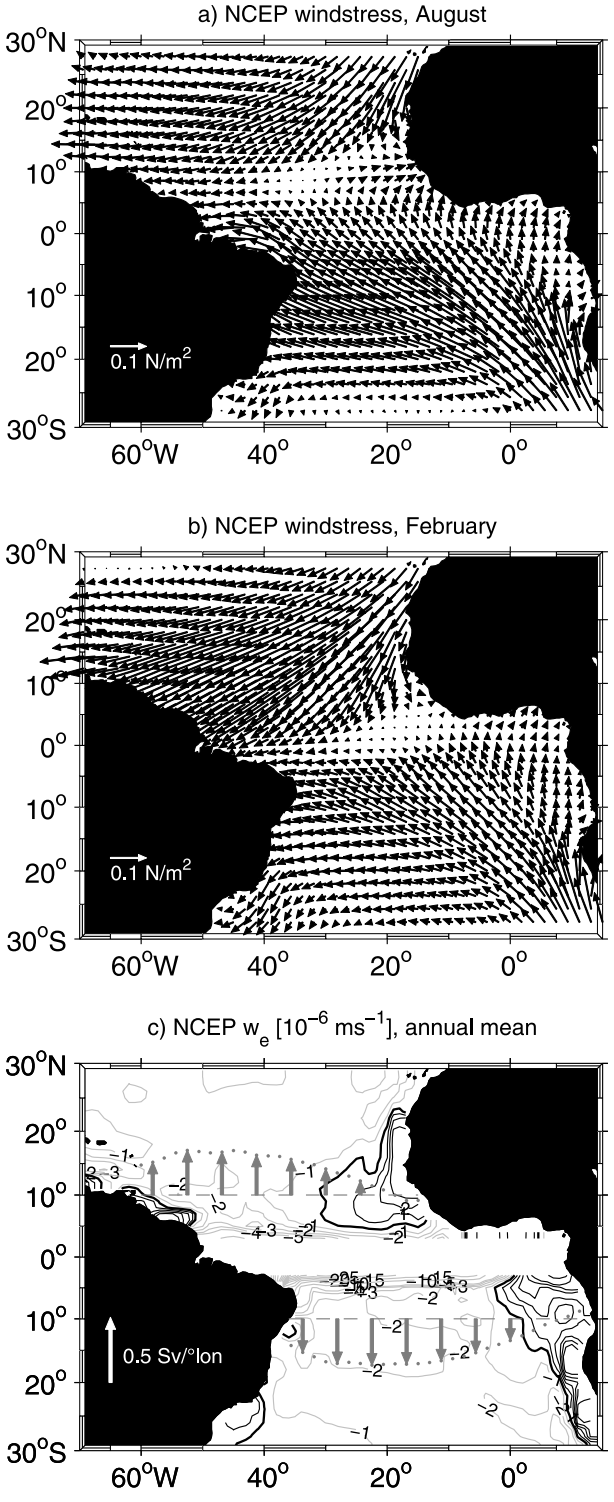

Figure 10. Wind stresses (NCEP) over the tropical and subtropical Atlantic for a) August and b) February, c) annual-mean Ekman pumping (outside ±3º latitude belt); also shown, in c), are meridional Ekman transports (vector at lower left = 0.5 Sv/degree longitude) across 10°N and 10°S.

Guinea Dome and offshore of Northwest Africa. Similarly, the area integral of positive w_{ek} for $x > 5°W$, $20ºS > y > 5°S$ plus the coastal Ekman divergence driven by the alongshore winds yields an upper estimate on coastal and Angola-Dome upwelling of 5.5 Sv. The total eastern-boundary Ekman divergence for the Atlantic is therefore about 10 Sv, similar to the eastern Pacific and a substantial fraction of the equatorial 10°N/10°S divergence (23 Sv). As stated in Section 3.1, some amount of this eastern upwelling occurs from 10°S–10°N and so contributes to the Ekman divergence across 10°N/10°S; thus, this amount must be subtracted from the divergence to estimate equatorial open-ocean upwelling.

From recent satellite observations, an ITCZ has also been identified in the western tropical South Atlantic. It extends eastward from the Brazilian coast in the latitude range 3–10°S during boreal summer [*Grodsky and Carton*, 2003], and is associated with wind convergence, high SST, reduced surface salinities, and increased precipitation. Its possible effects on the structure of the southern-hemisphere STC, if any, have not yet been investigated.

4.2. Observations

4.2.1. Subduction. For the North Atlantic, *Qiu and Huang* [1995] estimated an annual-mean subduction rate of 27 Sv. By calculating geostrophic pathways of the subducted waters, they further showed that most of the subducted water returns northward within the NEC and Gulf Stream, but they did not specifically estimate the southward transfer that would contribute to the northern STC. For the South Atlantic, *Karstensen and Quadfasel* [2002] estimated a total subduction of 22.5 Sv south of about 10°S, of which 18.7 Sv was inserted into density classes lighter than 26.8 kg m^{-3} that can upwell in the eastern tropical Atlantic (see Section 4.2.4). Much of the subducted water that is introduced into the southern SEC, however, reaches the western boundary south of the bifurcation latitude (12–15°S; Plate 3), returning southward within the Brazil Current.

4.2.2. Subsurface equatorward flow.

4.2.2.1. Western-boundary pathways: In the South Atlantic, the SEC carries thermocline waters subducted in the southeastern ocean toward the northwest. The bifurcation of the SEC occurs at 12–15°S, and from there the North Brazil Undercurrent (NBUC) transports the bulk of the STC waters equatorward. The NBUC has a strong maximum of more than 50 cm s^{-1} at a depth of about 250 m, with weak, or even reversed, surface currents due to the Ekman transports driven by the Southeast Trades (Figure 11a). It turns westward after passing Cape San Roque (at 5°S) and is augmented by the shallower inflow of the low-latitude SEC. This additional flow causes the NBUC to lose its undercurrent character, and it continues to flow northward as the surface-intensified North Brazil Current (NBC; Plate 3 and Figure 11b).

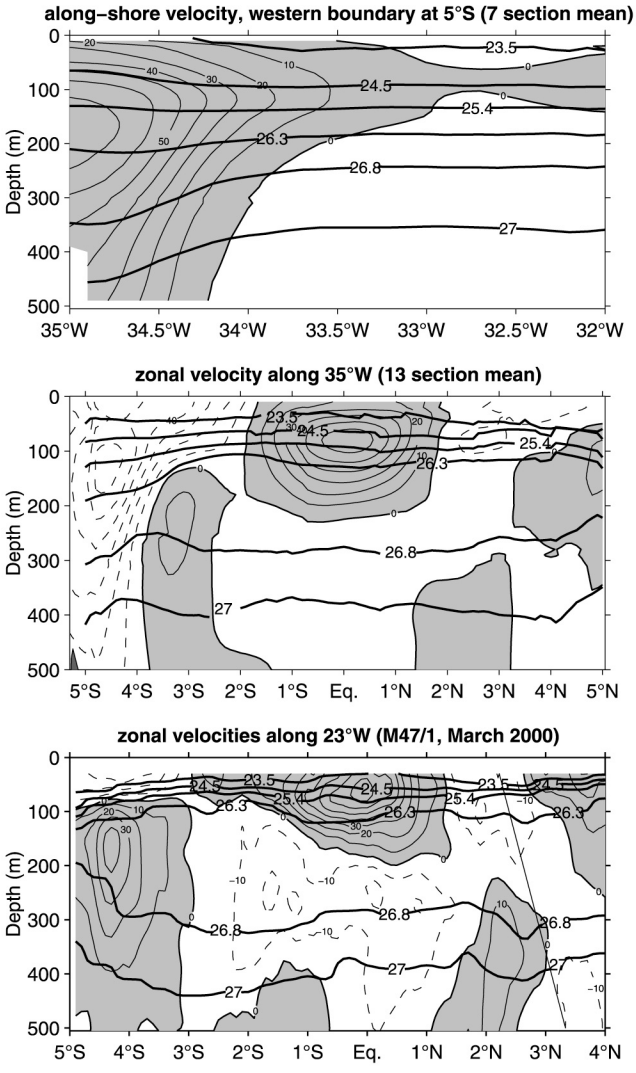

Figure 11. Mean current distributions for a) meridional flow of the North Brazil Undercurrent across 5°S (7 sections), and the zonal equatorial current system b) at 35°W (13 sections), c) at 23°W (1 section); also shown (heavy lines) are several relevant isopycnals. (After *Schott et al.* [2002b, 2003].)

Based on 7 shipboard current-profiling sections at 5°S, *Schott et al.* [2002b] estimated that the NBUC transports 25 Sv northward across that latitude (Figure 11a). This transport is a superposition of the MOC, the South Atlantic STC, and a recirculation of the southward interior Sverdrup transport, the latter estimated to be about 10 Sv near 5°S [*Mayer et al.*, 1998]. From 13 sections along 35°W, *Schott et al.* [2003] estimated an average NBC transport of 32 Sv northwest of Cape

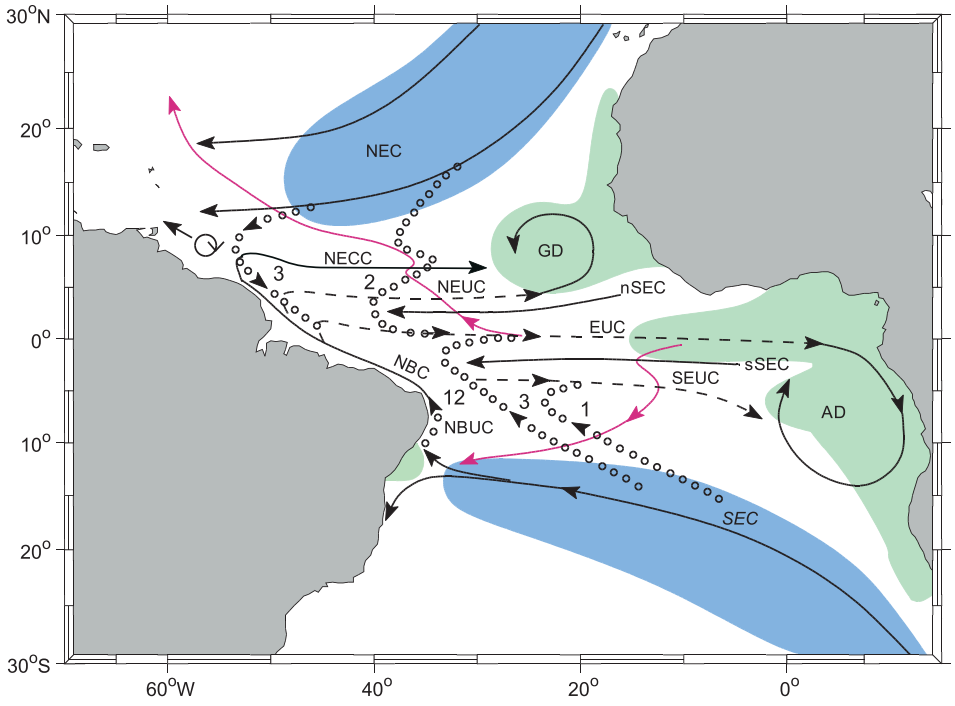

Plate 3. Schematic representation of the Atlantic STC circulation with subduction (blue) and upwelling (green) zones that participate in the STC. Current branches participating in STC flows are NEC, SEC, NECC and EUC as in Plate 2; NEUC, SEUC = North and South Equatorial Undercurrent; NBC, NBUC = North Brazil Current and Undercurrent; GD, AD = Guinea and Angola domes. Interior equatorward thermocline pathways dotted, transport estimates marked for interior and western boundary pathways; surface poleward pathways for the central basin (from drifter tracks, after *Grodsky and Carton* [2002]) marked by thin, magenta line; see text for details.

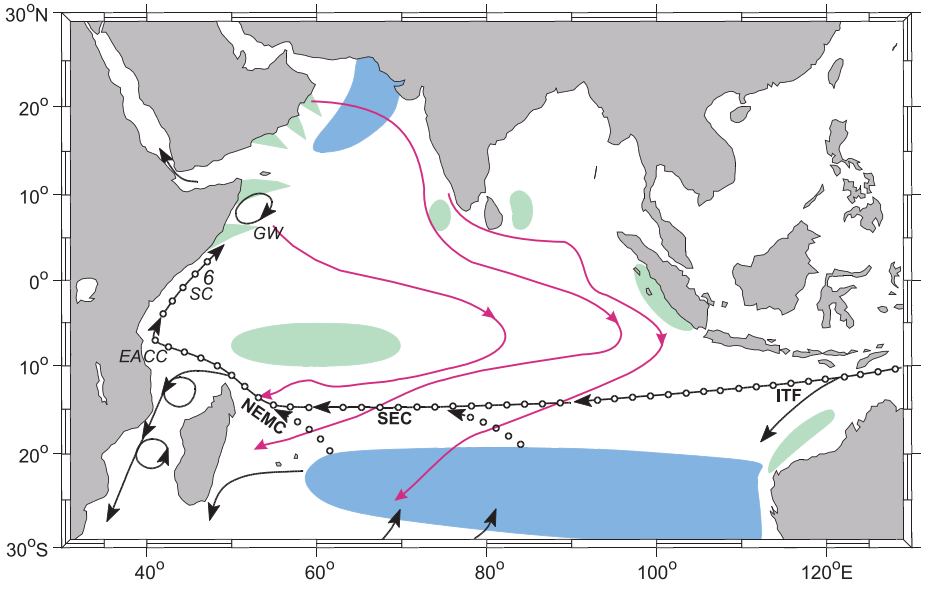

Plate 4. Schematic representation of the Indian Ocean Cross-Equatorial Cell (CEC) with subduction (blue) and upwelling (green) zones that participate in the CEC; ITF = Indonesian Throughflow, SEC = South Equatorial Current, NEMC = Northeast Madagascar Current, EACC = East African Coast Current, SC = Somali Current, GW = Great Whirl; also shown are model surface trajectories (magenta) of southward CEC return flow originating from upwelling sites off Somalia, Oman and west of India; see text for details. (After *Schott et al.* [2002a] and *Miyama et al.* [2003].)

San Roque with another 7 Sv of SEC flow just to its north, yielding a total of 39 Sv flowing across 35°W. *Schott et al.* [1998] reported 35 Sv of this amount crossing the equator at 44°W, after some loss to the South Intermediate Countercurrent (SICC). The NBC overshoots the equator [*Johns et al.*, 1998; *Schott et al.*, 1998] and, after passing through a retroflection zone known for its intense eddy-shedding activity [*Garzoli et al.*, 2003], most of it merges into various zonal currents in the interior ocean. When evaluating the NBUC currents at 5°S from the ADCP observations of *Schott et al.* [2002b] for the STC density range of $\sigma_\theta = 23.4–26.2$ kg m^{-3} (Figure 11a), a northward transport of 12 Sv results, as marked in Plate 3.

In the North Atlantic, thermocline water in the NEC is carried equatorward by the Guyana Undercurrent, which bends eastward to join the NECC at 5–8°N and the NEUC at 3–5°N. It is a very weak flow, transporting only about 3 Sv [*Wilson et al.*, 1994; *Bourles et al.*, 1999b; *Schott et al.*, 1998]. Model studies suggest that it may penetrate further southward during boreal winter to supply the EUC [*Schott and Boening*, 1991]. *Zhang et al.* [2003] estimate a western boundary undercurrent transport of 3.3±1.0 Sv, in agreement with the earlier observational estimates. The weakness of the northern equatorward STC flow compared to the southern one is of course a consequence of the Atlantic MOC, transporting about 15 Sv of warm water across the equator (see Section 4.3.2).

4.2.2.2. Interior pathways: In the tropical-subtropical Atlantic, the water masses subducted in the eastern subtropics and inserted into the thermocline by Ekman pumping are characterized by a potential-vorticity (PV) minimum. The Ekman upwelling associated with the ITCZ, however, brings stratified waters with higher PV into the density range of the subducted waters, causing them to make a westward detour around this barrier on their way south. This path is clearly seen in the PV distribution ($f/\Delta h$, where Δh is layer thickness) on the isopycnal surface $\sigma_\theta = 25.4$ kg m^{-3}, as determined by *Zhang et al.* [2003] from climatological hydrographic data (Figure 12a). Trajectories of the subducted waters on the $\sigma_\theta =$ 25.4 kg m^{-3} surface show that there are indeed interior pathways in the South Atlantic, facilitated by the narrowness of the PV barrier there (Figure 12b). For the South Atlantic, *Zhang et al.* [2003] determined the geostrophic transport across 6ºS, between the African coast and 34°W for various density classes (Figure 12c), obtaining a total of 4.0±0.5 Sv for the density range $\sigma_\theta = 23.5–26.3$ kg m^{-3}. For the North Atlantic, they estimated 2 Sv of equatorward interior flow across 10°N, concentrated in the density range $\sigma_\theta = 23.5–26.0$ kg m^{-3}. A similar calculation was carried out by *Lazar et al.* [2002], also yielding interior pathways. It should be noted that the lightest portions of the equatorward flow ($< \sigma_\theta = 24.0$ kg m^{-3}) are subducted at quite low latitudes and therefore do not really

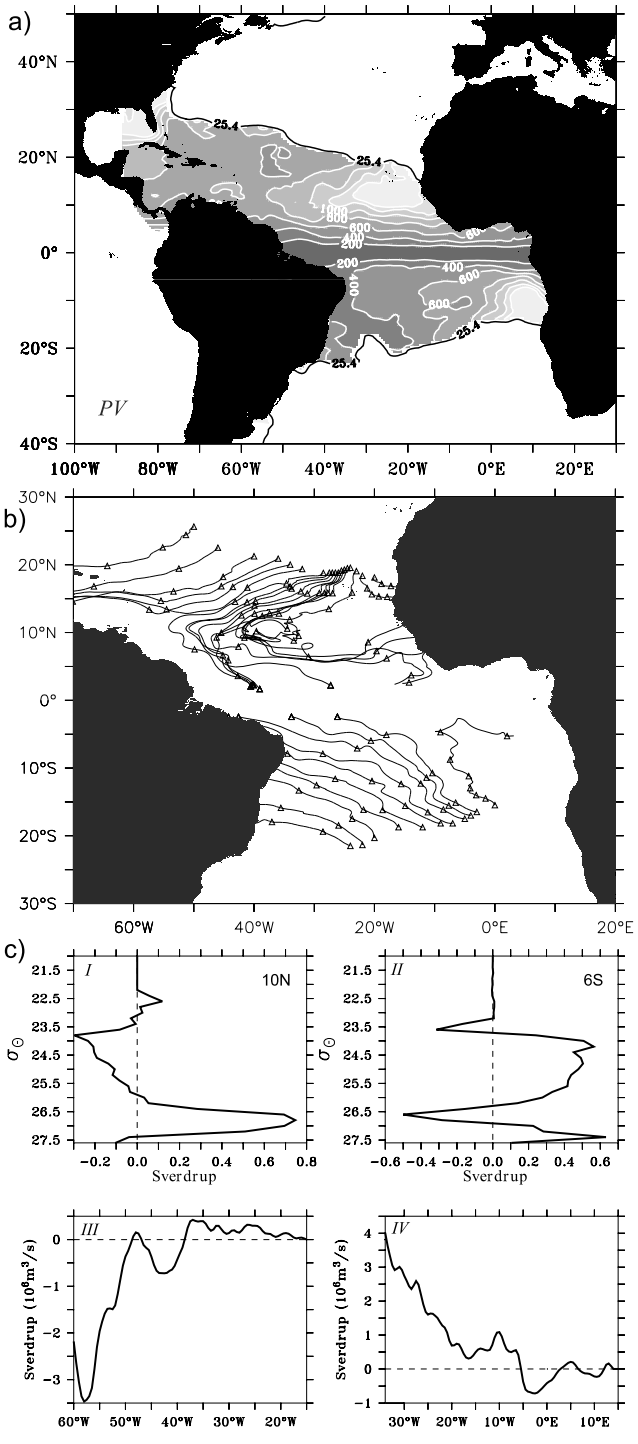

Figure 12. a) Distribution of potential vorticity ($f/\Delta h$, with Δh layer thickness, in units of 10^{-12}m^{-1}s^{-1}); b) geostrophic currents on the isopycnal surface $\sigma_\theta = 25.4$ kg m^{-3} for the tropical Atlantic, based on climatological hydrographic data; c) interior net meridional transports by density layers across 10°N (I: African coast to 60°W) and 6°S (II: African coast to 35°W) as well as accumulated layer transports across 10°N (II) and across 6°S (IV). (From *Zhang et al.* [2003].)

qualify as part of the STC, because they are not participating in a subtropical-tropical exchange.

4.2.3. Equatorial currents.

4.2.3.1. EUC: The EUC draws most of its water from the NBC retroflection (Plate 3). *Schott et al.* [2002b] reported that the undercurrent layer (σ_θ = 24.5–26.8 kg m^{-3}) is supplied by a northward flow of 13.4±2.7 Sv at 5°S, and estimated that about 80% of this flow enters the EUC. The EUC has a total eastward transport of 21.9±3.5 Sv in the mean section at 35°W, of which 8.6 Sv occur in the near-surface layer above σ_θ = 24.5 kg m^{-3} [*Schott et al.*, 2003]. The surface-layer eastward flow occurs predominantly during the spring when the ITCZ migrates close to the equator (Figure 10a,b), and weakened easterly, or even westerly, wind stresses drive the near-surface flow [*Bourles et al.*, 1999a; *Schott et al.*, 1998].

Farther east at 0°E, the transport is reduced to about 6 Sv [*Bourles et al.*, 2002]. These authors showed that during boreal summer the Atlantic EUC can even surface and terminate away from the boundary. The fate of the mean EUC at the eastern boundary and its possible supply of the Gabon-Congo Undercurrent or Angola Dome is still uncertain [*Stramma and Schott*, 1999].

4.2.3.2. North and South Equatorial Undercurrents: The NEUC and SEUC seem to be weak in the west and to strengthen into the central ocean. Their potential role in the STCs is to provide, from their shallower density layers, water for the off-equatorial eastern upwelling regimes along the coasts and in the Guinea and Angola domes. The SEUC is recognizable (Figure 11b) at a depth of about 100–400 m at 3–4°S in the density range 26.2–27.0 kg m^{-3}; its transport at 35°W is only 3 Sv, but at 23°W (Figure 11c) it has strengthened to about 10 Sv. Although a supply of the SEUC out of the NBC retroflection regime has not been established from ship surveys, the SEUC is distinguishable from the low-oxygen interior thermocline waters of the tropical South Atlantic by a relative oxygen maximum [*Arhan et al.*, 1998]. An interpretation is that it is supplied by a mixture of NBUC waters with interior SEC recirculations. Mean transports from sections further east still have to be composed from the sparse data base.

Since the equatorward flow of subducted water in the interior ocean occurs in the density range σ_θ = 23.5–26.3 kg m^{-3} [*Zhang et al.*, 2003], most of it can pass over the SEUC in the western basin (Figure 11b) but not at 23°W in the central basin where isopycnals σ_θ = 25.4 kg m^{-1} and deeper pass through its upper part (Figure 11c). Thus, the denser part of the subducted water (Figure 12c) cannot reach the EUC. *Zhang* [2003; pers. comm.] estimated that about 1 Sv of the interior equatorward thermocline flow is trapped by the SEUC in this way and carried eastward with it.

4.2.3.3. Tropical cells: From their ADCP section analysis, *Molinari et al.* [2003] inferred the existence of a North Atlantic TC, consisting of shallow upwelling at the equator and downwelling from 3–6°N. For the downwelling branch, *Grodsky and Carton* [2002] estimated a transport of 42 Sv for 35°W–10ºE from drifter convergences. The existence of a TC in the tropical South Atlantic has not yet been quantified. In any event, as for the Pacific, the presence of Atlantic TCs has to be taken into account when evaluating the wind forcing and net meridional upper-layer STC transports, that is, the relevant quantifications need to be carried out poleward of about 6° latitude.

4.2.4. Upwelling.

4.2.4.1. Source depth of upwelled waters: The core of the Atlantic EUC lies in the density range σ_θ = 24.5–26.8 kg m^{-3}, and the SEUC and NEUC extend to densities of the order σ_θ = 27.0 kg m^{-3}. Since the σ_θ = 26.25 kg m^{-3} isopycnal within the EUC reaches the surface at the Greenwich meridian [*Bourles et al.*, 2002], only densities near and less than this value can upwell to the surface at the equator [*Snowden and Molinari*, 2003]. The fate of the denser water is unclear, but it may upwell in the off-equatorial areas.

4.2.4.2. Equatorial upwelling: From an evaluation of early direct current sections across the equator, *Gouriou and Reverdin* [1992] estimated a divergence of 15 Sv for the 4–35°W band, and concluded that upwelling into the surface layer was confined to the upper part of the EUC. From an average of 12 cross-equatorial western Atlantic ADCP sections extending for 10° of longitude centered near 35°W, *Molinari et al.* [2003] estimated an upwelling transport of about 11 Sv. These estimates are comparable to upwelling transports obtained from inverse-model analyses of the divergence across off-equatorial sections. *Lux et al.* [2001], for example, derived an upwelling transport of 7.5 Sv out of the thermocline water layer (σ_θ = 24.58–26.75 kg m^{-3}) for a box closed by zonal sections at 7.5°N and 4.5°S. Earlier, *Roemmich* [1983] obtained an upwelling transport of 6–10 Sv across σ_θ = 26.2 kg m^{-3} for basin-wide sections at 10°N and 10°S, the spread of values depending on model assumptions. When comparing these estimates with the Ekman divergence of about 25 Sv across 10°N/10°S, it has to be considered that diapycnal upwelling velocities have a sharp profile and maximum upwelling values may not be reached when averaging over density ranges.

4.2.4.3. Off-equatorial upwelling: Off-equatorial upwelling happens along the eastern coasts and in two cyclonic domes, namely, the Guinea and Angola domes in the northern and southern hemispheres, respectively (Plate 3), which are driven by the regions of strong positive w_{ek} in the eastern tropical ocean (Figure 10). Upwelling estimates based on observations have not been reported for these regions, but, as noted above (Section 4.1), their combined Ekman upwelling effect (10 Sv) is not negligible. Their effects, while not known in detail, are nevertheless included in aforementioned inverse studies for those contributions that fall inside the northern and southern boundaries of their respective analysis domains.

4.2.5. Poleward surface flow. Surface-drifter pathways for the tropical Atlantic were determined by *Grodsky and Carton* [2002]. As for the Pacific (Section 3.2.5; Figure 6), they indicate that the STC return flow is carried westward by the zonal currents, except for an eastward portion in the NECC. Consequently, much of the upwelled water returns to the subtropics west of the subduction sites, as indicated in Plate 3 for two trajectories from the central equatorial basin. Again, it has to be noted that these drifter trajectories are not the tracks of real water parcels since they cannot follow downward motions at TC convergences; hence real trajectories would be deflected even more westward than those of Plate 3. This property ensures that much of the STC water does not return directly to the equator, so that the STCs are primarily closed indirectly after one or more recirculations in the Subtropical Gyre, or even an excursion into the subpolar region. Similar to the Pacific, pathways in the eastern basin also extend eastward to be trapped in the Gulf of Guinea.

4.3. Models

4.3.1. STC pathways and exchange windows. A variety of model studies have addressed Atlantic STC pathways and exchange windows between the subtropical subduction regions and the tropical and eastern upwelling regions. *Malanotte-Rizzoli et al.* [2000] used an intermediate-resolution (non-eddy resolving) OGCM, driven by COADS climatology and obtained PV distributions that looked qualitatively similar to those observed (Figure 12a). Regarding the exchange windows, they find an interior exchange zone in the northern hemisphere, whereas all the waters subducted in the eastern South Atlantic take the western-boundary pathway. As expected, the seasonal effect of the northern PV barrier is most pronounced in late boreal summer and much reduced in winter, so that the annual mean is dominated by the summer situation. They attributed the stronger than observed equatorward northern thermocline flow in their simulation to their model's having a somewhat weak MOC.

It is obvious that there must be a dependence of the exchange windows on the patterns and intensity of the wind stress climatology, since that determines upwelling and the PV barrier. *Inui et al.* [2002] studied the differences in STC pathways between the commonly used *Hellermann and Rosenstein* [1983] and *da Silva et al.* [1994] forcing fields. They found that for the stronger *Hellerman and Rosenstein* [1983] forcing the interior exchange window is much reduced in comparison to the weaker *da Silva et al.* [1994] forcing. This calculation was confirmed by a similar model study with both wind stress climatologies carried out by *Lazar et al.* [2002].

4.3.2. Effect of the MOC. Several investigators have studied the interaction of the Atlantic MOC with the STC. *Fratantoni et al.* [2000] compared two solutions to a six layer isopycnal model of the tropical Atlantic, one forced by wind alone and the other by winds and a 15-Sv MOC imposed at the model's northern and southern boundaries. A similar calculation was carried out by *Boening* [2002; pers. comm.] using an Atlantic-basin GCM. Both studies found that the STCs were nearly symmetric about the equator in the solution forced only by winds. In contrast, for the solution forced by wind and the MOC, the northern cell was so weak that there was only about 2 Sv of equatorward thermocline flow in the northern hemisphere, similar to the observational evidence presented above.

The transports of solutions forced by both winds and the MOC are approximately a linear superposition of the transports from solutions forced by MOC and wind forcing alone. This linearity, however, is not at all true for the mesoscale variability. The eddy kinetic energy at the western boundary is greatly enhanced with the addition of the MOC. *Fratantoni et al.* [2000] attribute this to the combined effects of increased current shear, advection of potential vorticity from the equatorial waveguide by the strengthened NBC and enhanced potential vorticity gradient. In their model, NBC eddy shedding only occurs in the combined forcing case.

5. INDIAN OCEAN

In the Indian Ocean, the Southeast Trades do not extend to the equator, and the annual-mean equatorial winds have a slight westerly component (Figure 13c). As a result, there is no annual-mean, equatorial upwelling as in the other oceans. Instead, there are prominent upwelling regions in the northern hemisphere off Somalia, Oman, and India during the summer monsoon. Since subduction occurs predominantly in the southeastern, subtropical Indian Ocean, the shallow overturning circulation associated with these upwelling regions involves interhemispheric flow, forming the Cross-equatorial Cell (CEC). There are also regions of open-ocean upwelling in the southern tropical Indian Ocean and off northwestern Australia that generate intra-hemispheric

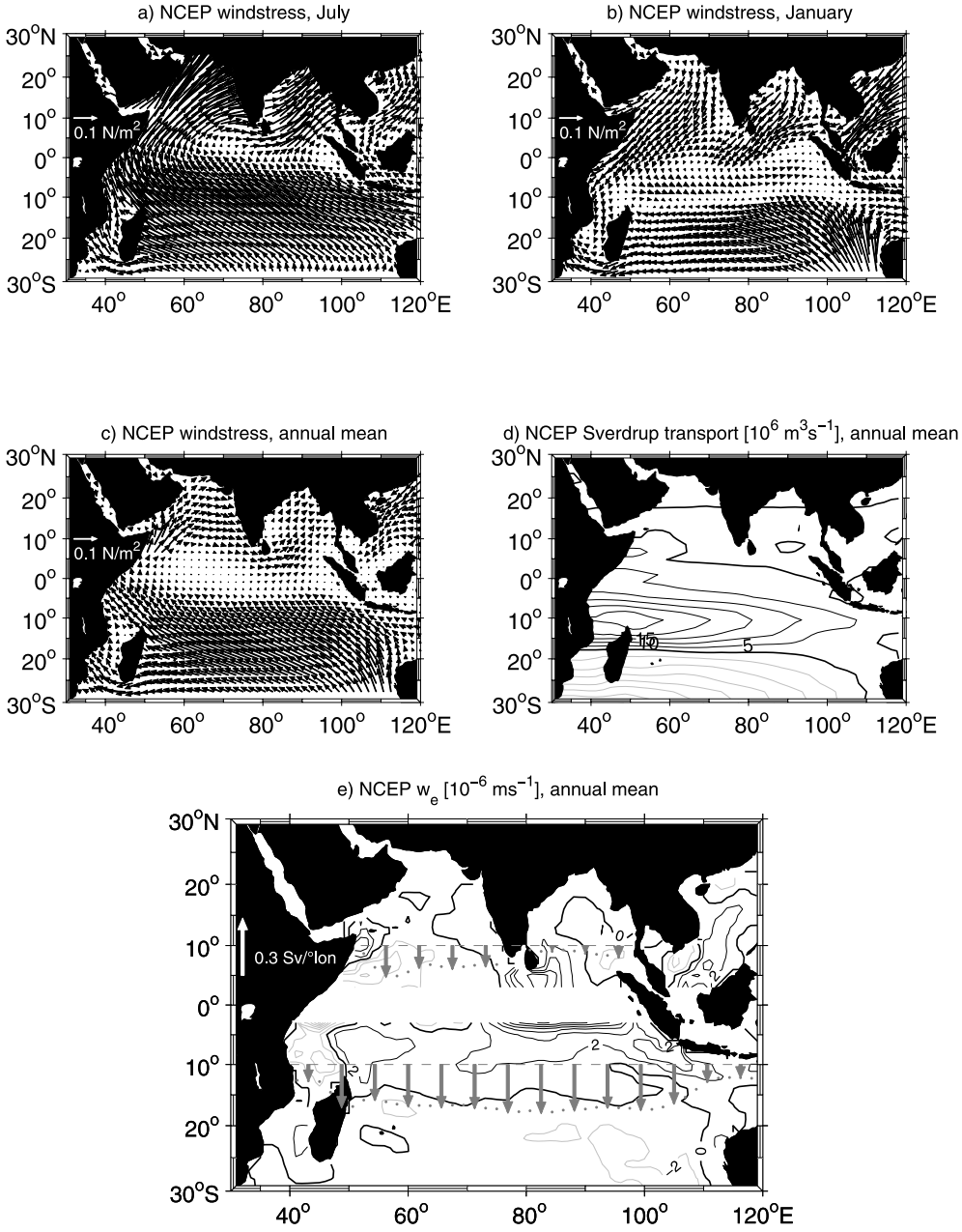

Figure 13. Wind stresses (NCEP) in the Indian Ocean for a) July, b) January, c) the annual mean; d) Sverdrup transport function, and e) annual mean of Ekman pumping (outside ±3° latitude belt), with meridional Ekman transports (vector at left = 0.3 Sv/degree longitude) across 10°N and 10°S.

overturning cells. Superimposed on the basin circulation is the ITF, allowing for complex pathways relating the CEC and hemispheric cells with the other oceans.

5.1. Wind Stress

5.1.1. Monsoon variability. The wind-stress fields for July and January show the drastic changes of the monsoons (Figs. 13a,b). During the northern summer, the Southeast Trades attain their seasonal maximum and extend almost to 5°S, their most northerly position. At this time, they flow into the Arabian Sea over the western basin, forming a narrow atmospheric jet with strong northward cross-equatorial stresses (the Findlater Jet; Figure 13a). As a result, in the Arabian Sea there is Ekman convergence and mixed-layer warming southeast of the jet, and Ekman divergence and

cooling northwest of it. North of the equator, the summer-monsoon winds have an eastward component (Figure 13a) and south of it (in the domain of the Southeast Trades) they have a westward component, that is, they drive southward Ekman transports on both sides of the equator. The equatorial winds are directed primarily northward *against* the off-equatorial Ekman transports in both hemispheres (Figure 13a), and they are strongest in the west.

During the winter monsoon, the Southeast Trades are confined south of 10°S, and there is a belt of eastward wind stress between 10°S and the equator (Figs. 13b). Ekman divergence and thermocline doming along the northern edge of the Trades are largest at this time. The zonal-mean stresses are eastward north of the equator and westward south of it. Thus, the Ekman transport is directed northward on both sides of the equator, the opposite situation from the summer. On the equator, the meridional stress is (weakly) southward, again against the Ekman transport.

The equatorial wind stress is eastward during the intermonsoon seasons (April–June and October–December), so that there is Ekman convergence on the equator. These winds drive semiannual eastward surface jets, leading to a deep, annual-mean thermocline in the eastern equatorial ocean [*Wyrtki*, 1973].

5.1.2. Sverdrup and Ekman transports. The annual-mean wind stress distribution is dominated by the summer-monsoon pattern, having anticyclonic stresses over the Arabian Sea (Figure 13c). The resulting mean Sverdrup transport function (Figure 13d) shows the subtropical and SEC circulation of the South Indian Ocean, with a weak cell in the Somali Current area. Using the NCEP climatology for the time period 1990–98, there is a mean southward transport of 6.5±0.9 Sv, based on the mean values for individual years.

As noted by *Godfrey et al.* [2001] and *Miyama et al.* [2003], the zonal component of the wind stress nearly vanishes at the equator during both monsoons, and it is roughly proportional to the distance from the equator on either side. For such a wind field ($\tau^x \propto y$), the Ekman pumping velocity, $-(\tau^x/f)_y$, vanishes completely. It follows that no pressure gradients and, hence, no geostrophic currents are generated, so that the flow field is composed entirely of Ekman drift. For this wind field, then, the concept of Ekman flow is valid all the way to the equator (i.e., in the limit $y \to 0$). Consistent with this property, $-\tau^x_y/\beta = -\tau^x/f$ so that the Sverdrup and Ekman transports are equal, a relation that is valid even at the equator. As a consequence, the cross-equatorial Ekman/Sverdrup flow is very shallow, providing the driving force for the CEC.

The near-equivalence of Ekman and Sverdrup transports has been confirmed by *Schott et al.* [2002a]. For the NCEP winds averaged from 1990–98, the annual-mean Ekman transports across 3°N and 3°S are −6.9±3.6 Sv and −6.0±3.9 Sv, respectively, and the cross-equatorial Sverdrup transport is −6.5±0.9 Sv. The same averages for the ERS-1/2 scatterometer winds yield Ekman transports of 7.4±4.0 Sv and 9.3±6.4 Sv with an across-equatorial Sverdrup transport of −6.4±2.6 Sv.

The longitudinal distributions of the annual-mean Ekman transports across 10°N and 10°S are sketched in Figure 13e. They underscore the completely different behavior of the Indian Ocean in comparison to the Atlantic (Plate 3) and Pacific (Plate 2) Oceans, with (weak) mean southward Ekman transports across 10°N. South of about 8°S, the Southeast Trades are present throughout the year. They are associated with a band of intensified w_{ek} from 2–12°S and 55–90°E (Figure 13e). Ekman divergence estimates for the region are almost 10 Sv [*Schott et al.*, 2002a], and this divergence drives the Indian Ocean's southern-hemisphere STC.

As discussed above, the main driver of the Indian Ocean cross-equatorial cell (CEC) is the cross-equatorial Sverdrup transport. Time series of this field show intraseasonal variations of 5 Sv or more and year-to-year differences of 2–3 Sv. These transport variations are comparable to those in the other two oceans, but they amount to a much larger fraction for the mean CEC than for the mean STCs in the Pacific and Atlantic Oceans.

5.1.3. Subduction. Subduction in the Indian Ocean occurs predominantly in the southeastern subtropical Indian Ocean. Based on their global analysis of climatological data, *Karstensen and Quadfasel* [2002] estimated that a total of 36 Sv is subducted into the 23–27 kg m^{-3} density range in that region. Of this amount, 12.2 Sv enters into densities less than 25.7 kg m^{-3}, corresponding to an upwelling depth off Somalia of about 150 m. A small amount of subduction, estimated to be about 0.5 Sv in the annual mean by *Karstensen* [2003; pers. comm.], also happens in the northern Arabian Sea during the winter monsoon in density classes that can upwell locally (Plate 4). A similar amount of surface water is transformed into thermocline waters in the Red Sea and Arabian Gulf, but into density classes of 27.2 and 26.6 kg m^{-3}, respectively, too dense for upwelling [*Schott et al.*, 2002a].

5.1.4. Southern-hemisphere subsurface flow. Given the structure of the southern-hemisphere winds (Figure 13c), we can expect that south of the equator the Indian Ocean's shallow overturning circulation has a structure like that in the other oceans, with subsurface water following the western-boundary pathway to the equator since $\tau^x(0) \approx 0$ so that $x_e(0) \to -\infty$ [Eq. (7)]. Indeed, this structure is suggested by the distributions of salinity and nutrients in the thermocline (Schott *et al.*, 2002a). Subducted water masses are carried

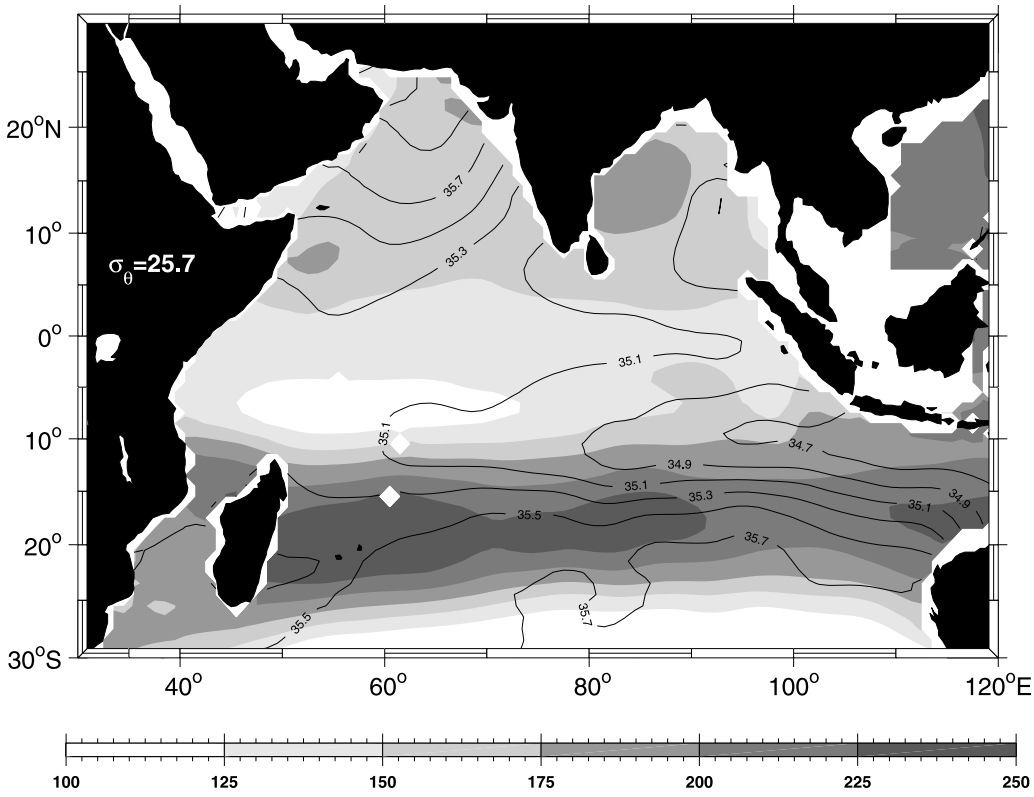

Figure 14. Depths (shading) of and salinities (contours) on potential density surface 25.7 kg m^{-3} for the annual-mean distributions, showing spreading of low-salinity ITF waters and doming northeast of Madagascar.

westward within the South Equatorial Current (SEC). The SEC waters bifurcate at the Madagascar coast, with part turning southward and the rest eventually joining the East African Coastal Current (EACC) to flow to the equator. The denser waters do not participate in the CEC, either retroflecting southeast of Madagascar or flowing out of the basin within the Agulhas Current.

Salinity (Figure 14) and nutrient distributions further indicate a connection to the ITF region. In a recent inverse modeling study, *Ganachaud et al.* [2000] emphasized the connection of the Throughflow to the southern Indian Ocean via the Mozambique Current. Evidence from drifter trajectories and earlier regional budget studies [*Swallow et al.*, 1991] indicates that the near-surface SEC water that arrives north of Madagascar mostly continues to flow northwestward toward the EACC and Somali Current (Plate 4); it is only the deeper thermocline flow that supplies the Mozambique Current.

5.1.5. Cross-Equatorial Cell.

5.1.5.1. Subsurface cross-equatorial flow: *Schott et al.* [1990] observed the cross-equatorial western-boundary flow with moored stations. They found that the annually reversing part of the Somali Current was restricted to be not much deeper than the upper 100 m (Figure 15a,b), with the stronger northward flow during the summer monsoon resulting in an annual northward mean of 3.5 Sv from the surface to 100 m, while from 100–400 m the flow was northward in both seasons. *Schott et al.* [2002a] derived a total of 6.3 Sv for the 50–300 m layer, which carries water in the density ranges that upwell off Somalia. The deeper portions of the northward flow, about 1.6 Sv from 300–500 m must also participate in the northern-hemisphere upwelling, since there is no southward return flow at these densities elsewhere along the equator. (Presumably, all subsurface cross-equatorial flow occurs near the western boundary where mixing and strong nonlinearities can change the sign of its potential vorticity.)

5.1.5.2. Upwelling: During the Southwest Monsoon, coastal upwelling off Somalia typically occurs in wedge-shaped areas, formed by offshore advection along the northern flanks of two prominent summertime gyres, the "Southern Gyre" at 3–5°N and the "Great Whirl" at 8–10°N [*Schott and McCreary*, 2001]. Although upwelling densities as high as $\sigma_\theta = 6.8$ kg m^{-3} have been observed off Somalia, the typical upwelled water is lighter than 25.7 kg m^{-3}.

From shipboard sections off Somalia, the Southern Gyre outflow of upwelled water was estimated by *Schott et al.* [2002a] to be about 9 Sv. The Great-Whirl outflow has two portions, one through the passage between Socotra and the African continent (Plate 4) and another by offshore and southeastward recirculation, both branches taking up heat and losing density. *Schott et al.* [2002a] estimated a combined upwelling transport of 12.5 Sv for the summer monsoon and 4.2 Sv for the annual mean. Along the Omani coast, coastal upwelling associated with filaments connected to topographic features

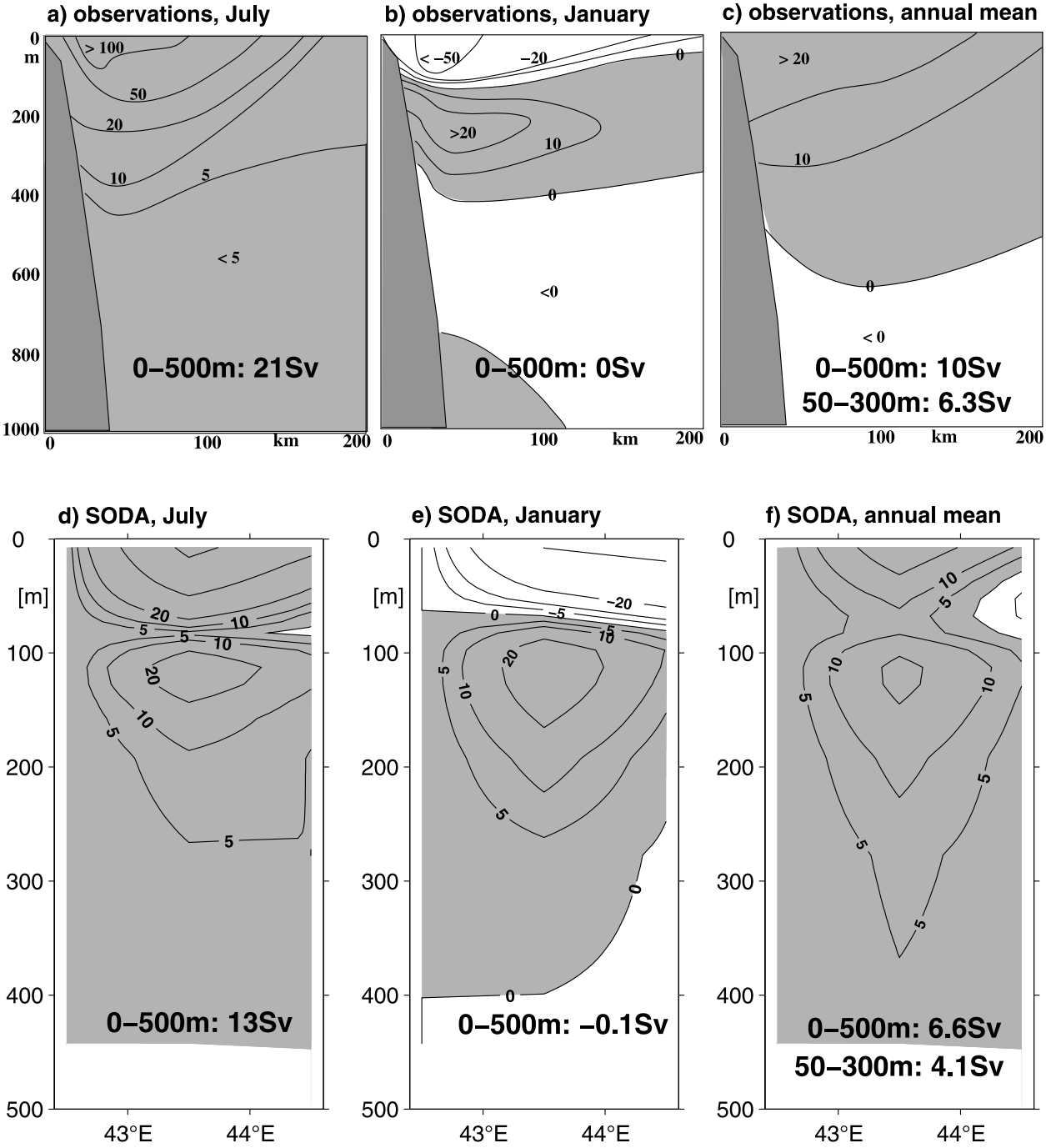

Figure 15. Observed meridional currents and transports of the Somali Current at the equator: a) summer monsoon, b) winter monsoon, c) mean; d)–f) same as a)–c) but from SODA model.

carry the upwelled waters far into the interior Arabian Sea. From various pieces of evidence, *Schott et al.* [2002a] estimated this upwelling to be about 3 Sv for the monsoon season or 1 Sv annually.

There is also open-ocean upwelling in the northern Indian Ocean during the summer monsoon. It has been emphasized in several modeling studies with regard to cyclonic domes east and west of southern India and Sri Lanka [*McCreary et al.*, 1993; *Vinayachandran and Yamagata*, 1998; *Miyama et al.*, 2003], which are driven by the positive Ekman pumping there (Figure 13e). Presumably, open-ocean upwelling also occurs in the Arabian Sea west of the Findlater Jet; however, it has been discounted as a significant upwelling source, likely because its effects are overwhelmed by the nearby Somali and Omani coastal upwelling and by local mixed-layer deepening [*McCreary et al.*, 1993; *McCreary et al.*, 1996; *Lee et al.*, 2000].

5.1.5.3. Surface cross-equatorial flow and equatorial roll: As discussed in Section 5.1, the wind-stress distribution suggests that the CEC is closed by a surface, southward Ekman/Sverdrup transport in the interior ocean. *Schott et al.* [2002a] noted the agreement between the observed northward Somali Current in depth range 50–300 m and the Sverdrup transport, both carrying about 6 Sv (Plate 4). Drifters provide observational evidence for this interior flow, indicating southward flow on either side of the equator to within ±3°. Close to the equator, however, the flow is masked by the equatorial roll, as discussed next.

Solutions forced by meridional winds at the equator [*Wacongne and Pacanowski*, 1996; *Miyama et al.*, 2003] suggest that there should be a vertical-meridional overturning circulation within a narrow band around the equator, with northward (southward) surface currents on the equator during the summer (winter) monsoon and subsurface counterflow underneath. This counterflow connects the southward (northward) Ekman transports from one side of the equator to the other during the summer (winter) monsoon. Based on shipboard ADCP sections taken during the summer monsoon in the western basin where strong northward winds exist on the equator (Figure 13a), *Schott et al.* [2002a] reported observational evidence for the subsurface flow of the roll at speeds exceeding 20 cm s^{-1}. Evidence for the reverse circulation during the winter monsoon was also found, but the roll was not as well developed at that time.

Whether the rolls can cause diapycnal fluxes depends on whether or not they penetrate through the bottom of the mixed layer. In the observations, however, the evidence points to the roll being dominantly restricted to the surface-mixed layer or at least uppermost part of the thermocline, leading *Schott et al.* [2002a] to the conclusion that the equatorial roll has small diapycnal effects and is therefore of little consequence for the meridional heat transport. This conclusion was confirmed by the model study of *Miyama et al.* [2003] (see Section 5.3).

Estimation of near-surface mean flows from drifter trajectories is much more difficult than for the other two oceans because of the seasonal reversal of the monsoon circulation north of about 8°S and the existence of the equatorial roll, the latter preventing drifters from being directly advected across the equator by the Ekman transports in both hemispheres. Therefore, likely mean surface trajectories have been inserted into Plate 4 from the model study of *Miyama et al.* [2003]. Three trajectories are shown from a simulation based on forcing by annual-mean winds, which emanate from the upwelling regimes of Somalia, the eastern Arabia Peninsula and west of India. They all slant to the southeast in the northern hemisphere and down to about 5°S, then reverse to slant to the southwest. As in the other oceans, much of the surface return flow does not return to the southeastern subduction regime, again requiring indirect STC recirculations with the subtropical or subpolar Indian Ocean, or even an interocean transfer into the Atlantic.

5.1.6. Southern-hemisphere STC. There are indications of open-ocean upwelling within the band of intensified Ekman pumping from 5–12ºS noted in Section 5.1. Direct evidence of this upwelling, including transport estimates from ocean measurements, is still lacking. It is suggested, however, by the doming of the thermocline along the northern edge of the Southeast Trades (Figure 14). Although not obvious in SST maps because it is masked by the general meridional temperature increase in that region, it is also suggested by satellite color images that show a chlorophyll maximum in that region [*Murtugudde et al.*, 1999]. As determined from numerical simulations, the region has an annual-mean upwelling transport of 5–10 Sv (*McCreary et al.* [1993]; *Ferron and Marotzke* [2003]; *Miyama et al.* [2003]; Figure 16 below), consistent with the amplitude of the Ekman divergence there (Section 5.1.2).

This upwelling regime points toward the existence of a second overturning circulation, the Indian Ocean STC. The subsurface pathways associated with this cell have not been determined from observations. Possible sources for the thermocline water that supplies the upwelling are subduction in the southeastern Indian Ocean, recirculation from the western Indian Ocean, and the ITF. In the *McCreary et al.* [1993] solution, all the water comes from the second source: Just south of the equator part of the subsurface EACC bends offshore to eastward into the upwelling band (see their Figure 3).

5.1.7. Other overturning cells. There is another regime of southern-hemispheric upwelling along the northwest Aus-

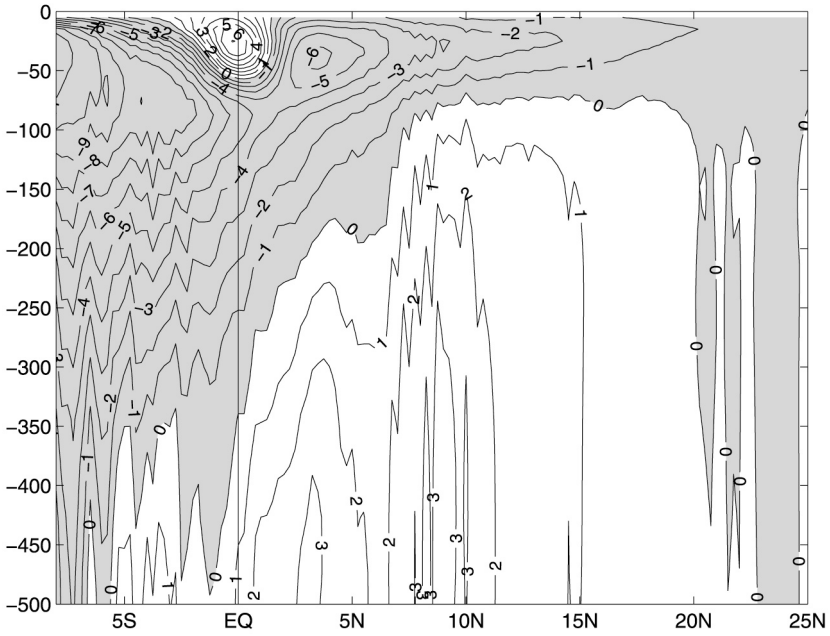

Figure 16. Meridional overturning function of the JAMSTEC model of *Miyama et al.* [2003] for the upper 500 m of the Indian Ocean.

tralian shelf and Arafura Sea, generating another overturning cell. *Godfrey and Mansbridge* [2000] established mass budgets for the combined region based on Ekman and geostrophic currents, estimating an annual-mean upwelling transport of 1.4 Sv (Plate 4), so that cell is weak.

Finally, IOD episodes are marked by westward wind anomalies along the equator, leading to significant uplifting of the thermocline and SST reduction in the eastern equatorial ocean and off Sumatra [*Saji et al.*, 1999; *Feng and Meyers*, 2003], but their contribution to mean upwelling is estimated to be small [*Schott et al.*, 2002a].

5.2. Models

A number of modeling studies have addressed the Indian Ocean overturning circulations [*McCreary et al.*, 1993; *Wacongne and Pacanowski*, 1996; *Garternicht and Schott*, 1997; *Ferron and Marotzke*, 2003; *Miyama et al.*, 2003]. Here, we review results from *Miyama et al.* [2003], who compared solutions to a variety of ocean models: a $1^1/_2$-layer model and a linear, continuously stratified model in order to explore the dynamics of cross-equatorial flows; a $2^1/_2$-layer model without the IT; a $4^1/_2$-layer model with the throughflow included; and the Japan Marine Science and Technology Center (JAMSTEC) global GCM in order to investigate circulation pathways. We also discuss output from the Simple Ocean Data Assimilation (SODA) product of *Carton et al.* [2000] that was analyzed by *Schott et al.* [2002a]. In SODA, a variety of ocean measurements (altimetry, surface temperatures, XBT track-lines, hydrographic stations, etc.) are assimilated into an ocean model, with a horizontal resolution of 1° × 1° at midlatitudes and 1° × 0.45º (longitude–latitude) in the tropics, 20 vertical levels, and a 15-m resolution near the sea surface.

5.2.1. Pathways. Flow pathways in both the model solutions and SODA compare well with the observed currents. The mean surface circulation of SODA shown by current vectors for the upper 15 m (Plate 5) indicates the dominant effect of the summer monsoon, with a northward Somali Current and anticyclonic circulation across the Arabian Sea. The structure of SODA's cross-equatorial Somali Current (Figure 15d–f) compares well with the observed one (Figure 15a–c). On the other hand, in SODA the total cross-equatorial Somali Current transport above 500 m (6.6 Sv) and the thermocline transport in the 50–300 m range (4.1 Sv) are weaker than observational estimates, while its upwelling corresponds to the numbers given above (see below).

The meridional overturning circulation in the JAMSTEC solution (Figure 16) has a cross-equatorial transport of 5 Sv. Of course, the overturning circulation illustrated by this 2-d streamfunction is deceptively simple; for example, the solution's subsurface northward branch occurs mostly in the Somali Current, whereas its near-surface southward branch occurs across the interior of the basin primarily as an Ekman/Sverdrup flow.

Note that the JAMSTEC streamfunction has a well-developed equatorial roll. The existence of the roll is confirmed in model surface trajectories, which sometimes carry out several orbits within the roll before extending into the southern hemisphere. A consequence of the northward surface flow associated with the roll is that model surface drifters only cross the equator in the far-eastern ocean, a property that can be inferred from the structure of the near-equatorial flow field

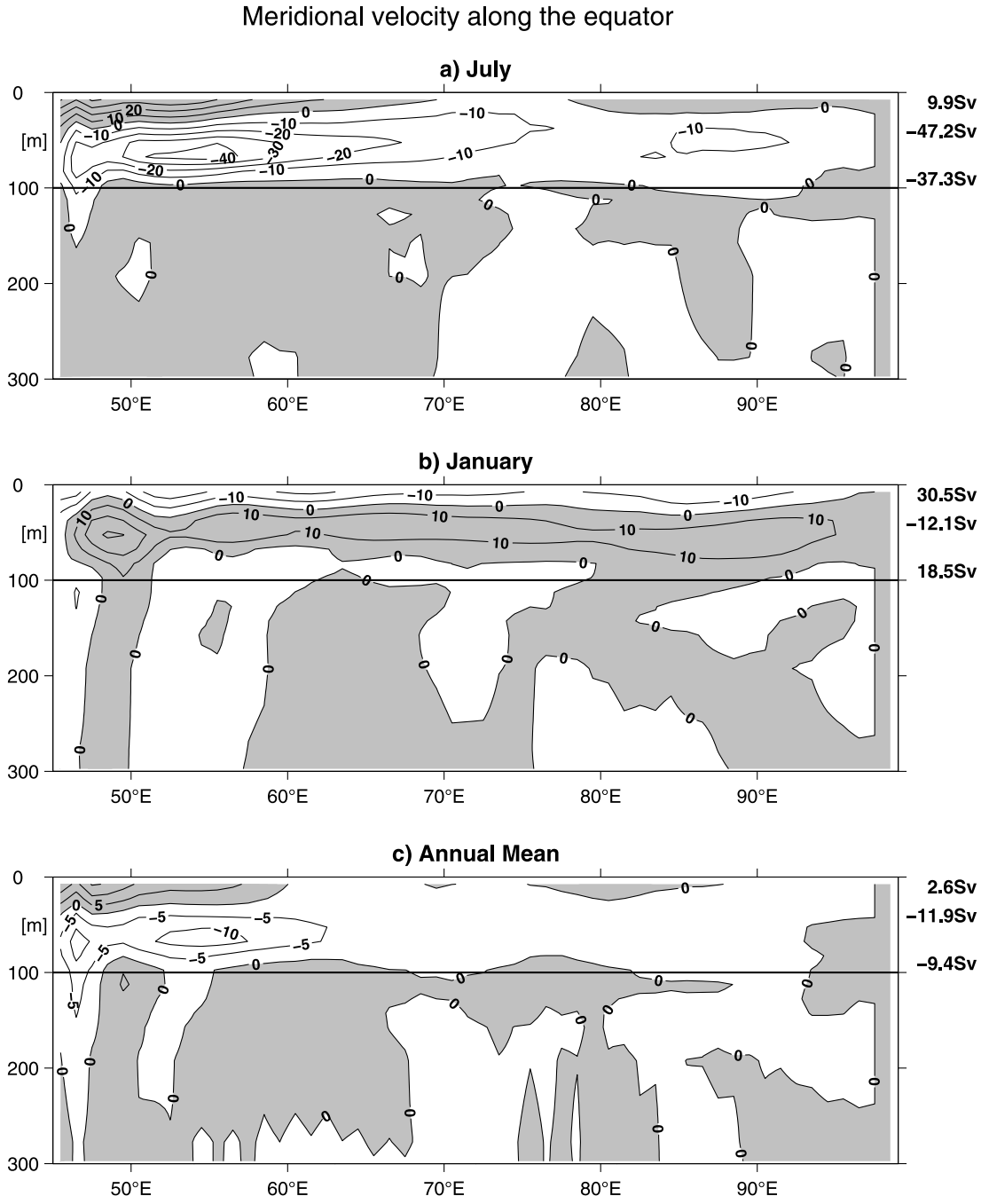

Figure 17. The equatorial roll in the SODA model, shown by the meridional velocities (cms^{-1}), along the equator for a) July, b) January and c) annual mean. Positive (shaded) is northward. Also shown (right margin) are northward, southward and net transports in 0–100-m layer. (From *Schott et al.* [2002a].)

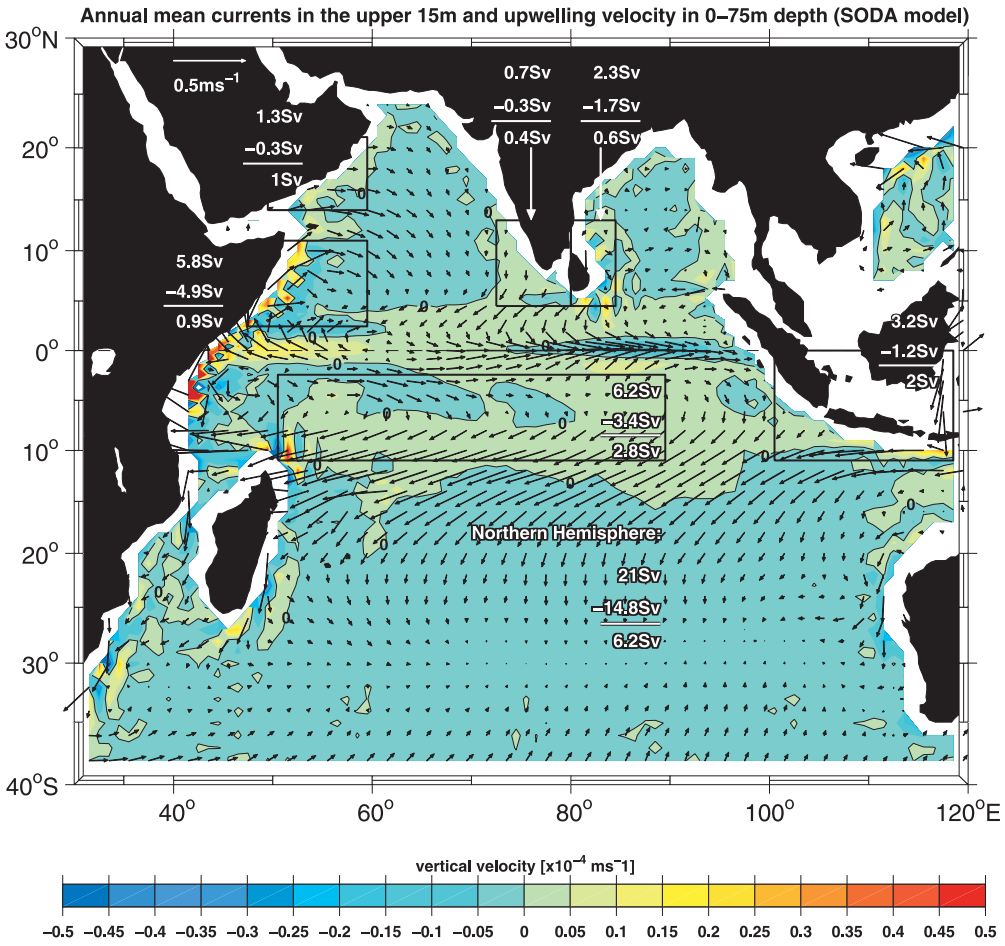

Plate 5. Mean currents (upper 15 m, not every grid point shown; current scale see upper left) and vertical velocity at 75-m depth of SODA model. Shown for marked boxes are upwelling (positive), downwelling (negative) and net transports in Sv across 75-m level. (From *Schott et al.* [2002a].)

(Plate 5). The equatorial roll in the SODA product is developed during the summer monsoon in response to the strong northward winds over the western equatorial ocean, with northward surface flow and southward subsurface flow (Figure 17a); it has a reversed rotation during the winter monsoon (Figure 17b), and is dominated by the summer conditions in the annual mean (Figure 17c).

Miyama et al. [2003] investigated the sources of waters that upwell in the northern hemisphere by tracing particle trajectories backwards from individual upwelling zones. In the JAMSTEC solution, water came from three regions: flow into the basin from south of 30°S, subduction in the southeastern Indian Ocean north of 30°S, and from the Pacific via the ITF. Particles from the Throughflow could follow either a shallow, fast (<4 years) pathway to the upwelling regions or a deep, slow (>10 years) one that involved subduction (Plate 6). The authors provided transports for each of the sources (9.7, 4.7, and 5.1 Sv, respectively, in their Table 2), but were not able to quantify precisely the contribution of each type to the 6-Sv cross-equatorial transport.

5.2.2. Northern-hemisphere upwelling. The model solutions and SODA all produce similar values for the net annual-mean upwelling in the northern hemisphere, a consequence of its being determined by the cross-equatorial Ekman/Sverdrup transport and, hence, solely by the winds. In contrast, the solutions differ markedly in the division of transport between *individual* upwelling regions, indicating that local upwelling is a highly model-dependent process.

Off Somalia, the annual-mean SODA upwelling across 75 m is 5.8 Sv (Plate 5), a value between the low and high estimates of *Schott et al.* [2002a]. This value, however, is nearly compensated by 4.9 Sv of downwelling in the region, yielding an annual-mean upwelling of only 0.9 Sv, much too small in comparison to observed estimates. In the three solutions analyzed by *Miyama et al.* [2003], the net annual-mean upwelling in the region varied from 1.3–3.1 Sv, still somewhat small compared to observations. Off Oman, the net upwellings in SODA and the *Miyama et al.* [2003] solutions vary from 1.0–1.9 Sv, in reasonable agreement with observations. Offshore from southern India and Sri Lanka, there is a total upwelling of 3.0 Sv (1.0 Sv net) in the SODA model (Plate 5), mostly east of 80°E where there is Ekman suction driven by large and positive wind curl. Similarly, the net upwelling transports in the *Miyama et al.* [2003] solutions vary from 1.2–1.8 Sv.

5.2.3. Southern-hemisphere upwelling. For the upwelling band northeast of Madagascar (2–12°S, 50–90°E), *Miyama et al.* [2003] obtained upwelling transports of 5–8 Sv, depending on model type. In SODA, the average upwelling transport across 75 m from 1990–99 is 6.2 Sv, but there was also downwelling of 3.4 Sv across that level, leaving a net upwelling of 2.8 Sv, small compared to the Ekman divergences and model simulations.

6. VARIABILITY

Interest in understanding STC variability stems from its possible influence on equatorial upwelling and SST, and hence climate. So far, observational evidence of STC variability is restricted to the Pacific because of its exceptional coverage of the near-equatorial zone over the past two decades. While modes of variability involving subtropical-tropical SST and ocean advection have also been determined for the Atlantic (e.g., *Huang and Shukla* [1997]) and Indian (e.g., *Xie et al.* [2002]) Oceans, observational evidence for the involvement of the STCs or CEC (Indian Ocean) in climate anomalies in these oceans is so far not available.

6.1. Observations

6.1.1. Pacific. In the North Pacific, one manifestation of Pacific decadal variability is a contrast between anomalously cold SSTs in the center of the basin with anomalously warm SSTs around the eastern boundary, and vice versa [*Mantua et al.*, 1997]. Analysis of subsurface temperature data suggests that when these anomalous SSTs subduct, they gradually propagate downward and southwestward to cool or warm the subtropical thermocline [*Deser et al.*, 1996]. Without salinity data, however, it is difficult to determine whether these anomalies result from changes in the temperature-salinity (T-S) properties of the subducted water or from wind-forced changes in the pycnocline depth.

Considerably less work has been done on the variability of air-sea fluxes and subduction in the South Pacific. This lack is due partly to the relative dearth of oceanic and atmospheric observations there, and partly to the perception that the region exhibits little low-frequency variability; however, a study of the NCEP reanalysis product did show low-frequency variability in the southern hemisphere with a character and magnitude similar to that seen in the north [*Garreaud and Battisti*, 1999]. *Kessler* [1999] provides one of the few pertinent studies of South Pacific variability, focusing on T-S properties of the core isopycnal in the salty tongue of subtropical water that reaches the equator to feed the EUC, a shallow feature that overlies the mode water formed just to its south [*Wong and Johnson*, 2003]. He showed that there is considerable interannual variability along 5–10°S, attributing it to advection and changes in the SEC associated with El Niño. Additionally, there is an interdecadal trend over the record length from 1983–1997, with

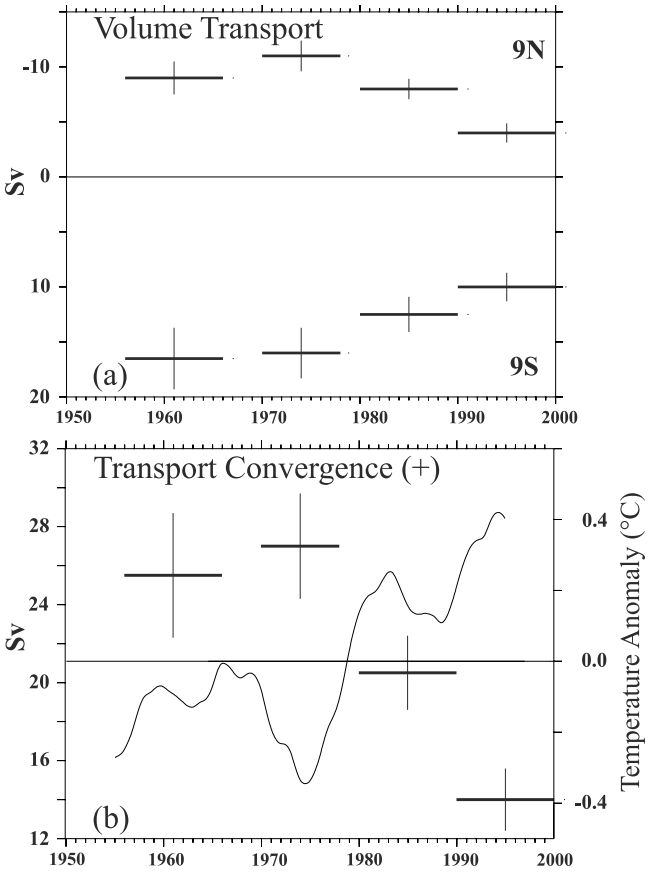

Figure 18. STC variability in the Pacific during 1955–2000, documented by decadal means of a) interior equatorward geostrophic thermocline transports across 9°N and 9°S and b) their sum, showing decrease of STC thermocline convergence from 27 Sv in the 70's to 14 Sv in the 90's; simultaneously, a warming of the equatorial Pacific (curve in b) by about 0.6°C is observed. (From *McPhaden and Zhang* [2002].)

a tendency toward a warmer, saltier tongue, for which he could find no satisfactory explanation.

In their upwelling study (see Section 3.2.4), *Meinen et al.* [2001] also examined the seasonal-to-interannual variability of equatorial upwelling across 50 m in an equatorial box extending from 5°S to 5°N and from 155°E to 95°W. On seasonal time scales, the divergence is mostly determined by variations in zonal geostrophic and meridional Ekman transports. During the 1997–1998 El Niño, the meridional geostrophic convergence was nearly eliminated as the thermocline flattened and the Ekman divergence was reduced even more, halving the upwelling across 50 m. During La Niña phases, they found increased Ekman transports and divergences due to the strengthened trades. It is not clear, however, that these changes represent variations in STC strength, since the edges of the box are located well inside the tropics, not near the subtropical/tropical boundary.

Evidence for interdecadal variability of the strength of the Pacific STCs was recently documented by *McPhaden and Zhang* [2002]. They determined the interior, geostrophic, equatorward convergences across 9°S and 9°N during the past 50 years (Figure 18a), finding that the total convergence reduced from 27±1 Sv during the decade before the mid-1970's regime shift [*Mantua et al.*, 1997] to only 14±1.5 Sv in the 1990's (Figure 18b). There were comparable reductions in estimates of the same quantities when the Sverdrup relation was applied to various wind products, as well as in the poleward Ekman transports. They inferred a weakening of both the North and South STCs over this time period, and hence of the equatorial upwelling. In support of this idea, they noted that there was a gradual increase in NINO3 SST during the same time span.

6.1.2. Atlantic. Aspects of the Atlantic STCs exhibit interannual-to-decadal variability. There are equatorial SST anomalies at interannual periods, corresponding to an Atlantic ENSO, and also at decadal periods [*Carton et al.*, 1996; *Huang and Shukla*, 1997]. The Ekman divergence between 10ºN and 10ºS has amplitudes of several Sverdrups at these time scales (Plate 1), and temperature variability at thermocline levels has been documented in several studies. The transfer of South Atlantic thermocline waters by North Brazil Current rings (Section 4) also undergoes longer period variations [*Goni and Johns*, 2003], which likely has consequences for the distribution of water masses and STC pathways. To date, though, there is no Atlantic counterpart to the *McPhaden and Zhang* [2002] Pacific STC variability study that would point toward these individual variations being collectively associated with Atlantic STC variability.

6.1.3. Indian Ocean. In the Indian Ocean, interannual variability occurs in both the Cross-equatorial Cell (CEC; Section 5.2.3) and in the STC of the southern hemisphere (Section 5.1.6). Variability of the cross-equatorial heat transport was suggested by *Loschnigg and Webster* [2000] to affect northern hemisphere SST and thereby to influence the following monsoon. In the southern hemisphere, tropical and subtropical anomalies associated with IOD events [*Saji et al.*, 1999; *Feng and Meyers*, 2003] have been found to affect SST strongly at interannual time scales in the upwelling zone northeast of Madagascar. The upwelling is interrupted by Rossby waves arriving from the east that increase upper-layer thickness and SST, causing increased atmospheric convection and enhanced cyclogenesis [*Webster et al.*, 1999; *Xie et al.*, 2002]. Since anomalous Ekman downwelling is involved, this phenomenon may be considered to be an anomaly of the Indian Ocean's southern-hemisphere STC. Similarly, the upwelling

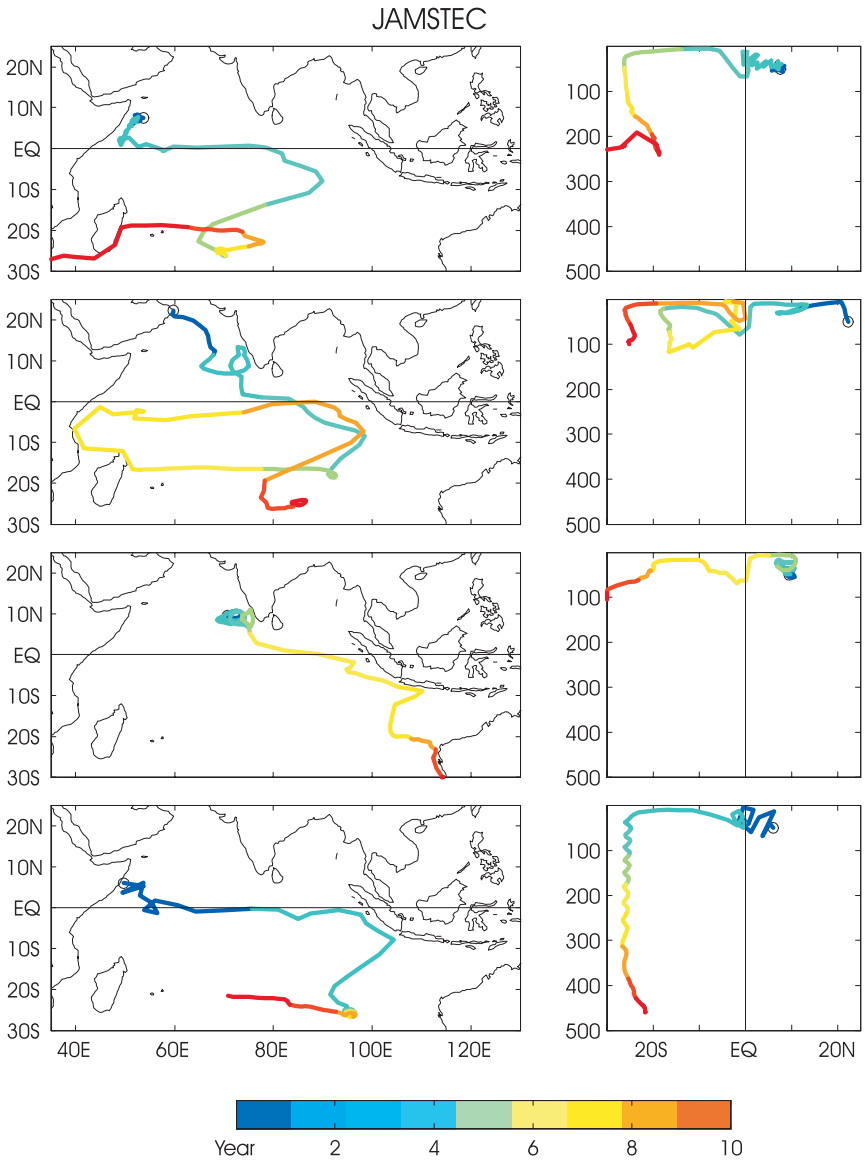

Plate 6. Typical Indian Ocean particle trajectories in the JAMSTEC model studies by *Miyama et al.* [2003], traced backward from the upwelling to the subduction zones, showing x–y and y–z views in corresponding left and right panels.

off Sumatra undergoes substantial variations [*Susanto and Gordon*, 2001; *Feng and Meyers*, 2003], also suggesting shallow cell anomalies.

6.2. Models

A number of recent modeling studies have been carried out to investigate the role of STC variability in climate variability. Two processes have been proposed for this influence. In one process, SST anomalies are subducted into the thermocline in the eastern subtropics, are advected to the equatorial ocean at thermocline levels with a time lag of the order of a decade, and influence equatorial SST when they upwell there (the $\bar{\mathbf{v}}T'$ hypothesis, first proposed by *Gu and Philander* [1997]). In the other, STC strength responds to interannual-to-decadal variability of the winds, thus altering the amount, rather than temperature, of the water that is upwelled in the equatorial cold tongue (the $\mathbf{v}'\bar{T}$ hypothesis; *Kleeman et al.* [1999]).

6.2.1. $\bar{\mathbf{v}}T'$ processes. Existing solutions suggest that $\bar{\mathbf{v}}T'$ processes are not adequate for generating equatorial SST anomalies of realistic amplitude at decadal time scales. In the Pacific, *Schneider et al.* [1999] reported a weak response in their wind-forced GCM solution, noting that northern-hemisphere isopycnal-thickness anomalies (assuming a climatological T-S relationship) were advected equatorward by the mean circulation, but only as far south as 18°N; equatorward of that latitude, temperature anomalies resulted from changes in the pycnocline depth forced by local wind variability. *Nonaka and Xie* [2000], *Shin and Liu* [2000], and *Hazeleger et al.* [2001] also noted a weak equatorial response in their GCM solutions forced by realistic midlatitude temperature anomalies.

Schneider [2000] discussed the potential climatic influence of "spiciness" anomalies in the Pacific region of his coupled-model solution. Spiciness anomalies are temperature anomalies accompanied by salinity anomalies such that there is no density change. He noted that such anomalies were subducted into the thermocline in the subtropics and subsequently advected to the equator by the STCs, where they perturbed tropical climate. Essentially, spiciness anomalies behave like "passive" tracers, which do not feedback to affect the pressure field and, hence, the circulation. (In contrast, a temperature anomaly alone is an "active" tracer that does affect pressure.) *Liu and Shin* [1999], *Nonaka et al.* [2000], and *Nonaka and Xie* [2000] have considered the propagation of both active and passive tracers, the latter study concluding that uncompensated temperature anomalies propagate less readily to the equator than a passive tracer.

In the Atlantic, *Lazar et al.* [2001] inserted a warm temperature anomaly (2.2°C) into the eastern subtropical subduction area of their OGCM, and followed its propagation across the South Atlantic and to the equator for a period of 10 years; during years 6–8, there was an increase in equatorial temperature along the $\sigma_\theta = 25.3$ kg m^{-3} surface, but only by 0.2°C. Noting an increase in the anomaly across the South Atlantic, the authors conclude that they are not just passively advected along with the mean thermocline flow but are partly salinity-compensated (a partial spiciness anomaly), indicating the need to observe both salinity and temperature variability in STC studies. They also concluded that, in addition to mean advection, wave processes associated with such dynamic anomalies need to be taken into account.

6.2.2. $\bar{\mathbf{v}}T'$ processes. Concerning $\bar{\mathbf{v}}T'$ processes, *Klinger et al.* [2002] used a $3^1/_2$-layer ocean model (a thermodynamic version of the *Lu et al.* [1998] model discussed in Section 3.3) to investigate the influence of switched-on and periodic, off-equatorial winds on the Pacific STCs and equatorial SST. They showed that decadal wind anomalies along the tropical-subtropical boundary can alter the STC transport, leading to significant changes in equatorial SST, whereas wind anomalies at midlatitudes do not. They also showed that the various STC branches respond at quite different time scales, with the surface branch adjusting much more rapidly than the subsurface one. As a result, only at periods considerably longer than a decade can STC variability be assumed to be quasi-steady. It follows that quasi-steady theories of climate variability (e.g., *Huang and Pedlosky* [1999]) should be viewed with caution.

Nonaka et al. [2002] confirmed the importance of tropical-subtropical wind anomalies in causing STC variability in their GCM solution forced by NCEP reanalysis winds. They showed that at decadal time scales weaker (stronger) STC transports are associated with warmer (cooler) equatorial SST anomalies (Plate 7a) and more (less) heat content (Plate 7b). (The green-dashed line in Plate 7a is a trend in STC strength, removed from the green curve. It indicates that the model STCs weakened by 6 Sv from 1965–1990, consistent with but weaker than the observed weakening noted by *McPhaden and Zhang* [2002].) In contrast, there was no such relationship at interannual time scales, pointing toward fundamentally different dynamics for interannual and decadal variability (see their Figure 2). They also noted the importance of forcing by near-equatorial, decadal winds, concluding that the model's decadal variability was initiated by near-equatorial wind anomalies and subsequently maintained by STC variability. Finally, they noted that there was a phase difference between two different measures of STC strength, with a measure based on heat transport $\mathcal{V}'$ leading another based on the two-dimensional streamfunction $\Delta\psi'$ (compare blue and green curves in Plate 7a), pointing toward the need for a definition of STC variability that takes into account the different spinup times of the various STC branches.

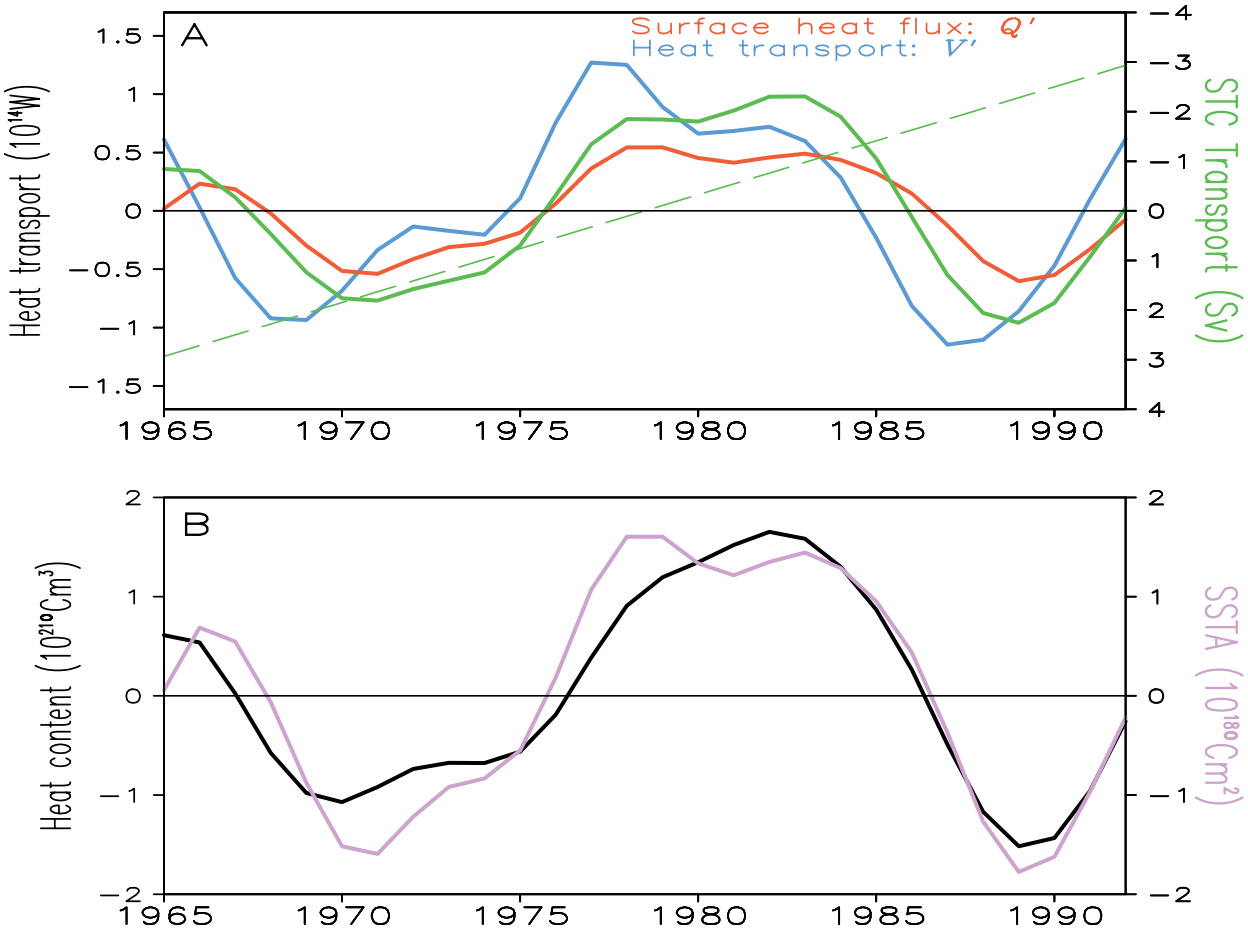

Plate 7. a) Decadal anomalies of heat transport $\mathcal{V}'$ across 10°S and 15°N (blue line; left axis), surface heat flux Q' integrated over the area extending across the Pacific and from 10°S and 15°N basin A (red line; left axis), and STC strength $\Delta\psi'$ (green solid line; right axis) for a solution forced by winds without equatorial anomalies (Solution NoEQ). b) Decadal anomalies of heat content from 10°S to 15°N and from the surface to 500 m H' (black line; left axis), and SST anomalies averaged over area A (purple line; right axis) for solution NoEQ. Trends are removed from all curves, with the trend of $\Delta\psi'$ plotted in the green dashed line in a). The $\Delta\psi'$ curves are reversed for easy comparison with other curves. (From *Nonaka et al.* [2002].)

Kleeman et al. [1999] and *Solomon et al.* [2003] developed an intermediate coupled model to explore the potential influence of STC variability. Their solutions developed two modes of oscillation: an ENSO-like interannual mode (~4 year) and a decadal one (~13 year). The decadal mode was generated in northern midlatitudes, and was similar in structure to the *Latif and Barnett* [1994] mode. It was found to influence the equatorial cold tongue by altering the transport of the ocean model's northern STC ($\mathbf{v}'\overline{T}$ hypothesis), thereby causing ENSO Decadal Variability (EDV). The STC transport was determined largely by the Ekman transport across the edge of the tropical warm pool, thereby linking subtropical wind variability to equatorial SST anomalies. *Solomon et al.* [2003] noted that for weaker midlatitude coupling, the decadal mode was damped but could still be maintained by tropical air-sea interactions (the ENSO mode) through tropical-to-midlatitude atmospheric teleconnections. In this parameter range, then, both tropical and midlatitude processes are required to cause PDV and EDV, a property consistent with the conclusions of *Nonaka et al.* [2002].

Latif and Lohmann [2003, pers. comm.] discussed Atlantic SST anomalies in a solution to the MPI OPYC coupled model. They found that, although Atlantic anomalies existed at decadal time scales, they had small amplitudes in the tropics compared to those in the Pacific. Since the Atlantic STC anomalies last for decadal time scales, though, they may still be climatically significant.

7. SUMMARY AND CONCLUSIONS

We have reviewed observational evidence and model results for the STCs in all the oceans and for the CEC in the Indian Ocean. Here, we summarize our findings and comment on outstanding issues.

7.1. Theory

Basic STC dynamics can be understood within the framework of a $2^1/_2$-layer model (Section 2). In this model, the existence and strength of the STCs is determined by the tradewinds across the subtropical/tropical boundary: They cause poleward Ekman drift that drains near-surface water out of the tropics by Ekman drift, thereby forcing a compensating return flow (Section 2.2). The existence of subsurface, equatorward currents in the interior ocean results from the nonlinear terms in Eqs. (1), which require that subsurface flow follows equatorward-bending characteristics (Section 2.3; *Luyten et al.* [1983]). Two key characteristics are the shadow-zone x_e [Eq. (6)] and bifurcation x_b streamlines (Figure 1): Only subsurface water located between these two streamlines flows to the equator to participate in the STC, the water west of x_b recirculating poleward within the subtropical gyre. Thus, it is primarily thermocline water subducted in the eastern subtropics that participates in the STCs. Thermocline water can flow directly to the equator in the interior ocean (the interior pathway) provided that $x_e(0) > 0$ (as for the dashed curve in Figure 1; Section 2.4). The ITCZ, however, can distort or even block interior pathways, by bending characteristics more to the west on its northern flank where $|w_e|$ is small. If the ITCZ is sufficiently strong, $x_e(y)$ intersects the western boundary before it can approach the equator even if $x_e(0) > 0$. For a weaker ITCZ, it first bends westward but then returns eastward to extend to the equator, creating a sinuous interior pathway, for example, as in Figs. 8 and 9. According to (5), the ITCZ's influence on characteristics has a convenient interpretation in terms of wind-driven currents, with characteristics bending westward in the NEC and eastward in the NECC. Another interpretation is that the ITCZ creates a "PV barrier" by uplifting stratified waters with high PV, thereby forcing low-PV subducted waters to take a westward detour around these zones.

7.2. Pacific and Atlantic Oceans

7.2.1. Subduction. Available estimates of subduction rates were obtained by combining Ekman transports determined from climatological winds with referenced geostrophic currents from the mean hydrographic data base. Using this approach, estimates of the total subduction rates in both hemispheres are large, 35 Sv (27 Sv) and 44 Sv (23 Sv) for the North and South Pacific (Atlantic), respectively [*Huang and Qiu*, 1998; *Karstensen and Quadfasel*, 2002]. Only fractions of these totals, however, are subducted in regions with pathways that extend to the equator and density classes that upwell there. It should also be noted that subduction is not restricted to the subtropics, a consequence of the lateral-induction term that results from near-surface flow across a negative gradient of mixed-layer thickness; it can happen even in low latitudes where the Ekman pumping is weak or absent [*Karstensen and Quadfasel*, 2002]. By definition, however, tropical subduction should not be considered part of the STC.

7.2.2. Interior and western-boundary pathways. In the Pacific and Atlantic Oceans, thermocline water moves to the equator via western-boundary and interior pathways (Plates 2 and 3). In the North (South) Pacific, about 14 Sv (15 Sv) of thermocline water takes the western-boundary pathway, with the northern branch first feeding the NECC before joining the EUC and the southern branch moving directly to the equator in the NGUC. Actually, the northern western boundary current carries 23 Sv southward, but about 9 Sv of this North Pacific water feeds the Indonesian Throughflow near the equator.

In the North (South) Atlantic, the western-boundary pathway carries about 3 Sv (12 Sv) to the EUC, the northern branch being nearly blocked by the MOC (see Section 7.4). In the Pacific, the transports of the interior pathways were recently quite well determined by *Sloyan et al.* [2003], who applied a box inverse model to the multitude of direct current observations compiled along cross-sections by the TAO project. They found 5 Sv for the northern interior pathway and 15 Sv for the southern one (Plate 2). In the Atlantic, preliminary estimates of STC transports were derived by *Zhang et al.* [2003] based on geostrophic currents derived from the climatological hydrographic data base, yielding 2 Sv for the northern and 4 Sv for the southern interior STC transport (Plate 3). The interior equatorward STC pathways (dotted in Plates 2 and 3) are deflected eastward (by the NECC) and westward (by the SEC), and therefore particles have to describe wide excursions before joining the EUC (Figs. 8 and 9).

7.2.3. Equatorial currents. The Pacific and Atlantic EUCs are the primary equatorial branches of the STCs. In the western regions, they are both predominantly supplied from the southern hemisphere by the NGUC and NBUC, respectively (Plates 2 and 3), a consequence of interactions with interocean circulations (see Section 7.4 below). The EUCs in both oceans slant upwards across isopycnals to the east (e.g., Figure 5d) with maximum transports of about 40 Sv and 20 Sv, respectively. They seem to terminate near the eastern boundary, and a clear connection to the eastern-boundary circulations has not been established. Water-mass properties, however, suggest that EUC water flows southward, rather than northward, near the eastern boundary.

There are off-equatorial undercurrents in each ocean, located 3–5° on either side of the equator, the NSCC and SSCC (or Tsuchiya Jets) in the Pacific and the NEUC and SEUC in the Atlantic. Source waters for these flows appear to be western-boundary currents, with the exception of the SEUC for which the connection to the NBC retroflection region is not clear [*Arhan et al.*, 1998; *Schott et al.*, 1998]. They diverge poleward [*Johnson and Moore*, 1997; *Rowe et al., 2000*] as they flow eastward, as shown schematically in Plates 2 and 3. They are merged with the EUC in the western Pacific (Figure 5), but are clearly separate from the EUC in the western Atlantic (Figure 11b). The role of these currents in the STCs, if any, is still a matter of debate. For one thing, they occupy a certain density range that can block interior STC pathways (Figs. 4, 5). Indeed, the SEUC is estimated to block about 1 Sv out of 4 Sv interior thermocline flow across 6°S (*Zhang* [2003, pers. comm.]; dotted line in Plate 3). They can perhaps be viewed as a deep STC branch that upwells in off-equatorial regions. At present, though, their relation to eastern upwelling has not been quantitatively documented.

There is a region of Ekman convergence on either side of the equator, a consequence of the poleward increase of $|f|$. In response, water appears to downwell there and return to the equator at the top of the thermocline or even within the surface mixed layer, to form Tropical Cells (called Equatorial Cells in the latter case by *McCreary and Lu* [1994]). This tendency is particularly prominent at the northern edge of the Southeast Trades (4–6°N), where there is strong convergence associated with weaker winds in the ITCZ. For the Pacific, *Sloyan et al.* [2003] estimated the combined northern and southern TCs to have a strength of 35 Sv (with large error bars), whereas for the Atlantic *Grodsky and Carton* [2003] estimated the transport of the northern TC to be only 4 Sv based on drifter convergences. The TCs are also prominent features in numerical solutions; however, because they occur at shallow levels with little diapycnal exchange, their strength is much reduced when calculated in density coordinates [*Hazeleger et al.*, 2001]. The existence of the TCs requires that any measure of STC strength based on surface transports occurs poleward of the TC convergences (about 7°).

7.2.4. Upwelling. Because upwelling velocities are so small (∼1 m/day), upwelling transports are typically estimated indirectly, by calculating the horizontal transport divergence out of a closed box surrounding the region of interest. A complicating factor with this approach is that estimates depend on the chosen depth of the box, so that the calculation should be repeated for a range of depths to determine the maximum upwelling. In addition, the EUC shoals to the east, so the method typically yields higher values than the actual, across-isopycnal transport.

Applying these procedures to the central and eastern Pacific, *Sloyan et al.* [2003] estimated 37±4 Sv of equatorial upwelling in their box inverse model analysis, which is the best available estimate. For the Atlantic, with much less complete observational coverage, only local estimates of upwelling transports have been possible. It should be noted that equatorial upwelling alone is not a measure of STC strength, it has to be corrected for the contribution of the TCs, which never reaches the subtropics. There are no quantitative estimates of eastern-boundary and dome upwelling in either ocean that are based on modern methods.

Upper limits for upwelling transports can be determined from wind-stress divergences. For the Pacific, the total Ekman divergence across 10°S and 10°N is 54 Sv (for NCEP reanalysis stresses) and the coastal and dome upwelling is 10 Sv (Figure 2b). For the Atlantic, the divergence across 10°N and 10°S is 23 Sv; the divergence along coasts and in domes is also 10 Sv (Figure 10c), a significant amount in comparison to the Atlantic's equatorial upwelling.

7.2.5. Poleward surface flows. There is poleward Ekman drift of the surface flow field from the equator to the subtropics, the basic driving force of the STCs (Figs. 2b, 10c). At the same time, surface water is deflected westward by the NEC and SEC and eastward by the NECC on its way north. Therefore, surface pathways (Figure 6, Plate 2) are as sinuous as subsurface interior pathways (Figs. 8, 12), and much of the poleward return flow of the STC ends up westward of the subduction sites (Plates 2, 3). Direct closure within the STC is thus not possible for this flow, leading to interactions with the subtropical gyre and Subpolar Cell (SPC).

7.3. Indian Ocean

The Indian Ocean is unique among the three oceans, in not possessing an eastern upwelling zone and cold tongue. Instead, the mean equatorial winds are westerly, making the equator a downwelling regime so that the upwelling branches of the overturning cells all occur off the equator. In the annual mean, almost all subduction occurs in the southern hemisphere. Some of the subducted water upwells in the southern hemisphere, but a significant portion upwells north of the equator, thereby forming the Indian Ocean's distinctive CEC.

Almost all subduction occurs in the southern hemisphere. It is estimated to be 36 Sv, out of which 12 Sv enter density classes that can upwell in the northern hemisphere [*Karstensen and Quadfasel*, 2002]. The subducted waters flow westward in the SEC alongside waters originating from the ITF and joined by northward recirculation from the southern subtropics (Plate 4), so that it is not clear just what is the final mix of waters that supply the CEC. In the numerical solutions reported by *Miyama et al.* [2003], subsurface water also flows across 30ºS to participate in the CEC. There is also a small amount of subduction in the northern Arabian Sea, that might feed the upwelling there (Plate 4).

One measure of the strength of the CEC is the southward, near-surface transport across the equator (analogous to $M_1(y_d)$ in (2) for the STCs). For the particular mean wind field of the Indian Ocean, in which τ^x is roughly proportional to y near the equator, the cross-equatorial Sverdrup transport is nearly equal to the Ekman transport, a consequence of the property that

$$\lim_{y\to 0} \tau^x/f = \tau^x_y/\beta$$

for $\tau^x \propto y$ [*Godfrey et al.*, 2001; *Miyama et al.*, 2003]. *Schott et al.* [2002a] demonstrate this near-equality, finding that the winds drive a southward Ekman-Sverdrup transport of about 6 Sv. Consistent with this value, the CEC is closed by northward flow of the Somali Current at the thermocline level, which is also close to 6 Sv in western boundary observations (Figure 15). This strength is also consistent with the overturning streamfunction of the JAMSTEC GCM solution and other high-resolution models (Figure 16).

During the Southwest Monsoon, upwelling occurs in the northern hemisphere, mostly along the coasts of Somalia and Oman where it is driven by the intense Findlater Jet. It extends offshore from Somalia in wedges between large quasi-stationary gyres (the Southern Gyre and Great Whirl) and from Oman in filaments that extend well into the interior of the northern Arabian Sea (Plate 4). Model studies also suggest that there is open-ocean upwelling south of India and Sri Lanka, but observational evidence is not available to quantify it.

In addition to the CEC, the Indian Ocean appears to have another prominent overturning circulation confined to the southern hemisphere, the Indian Ocean STC. It is associated with upwelling driven by Ekman pumping along the northern edge of the Southeast Trades from 5–10°S (Plate 4). This cell was first reported in the modeling study of *McCreary et al.* [1993]. *Murtugudde et al.* [1999] noted its influence on ocean color.

7.4. Influence of Interocean Circulations

In the Pacific and Atlantic Oceans, one might expect the STCs to be nearly symmetric about the equator based on the structure of the wind fields that drive them (with poleward Ekman transports roughly equal in both hemispheres), but they are not. In the Atlantic, the reason for the asymmetry is the northward transport of 15–20 Sv by the warm limb of the Atlantic MOC. It strengthens the southern STC, but weakens the northern one so much that only small equatorward thermocline flow is observed in the northern hemisphere (Plate 3). In the Pacific, the asymmetry is due to the ITF with an estimated transport of 10–15 Sv [*Ganachaud et al.* 2000; *Sloyan et al.*, 2003]. The ITF is supplied by thermocline and intermediate water from the South Pacific, which must cross the equator and upwell to shallower levels before eventually merging into the ITF in the Makassar Strait (Plate 2). Thus, it also acts to strengthen the southern STC and weaken the northern one. Its effects, however, are less apparent than those of the Atlantic's MOC because of the much larger transports of the Pacific STCs.

In the Indian Ocean, the ITF alters the mix of waters that participate in the CEC. Water-mass properties indicate that a portion of ITF water participates in the cross-equatorial Somali Current but the ITF influence on CEC pathways is not clear. As the (model) surface pathways in Plate 4 indicate, the cross-equatorial return CEC flow from the northern upwelling sites can arrive west of the subduction regime, thus feeding into the gyre return flow or even into exchanges with the Atlantic.

7.5. STC Variability and Climate

Because the STCs account for a significant amount of poleward heat transport [*Talley*, 2003], their variability has been hypothesized to be involved in climate. In one hypothesis ($\mathbf{v}'\overline{T}$ processes), temperature anomalies subducted into the thermocline at midlatitudes are advected to the equator, where they upwell to affect SST [*Gu and Philander*, 1997]. In the other $\mathbf{v}'\overline{T}$ processes, variability in the strength of the STCs leads to SST anomalies [*Kleeman et al.*, 1999].

There is little observational evidence to support either hypothesis. In support of the former, *Deser et al.* [1996] reported the downward and equatorward propagation of temperature anomalies, but they did not follow them to the equator. In support of the latter, *McPhaden and Zhang* [2002] reported a decrease in the equatorward transport convergence across 9°N and 9°S in the Pacific Ocean from 27 Sv during the 1970's to about half that value during the 1990's. There was a similar decrease in Ekman transport divergence across these latitudes during the same time period, as well as an increase of equatorial SST by about 0.6°C (Figure 18b). A recent update of this calculation to 1998–2003 reveals a rebound of the STC strength associated with an SST cooling [McPhaden and Zhang, pers. comm., 2004].

Modeling studies generally suggest that $\overline{\mathbf{v}}T'$ processes do not generate significant equatorial SST anomalies [*Schneider et al.*, 1999; *Nonaka and Xie*, 2000; *Hazeleger et al.*, 2001; *Lazar et al.*, 2001], although there is an indication of the potential influence of spiciness anomalies [*Schneider*, 2000]. In contrast, ocean-only models forced by wind anomalies along the subtropical/tropical lead to changes in STC strength that, in turn, cause variations in equatorial SST that are consistent with observed decadal variability [*Klinger et al.*, 2002; *Nonaka et al.*, 2002], and intermediate coupled models have demonstrated the potential feedback of STC-driven SST anomalies to the atmosphere [*Kleeman et al.*, 1999; *Solomon et al.*, 2003]. A noteworthy result of the ocean-model studies is that the STC response is not quasi-steady even at quite low frequencies (periods of 10 years and longer), the surface branch responding more rapidly than the subsurface one.

7.6. Conclusions

We are only beginning to understand the role of STCs in ocean circulation and climate. Even their mean transports and pathways are still poorly determined from observations, and there are significant differences in their representation in different model types. In the Pacific our quantitative knowledge is fairly advanced [*Meinen et al.,* 2001; *Sloyan et al.*, 2003; *McPhaden and Zhang*, 2002] due to the continuous observational efforts related to the El Niño Southern Oscillation (ENSO) observing system [*McPhaden et al.*, 1998]. In contrast, the existing Atlantic data base is much weaker: Only in the western tropical Atlantic have continuous observations of western boundary STC components been started [*Molinari et al.*, 2003; Schott *et al.*, 2003].

There is a particular need for observational work to determine pathways of thermocline flow between identified subduction regions and the EUCs, as well as the potential participation of the off-equatorial undercurrents (NSCC and SSCC in the Pacific; NEUC and SEUC in the Atlantic) in the STCs. One method of pursuing STC pathways involves deploying Autonomous Profiling Explorers (APEX) that drift at shallow levels to provide velocity information there, but take temperature and salinity profiles to deeper levels at preselected time intervals to provide water mass information. As shown for the tropical Atlantic [*Schott et al.*, 2002b], however, floats at constant levels are of reduced usefulness as tracers for STC pathways since they cross density surfaces. Instead, isopycnic RAFOS floats are needed, which can be analyzed as true density-surface followers similar to model Lagrangian studies (e.g., Figure 9a).

Regarding the surface circulation, the Atlantic is lacking not only in data on subsurface zonal currents but also in surface drifter data. In the Pacific, surface drifter data are sufficiently dense to quantify mean STC pathways, equatorial divergence, and off-equatorial TC convergence [*Johnson*, 2001]. In contrast, surface drifter data are much more sparse in the tropical Atlantic, especially in the east, making such estimates uncertain there [*Grodsky and Carton*, 2002; *Molinari et al.*, 2003].

Large uncertainties also surround subduction and upwelling by the STCs. So far, estimates of mean subduction rates have been limited to the evaluation of historical data sets. When fully implemented, the Array for Realtime Geostrophic Oceanography (Argo) Program [*Argo Science Team*, 1998] will provide sufficient CTD data from profiling floats to estimate nearly global fields of large-scale interior geostrophic circulation and mixed-layer properties. These data, combined with satellite scatterometer winds fields, should allow large-scale estimates of the temporal evolution of subduction from season to season. In addition, time series are required to understand the influence of high-frequency small-scale forcing in subduction. Regarding upwelling, we noted that the relation between the various zonal equatorial currents and the eastern coastal and dome upwelling zones is still largely unknown, although Ekman transport divergences hint at some importance of these zones for the STCs. Focused process studies are needed to fill these knowledge gaps.

For determining potential STC predictability, transports by the STC branches need to be measured continuously at key locations, and then related to indicators of STC strength (such

as Ekman divergence at 10ºS/10ºN), to equatorial SST variability, and to model simulations. Key locations are the low-latitude western boundary currents and cross-equatorial sections in the interior ocean, to measure the transports of the western-boundary and interior STC pathways, respectively. The interior observations, which are already underway in the Pacific, need to be extended meridionally beyond the latitudes of the TC convergences. While seasonal ship sections might provide sufficient temporal coverage for the STC variability time scale (Plate 7), aliasing by Tropical Instability Waves (and possibly their role in STC currents and stratification) may be substantial, requiring longer-term moored stations. Several such studies are presently being discussed within the international Climate Variability and Predictability studies (CLIVAR) program.

Regarding modeling studies, it is important to determine the causes (model resolution, mixing parameterizations, forcing, etc.) for the considerable differences in mean STC transports and pathways among models. It is equally important to understand the processes that govern STC variability and its influence on equatorial SST in greater detail. Finally, models can be used to develop a comprehensive measure for STC strength and variability; there are indications that variability of the meridional streamfunction, which implicitly assumes that surface and subsurface branches respond at the same time scale, is not adequate.

In conclusion, we have shown here that STCs and the CEC play important roles in the mean circulation of all three tropical-subtropical oceans, and that there is evidence for their participation in climate anomalies. We are, however, only at the beginning to develop a quantitative understanding of the overturning circulations and their variability. Further progress requires new dedicated observational activities and modeling efforts.

Acknowledgments. We thank Rena Schoenefeldt, Verena Hormann and Jens Schafstall (all of IFM-GEOMAR) for help with the graphic presentations; J. Karstensen (IFM-GEOMAR) for supplying subduction transports for the three southern oceans, and Lothar Stramma (IFM-GEOMAR) for critical readings of several versions of the manuscript. Fritz Schott acknowledges support from the German CLIVAR program through Contract 03F0246A. Julian McCreary acknowledges support from the Frontier Research System for Global Change through its sponsorship of the IPRC. Gregory Johnson acknowledges support from the NOAA Office of Oceanic and Atmospheric Research. This manuscript is SOEST contribution No. 6350, IPRC contribution No. 265, and PMEL contribution No. 2623.

REFERENCES

Argo Science Team, On the design and implementation of Argo: An initial plan for a global array of profiling floats, *International CLIVAR Project Office Report 21*, 32 pp., 1998.

Arhan, M., H. Mercier, Y. Gouriou, and B. Bourlès, Hydrographic sections across the Atlantic Ocean at 730'N and 430'S, *Deep Sea Res.*, *Part I*, *45*, 829–872, 1998.

Blanco, J. L., A. C. Thomas, M.-E. Carr, and P. T. Strub, Seasonal climatology of hydrographic conditions in the upwelling region off northern Chile, *J. Geophys. Res.*, *106* (C6), 11,451–11,467, 2001.

Blanke, B., and S. Raynaud, Kinematics of the Pacific equatorial undercurrent. An Eulerian and Lagrangian approach from GCM Results, *J. Phys. Oceanogr.*, *27*, 1038–1053, 1997.

Bourlès, B., Y. Gouriou, and R. Chuchla, On the circulation in the upper layer in the western equatorial Atlantic, *J. Geophys. Res.*, *104*(C9), 21,151–21,170, 1999a.

Bourlès, B., R.L. Molinari, E. Johns, W.D. Wilson, and K.D. Leaman, Upper layer currents in the western tropical Atlantic (1989–1991). *J. Geophys. Res.*, *104*(C1), 1361–1375, 1999b.

Bourlès, B., M. D. D'Orgeville, G. Eldin, Y. Gouriou, R. Chuchla, Y. DuPenhoat, and S. Arnault, On the evolution of the thermocline and subthermocline eastward currents evolution in the equatorial Atlantic, *Geophys. Res. Lett., 29*(16), doi:10.1029/2002GL015098, 2002.

Bryden, H. L., and E. C. Brady, Diagnostic model of the three-dimensional circulation in the upper equatorial Pacific Ocean, *J. Phys. Oceanogr.*, *15*, 1255–1273, 1985.

Butt, J., and E. Lindstrom, Currents off east coast of New Ireland, Papua-New Guinea, and their relevance to regional undercurrents in the western equatorial Pacific Ocean, *J. Geophys. Res.*, *99*, 12,203–12,514, 1994.

Carton, J. A., X. Cao, B. S. Giese, and A. M. da Silva, Decadal and interannual SST variability in the tropical Atlantic Ocean, *J. Phys. Oceanogr.*, *26*, 1165–1175, 1996.

Carton, J. A., G. Chepurin, X. Cao, and B. Giese, A simple ocean data assimilation analysis of the global upper ocean 1950–95. Part I: Methodology. *J. Phys. Oceanogr.*, *30*, 294–309, 2000.

da Silva, A. M., C. C. Young, and S. Levitus, *Atlas of Surface Marine Data 1994*. Vol. 3: Anomalies of heat and momentum fluxes; Vol. 4: Anomalies of fresh water fluxes NOAA Atlas NESDIS 8, U.S. Department of Commerce, NOAA, NESDIS, 413 pp., 1994.

Deser, C., A. Alexander, and M. S. Timlin, Upper-ocean thermal variations in the North Pacific during 1970–1991, *J. Clim.*, *9*, 1840–1855, 1996.

Esbensen, S. K., and V. Kushnir, The heat budget of the global ocean: An atlas based on estimates from marine surface observations. *Climatic Research Institution Rep. 29*, 27 pp., 1981.

Feng, M., and G. Meyers, Interannual variability in the tropical Indian Ocean: a two-year time-scale of Indian Ocean dipole, *Deep Sea Res., Part II*, *50*, 2263–2284, 2003.

Ferron, B., and. J. Marotzke, Impact of 4D-variational assimilation of WOCE hydrography on the meridional circulation of the Indian Ocean, *Deep Sea Res., Part II*, *50*, 2005–2021, 2003.

Fine, R. A., W. H. Peterson, and H. G. Ostlund, The penetration of the tritium into the tropical Pacific, *J. Phys. Oceanogr.*, *17*, 553–564, 1987.

Fratantoni, D. M., W. E. Johns, T. L. Townsend, and H. E. Hurlburt, Low-latitude circulation and mass transport pathways in a model of

the tropical Atlantic Ocean, *J. Phys. Oceanogr.*, *30*, 1944–1966, 2000.

Ganachaud, A., and C. Wunsch, Improved estimates of global ocean circulation, heat transport and mixing from hydrographic data, *Nature*, *408*, 453–457, 2001.

Ganachaud, A., C. Wunsch and J. Marotzke, The Meridional Overturning and Large-Scale Circulation of the Indian Ocean, *J. Geophys. Res.*, *105*, 26,117–26,134, 2000.

Garreaud, R. D., and D. S. Battisti, Interannual (ENSO) and interdecadal (ENSO-like) variability in the southern hemisphere tropospheric circulation, *J. Clim.*, *12*, 2113–2123, 1999.

Garzoli, S. L., A. Ffield, and Q. Yao, North Brazil current rings and the variability in the latitude of retroflection, in: *Interhemispheric water exchange in the Atlantic Ocean*, Goni, G.J., and P. Malanotte-Rizzoli (Editors), Elsevier Oceanography Series, pp.357–373, 2003.

Garternicht, U., and F. Schott, Heat fluxes of the Indian Ocean from a global eddy-resolving model, *J. Geophys. Res.*, *102*, 21,147–21,159, 1997.

Godfrey, J. S., G. C. Johnson, M. J. McPhaden, G. Reverdin, and S. Wijffels, The tropical ocean circulation. In: *Ocean circulation and climate*, Church, J., J. Gould, and G. Siedler (Editors), Academic Press, London, pp. 215–245, 2001.

Godfrey, J. S. and J. V. Mansbridge, Ekman transports, tidal mixing, and the control of temperature structure in Australia's northwest waters, *J. Geophys. Res.*, *105*(C10), 24,021–24,044, 2000.

Goni, G. J. and W. E. Johns, Synoptic study of warm rings in the North Brazil Current retroflection region using satellite altimetry, in: *Interhemispheric water exchange in the Atlantic Ocean*, Goni, G.J., and P. Malanotte-Rizzoli (Editors), Elsevier Oceanography Series, pp. 335–356, 2003.

Gordon, A. L., R. D. Susanto, and A. Ffield, Throughflow within Makassar Strait, *Geophys. Res. Lett.*, *26*, 3325–3329, 1999.

Gouriou, Y., and G. Reverdin, Isopycnal and diapycnal circulation of the upper equatorial Atlantic Ocean in 1983–1984, *J. Geophys. Res.*, *97*(C3), 3543–3572, 1992.

Grodsky, S.A. and J.A. Carton, Surface drifter pathways originating in the equatorial Atlantic cold tongue, *Geophys. Res. Lett.*, *29*(23), 62–65, 2002.

Grodsky, S. A., and J. A. Carton, The intertropical convergence zone in the South Atlantic and the equatorial Cold Tongue, *J. Clim.*, *16*(4), 723–733, 2003.

Gu, D., and S. G. H. Philander, Interdecadal climate fluctuations that depend on exchanges between the tropics and extratropics, *Science*, *272*, 805–808, 1997.

Hautala, S., and D. Roemmich, Subtropical mode water in the northeast Pacific basin, *J. Geophys. Res.*, *103*, 13,055–13,066, 1998.

Hazeleger, W., P. de Vries, and G. J. van Oldenborgh, Do tropical cells ventilate the Indo-Pacific equatorial thermocline?, *Geophys. Res. Lett.*, *28*, 1763–1766, 2000.

Hazeleger, W., M. Visbeck, M. Cane, A. Karspack, and N. Naik, Decadal upper ocean temperature variability in the tropical Pacific, *J. Geophys. Res.*, *106*, 8971–8988, 2001.

Hellerman, S., and M. Rosenstein, Normal monthly wind stress over the world ocean with error estimates, *J. Phys. Oceanogr.*, *13*, 1093–1105, 1983.

Huang, B., and Z. Liu, Pacific subtropical-tropical thermocline water exchange in the National Centers for Environmental Prediction ocean model, *J. Geophys. Res.*, *104*, 11,065–11,076, 1999.

Huang, R. X., and J. Pedlosky, Climate variability inferred from a layered model of the ventilated thermocline, *J. Phys. Oceanogr.*, *29*, 779–790, 1999.

Huang, R. X., and B. Qiu, The Structure of the wind-driven circulation in the subtropical south Pacific Ocean. *J. Phys. Oceanogr.*, *28*, 1173–1186, 1998.

Huang, B., and J. Shukla, Characteristics of the interannual and decadal variability in a general circulation model of the tropical Atlantic Ocean, *J. Phys. Oceanogr.*, *27*(8), 1693–1712, 1997.

Huyer, A., M. Knoll, T. Paluskiewicz, and R. L. Smith, The Peru Undercurrent: a study in variability, *Deep Sea Res.*, *Suppl. 1*, *38*, 247–271, 1991.

Inui, T., A. Lazar, P. Malanotte-Rizzoli, and A. Busalacchi, Wind stress effects on subsurface pathways from the subtropical to tropical Atlantic, *J. Phys. Oceanogr.*, *32*(8), 2257–2276, 2002.

Johns, W. E., T. N. Lee, R. C. Beardsley, J. Candela, R. Limeburger, and B. Castro, Annual cycle and variability of the North Brazil Current, *J. Phys. Oceanogr.*, *28*, 103–128, 1998.

Johns, W. E., R. Zantopp, and G. J. Goni, Cross-gyre transport by North Brazil Current rings, in: *Interhemispheric water exchange in the Atlantic Ocean*, Goni, G.J., and P. Malanotte-Rizzoli (Editors), Elsevier Oceanography Series, pp. 411–441, 2003.

Johnson, G. C., The Pacific Ocean subtropical cell surface limb, *Geophys. Res. Lett.*, *28*, 1771–1774, 2001.

Johnson, G. C., and M.J. McPhaden, Interior pycnocline flow from the subtropical to the equatorial Pacific Ocean, *J. Phys. Oceanogr.*, *29*(12), 3073–3089, 1999.

Johnson, G. C., M. J. McPhaden, and E. Firing, Equatorial Pacific Ocean horizontal velocity, divergence, and upwelling, *J. Phys. Oceanogr.*, *31*(3), 839–849, 2001.

Johnson, G. C., and D.W. Moore, The Pacific Subsurface Countercurrents and an inertial model, *J. Phys. Oceanogr.*, *27*(11), 2448–2459, 1997.

Johnson, G. C., B. M. Sloyan, W. S. Kessler, and K.E. McTaggart, Direct measurements of upper ocean currents and water properties across the tropical Pacific during the 1990s, *Prog. Oceanogr.*, *52*, 31–61, 2002.

Karstensen, J. and D. Quadfasel, Formation of southern hemisphere thermocline waters: water mass conversion and subduction, *J. Phys. Oceanogr.*, *32*(11), 3020–3038, 2002.

Kessler, W. S., Interannual variability in the subsurface high-salinity tongue south of the equator at 165E, *J. Phys. Oceanogr.*, *29*(8), 2038–2049, 1999.

Kessler, W. S., Mean three-dimensional circulation in the northeast tropical Pacific, *J. Phys. Oceanogr.*, *32*, 2457–2471, 2002.

Kessler, W. S., G. C. Johnson, and D. W. Moore, Sverdrup and nonlinear dynamics of the Pacific Equatorial Currents. *J. Phys. Oceanogr., 33*, 994–1008, 2003.

Kleeman, R., J. P. McCreary Jr., and B. A. Klinger, A mechanism for generating ENSO decadal variability, *Geophys. Res. Lett.*, *26*(12), 1743–1746, 1999.

Klinger, B. A., J. P. McCreary Jr., and R. Kleeman, The relationship between oscillating subtropical wind stress and equatorial temperature, *J. Phys. Oceanogr.*, *32*, 1507–1521, 2002.

Latif, M., and T. P. Barnett, Causes of decadal climate variability over the north Pacific and North America. *Science*, *266*, 634–637, 1994.

Lazar, A., T. Inui, P. Malanotte-Rizzoli, A. J. Busalacchi, L. Wang, and R. Murtugudde, Seasonality of the ventilation of the tropical Atlantic thermocline in an ocean general circulation model, *J. Geophys. Res.*, *107*(C8), 3104, doi:10.1029/2000JC000667, 2002.

Lazar, A., R. Murtugudde, and A. J. Busalacchi, A model study of temperature anomaly propagation from the subtropics to tropics within the South Atlantic thermocline, *Geophys. Res. Lett.*, *28*, 1271–1274, 2001.

Lee, C. M., B. H. Jones, K. H. Brink, and A.S. Fischer, The upper ocean response to monsoonal forcing in the Arabian Sea, seasonal and spatial variability, *Deep Sea Res., Part II*, *47*, 1177–1226, 2000.

Levitus, S., Climatological atlas of the world ocean. *NOAA Profess. Paper No 13*, US. Dept. of Commerce, Rockville, MD, 173 pp., 1982.

Levitus, S., and T. Boyer, World Ocean Atlas 1994, Vol. 3: Salinity. *NOAA Atlas NESDIS 3*, U.S. Government Printing Office, Wash., D.C., 93 pp., 1994a.

Levitus, S., and T. Boyer, World Ocean Atlas 1994, Vol. 4: Temperature. *NOAA Atlas NESDIS 4*, U.S. Government Printing Office, Wash., D.C., 117 pp., 1994b.

Liu, Z., A simple model of the mass exchange between the subtropical and tropical ocean, *J. Phys. Oceanogr.*, *24*, 1153–1165, 1994.

Liu, Z., and S. G. H. Philander, How different wind stress patterns affect the tropical-subtropical circulations of the upper ocean, *J. Phys. Oceanogr.*, *25*, 449–462, 1995.

Liu, Z. and G. Philander, Tropical-extratropical oceanic exchange pathways, in: *Ocean Circulation and Climate: Observing and Modeling the Global Ocean*, G. Siedler et al. (Editors), pp. 247–254, 2001.

Liu, Z., S. G. H. Philander, and R.C. Pacanowski, A GCM study of the tropical-subtropical upper-ocean exchange, *J. Phys. Oceanogr.*, *24*, 2606–2623, 1994.

Liu, Z., and B. Huang, Why is there a tritium maximum in the central equatorial Pacific thermocline, *J. Phys. Oceanogr.*, *28*, 1527–1533, 1998.

Liu, Z., and S. Shin, On thermocline ventilation of active and passive tracers, *Geophys. Res. Lett.*, *26*, 357–360, 1999.

Loschnigg, J., and P.J. Webster, A coupled ocean-atmosphere system of SST modulation for the Indian Ocean. *J. Clim., 13*(19), 3342–3360, 2000.

Lu, P., and J. P. McCreary Jr., Influence of the ITCZ on the flow of the thermocline water from the subtropical to the equatorial Pacific Ocean, *J. Phys. Oceanogr.*, *25*, 3076–3088, 1995.

Lu, P., J. P. McCreary Jr., and B. A. Klinger, Meridional circulation cells and the source waters of the Pacific equatorial undercurrent, *J. Phys. Oceanogr.*, *28*, 62–83, 1998.

Lukas, R., The termination of the equatorial undercurrent in the eastern Pacific, *Prog. Oceanogr.*, *16*, 63–90, 1986.

Lumpkin, R. and K. Speer, Large-scale vertical and horizontal circulation in the North Atlantic Ocean, *J. Phys. Oceanogr.*, *33*, 1902–1920, 2003.

Lux, M., H. Mercier, and M. Arhan, Interhemispheric exchanges of mass and heat in the Atlantic Ocean in January–March 1993, *Deep Sea Res., Part I*, *48*, 605–638, 2001.

Luyten, J. R., J. Pedlosky, and H. Stommel, The ventilated thermocline, *J. Phys. Oceanogr.*, *13*, 292–309, 1983.

Luyten, J. R., and H. Stommel, Gyres driven by combined wind and buoyancy flux, *J. Phys. Oceanogr.*, *16*, 1551–1560, 1986.

Malanotte-Rizzoli, P. K. Hedstrom, H. Arango, and D.B. Haidvogel, Water mass pathways between the subtropical and tropical ocean in a climatological simulation of the North Atlantic ocean circulation, *Dyn. Atmospheres and Oceans*, *32*, 331–371, 2000.

Mantua, N. J., S. R. Hare, Y. Zhang, J. M. Wallace, and R. C. Francis, A Pacific interdecadal climate oscillation with impacts on salmon production, *Bull. Am. Meteorol. Soc.*, *78*, 1069–1079, 1997.

Marshall, J. C., A. J. G. Nurser, and R. G. Williams, Inferring the subduction rate and period over the North Atlantic, *J. Phys. Oceanogr.*, *23*,1315–1329, 1993.

Mayer, D. A., R. L. Molinari, and J. F. Fiesta, The mean and annual cycle of upper layer temperature fields in relation to Sverdrup dynamics within the gyres of the Atlantic Ocean, *J. Geophys. Res.*, *103*, 18545–18566, 1998.

McCreary, J. P., Jr., Modeling equatorial ocean circulation, *Ann. Rev. Fluid Mech.*, *17*, 359–409, 1985.

McCreary, J. P., Jr., P. K. Kundu, and R. L. Molinari, A numerical investigation of dynamics, thermodynamics and mixed-layer processes in the Indian Ocean, *Prog. Oceanogr.*, *31*, 181–244, 1993.

McCreary, J. P., Jr., and P. Lu, Interaction between the subtropical and equatorial ocean circulations: the subtropical cell, *J. Phys. Oceanogr.*, *24*(2), 466–497, 1994.

McCreary, J. P., Jr., K. E. Kohler, R. R. Hood, and D. Olson, A four-component model of biological activity in the Arabian Sea. *Prog. Oceanogr.*, *37*, 193–240, 1996.

McCreary, J.P., Jr., P. Lu, and Z. Yu, Dynamics of the Pacific Subsurface Countercurrents, *J. Phys. Oceanogr.*, *32*, 2379–2404, 2002.

McPhaden, M. J., A.J. Busalacchi, R. Cheney, J. R. Donguy, K. S. Gage, D. Halpern, M. Ji, P. Julian, G. Meyers, G. T. Mitchum, P. P. Niiler, J. Picaut, R.W. Reynolds, N. Smith, and K. Takeuchi, The Tropical Ocean-Global Atmosphere (TOGA) observing system: A decade of progress, *J. Geophys. Res.*, *103*, 14,169–14,240, 1998.

McPhaden, M. J., and D. Zhang, Slowdown of the meridional overturning circulation in the upper Pacific Ocean, *Nature*, *415*, 603–608, 2002.

Meinen, C. S., M. J. McPhaden, and G. C. Johnson, Vertical velocities and transports in the equatorial Pacific during 1993–1999, *J. Phys. Oceanogr.*, *31*, 3230–3248, 2001.

Miyama, T., J. P. McCreary Jr., T. G. Jensen, J. Loschnigg, S. Godfrey, and A. Ishida, Structure and dynamics of the Indian-Ocean cross-equatorial cell, *Deep Sea Res., Part II*, *50*, 2023–2047, 2003.

Molinari, R. L., S. Bauer, D. P. Snowden, G. C. Johnson, B. Bourles, Y. Gouriou, and H. Mercier, A Comparison of kinematic evidence for tropical cells in the Atlantic and Pacific oceans, in: *Interhemispheric Water Exchange in the Atlantic Ocean*, Goni, G.J., and P. Malanotte-Rizzoli (Editors), Elsevier Oceanographic Series, pp.

269–286, 2003.

Murtugudde, R., S. Signorini, J. Christian, A. Busalacchi, C. McClain, and J. Picaut, Ocean color variability of the tropical Indo-Pacific basin observed by SeaWiFS during 1997–98, *J. Geophys. Res.*, *104*, 18,351–18,366, 1999.

Nonaka, M., S.-P. Xie, and K. Takeuchi, Equatorward spreading of a passive tracer with application to North Pacific interdecadal temperature variations, *J. Oceanogr.*, *56*, 173–183, 2000.

Nonaka, M., and S.-P. Xie, Propagation of North Pacific interdecadal subsurface temperature anomalies in an ocean GCM, *Geophys. Res. Lett.*, *27*, 3747–3750, 2000.

Nonaka M., S.-P. Xie, and J. P. McCreary Jr., Decadal variations in the Subtropical Cells and equatorial Pacific SST, *Geophys. Res. Lett.*, *29*(7), 1116, doi:10.1029/2001GL013–717, 2002.

Pedlosky, J., An inertial theory of the equatorial undercurrent, *J. Phys. Oceanogr.*, *17*, 1978–1985, 1987.

Pedlosky, J., Entrainment and the termination of the equatorial undercurrent, *J. Phys. Oceanogr.*, *18*, 880–886, 1988.

Pedlosky, J., The link between western boundary current and equatorial undercurrent, *J. Phys. Oceanogr.*, *21*, 1553–1558, 1991.

Pedlosky, J., and R.M. Samelson, Wind forcing and the zonal structure of the equatorial undercurrent, *J. Phys. Oceanogr.*, *19*, 1244–1254, 1989.

Philander S. G. H., and R. C. Pacanowski, The generation of equatorial currents, *J. Geophys. Res.*, *85*, 1123–1136, 1980.

Qiu, B. and R. X. Huang, Ventilation of the North Atlantic and North Pacific: Subduction Versus Obduction, *J. Phys. Oceanogr.*, *25*, 2374–2390, 1995.

Quay, P. D., M. Stuiver, and W. S. Broeker, Upwelling rates for the equatorial Pacific Ocean derived from the bomb 14C distribution, *J. Mar. Res.*, *41*, 769–792, 1983.

Reverdin, G., C. Frankignoul, E. Kestenare, and M. J. McPhaden, Seasonal variability in the surface currents of the equatorial Pacific, *J. Geophys. Res.*, *99*, 20323–20344, 1994.

Roemmich, D., The balance of geostrophic and Ekman transports in the tropical Atlantic Ocean, *J. Phys. Oceanogr.*, *13,* 1534–1539, 1983.

Rothstein, L. M., R.-H. Zhang, A. J. Busalacchi, and D. Chen, A numerical simulation of the mean water pathways in the subtropical and tropical Pacific Ocean, *J. Phys. Oceanogr.*, *28*, 322–343, 1998.

Rowe, G., E. Firing, and G.C. Johnson, Pacific equatorial subsurface countercurrent velocity, transport, and potential vorticity, *J. Phys. Oceanogr.*, *30*, 1172–1187, 2000.

Saji, N. H., B. N. Goswami, P. N. Vinayachandran, and T. Yamagata, A dipole in the tropical Indian Ocean, *Nature*, *401*, 360–363, 1999.

Schneider, N., A decadal spiciness mode in the tropics, *Geophys. Res. Lett.*, *27*, 257–260, 2000.

Schneider, N, S. Venzke, A. J. Miller, D. W. Pierce, T. P. Barnett, C. Deser, and M. Latif, Pacific thermocline bridge revisited, *Geophys. Res. Lett.*, *26*, 1329–1332, 1999.

Schott, F., J. C. Swallow and M. Fieux, The Somali current at the equator: annual cycle of currents and transports in the upper 1000 m and connection to neighboring latitudes, *Deep Sea Res.*, *37*, 1825–1848, 1990.

Schott, F. and C.W. Böning, The WOCE model in the western equatorial Atlantic: upper-layer circulation, *J. Geophys. Res.*, *96*(C4), 6993–7004, 1991.

Schott, F., J. Fischer and L. Stramma, Transports and pathways of the upper-layer circulation in the western tropical Atlantic, *J. Phys. Oceanogr.*, *28*(10), 1904–1928, 1998.

Schott, F., and J. P. McCreary Jr., The monsoon circulation of the Indian Ocean, *Prog. Oceanogr.*, *51*, 1–123, 2001.

Schott, F., Dengler, M., and R. Schoenefeldt, The shallow thermohaline circulation of the Indian Ocean, *Prog. Oceanogr.*, *53*, 57–103, 2002a.

Schott, F., P. Brandt, M. Hamann, J. Fischer, and L. Stramma, On the boundary flow off Brazil at 5-10°S and its connection to the interior tropical Atlantic, *Geophys. Res. Lett.*, *29*(17), 1840, doi:10.1029/2002 GL014786, 2002b.

Schott, F., M. Dengler, P. Brandt, K. Affler, J. Fischer, B. Bourlès, Y. Gouriou, R. L. Molinari, and M. Rhein, The zonal currents and transports at 35W in the tropical Atlantic, *Geophys. Res. Lett.*, *30*(7), 1349, doi:10.1029/2002GL016849, 2003.

Shin, S., and Z. Liu, Response of equatorial thermocline to extratropical buoyancy forcing, *J. Phys. Oceanogr.*, *30*, 2883–2905, 2000.

Sloyan, B. M., G. C. Johnson, and W. S. Kessler, The Pacific cold tongue: A pathway for interhemispheric exchange, *J. Phys. Oceanogr.*, *33*(5) 1027–1043, 2003.

Snowden, D. P. and R .L. Molinari, Subtropical cells in the Atlantic Ocean: An observational summary, in: *Interhemispheric Water Exchange in the Atlantic Ocean*, Goni, G.J., and P. Malanotte-Rizzoli (Editors), Elsevier Oceanographic Series, pp. 287–312, 2003.

Solomon, A., J. P. McCreary Jr., R. Kleeman, and B.A. Klinger, Interannual and decadal variability in an intermediate coupled model of the Pacific region, *J. Clim.*, *16*, 383–405, 2003.

Stommel, H., Wind-drift near the equator, *Deep Sea Res.*, *6*, 298–302, 1960.

Stramma, L., and F. Schott, The mean flow field of the tropical Atlantic Ocean, *Deep Sea Res., Part II*, *46*, 279–303, 1999.

Susanto, D. R., and A .L. Gordon, Upwelling along the coasts of Java and Sumatra and its relation to ENSO, *Geophys. Res. Lett.*, *28*, 1599–1602, 2001.

Swallow, J. C., F. Schott, and M. Fieux, Structure and transport of the East African Coastal Current, *J. Geophys. Res.*, 96, 22,254–22,267, 1991.

Talley, L., Shallow, intermediate, and deep overturning components of the global heat budget, *J. Phys. Oceanogr.*, *33*, 530–560, 2003.

Tsuchiya, M., A subsurface north equatorial countercurrent in the eastern Pacific Ocean, *J. Geophys. Res.*, *77*, 5981–5986, 1972.

Tsuchiya, M., R. Lukas, R. A. Fine, E. Firing, and E. Lindstrom, Source waters of the Pacific equatorial undercurrent, *Prog. Oceanogr.*, *23*, 101–147, 1989.

Vinayachandran, P. N., and T. Yamagata, Monsoon response of the sea around Sri Lanka: generation of thermal domes and anticyclonic vortices, *J. Phys. Oceanogr.*, *28*, 1946–1960, 1998.

Wacongne, S. and R. Pacanowski, Seasonal heat transport in a primitive equations model of the tropical Indian Ocean, *J. Phys. Oceanogr.*, *26*(12), 2666–2699, 1996.

Webster, P. J., A. M. Moore, J .P. Loschnigg, and R.R. Leben, Coupled ocean-atmosphere dynamics in the Indian Ocean during 1997–98, *Nature*, *401*, 356–359, 1999.

Wijffels, S., E. Firing, and J. Toole, The mean structure and variability of the Mindanao Current at 8N, *J. Geophys. Res.*, *100*, 18,421–18,435, 1995.

Wilson, W. D., E. Johns, and R. L. Molinari, Upper layer circulation in the western tropical North Atlantic Ocean during August 1989, *J. Geophys. Res.*, 99, 22,513–22,523, 1994.

Wong, A. P. S., and G. C. Johnson, South Pacific eastern subtropical mode water, *J. Phys. Oceanogr.*, *33*, 1493–1509, 2003.

Wyrtki, K., Upwelling in the Costa Rica Dome, *U.S. Fish and Wildlife Service Fishery Bull.*, *63*, 355–372, 1964.

Wyrtki, K., An estimate of equatorial upwelling in the Pacific, *J. Phys. Oceanogr.*, *11*, 1205–1214, 1981.

Wyrtki, K., An equatorial jet in the Indian Ocean, *Science*, *181*, 262–264, 1973.

Xie, S.-P., H. Annamalai, F. Schott, and J. P. McCreary, Jr., Origin and predictability of South Indian Ocean climate variability, *J. Clim.*, *15*(8), 864–874, 2002.

Zhang, D., M. J. McPhaden and W. E. Johns, Observational evidence for flow between the subtropical and tropical Atlantic: The Atlantic Tropical Cells, *J. Phys. Oceanogr.*, *33*, 1783–1797, 2003.

Gregory C. Johnson, NOAA/Pacific Marine Environmental Laboratory, Seattle, Washington. (Gregory.C.Johnson@noaa.gov)

Julian P. McCreary, Jr., International Pacific Research Center, University of Hawaii, POST Bldg. 401, 1680 East West Road, Honolulu, Hawaii 96822. (jay@hawaii.edu)

Friedrich A. Schott, IFM-GEOMAR Leibniz Institut für Meereswissenschaften an der Universität Kiel, Düsternbrooker Weg 20, D-24105 Kiel, Germany. (fschott@ifm-geomar.de)